2012

Gβγ acts at an inter-subunit cleft to activate GIRK1 channels

Rahul Mahajan
Virginia Commonwealth University

Gβγ acts at an inter-subunit cleft to activate GIRK1 channels

by

Rahul Mahajan

Advisor: Dr. Diomedes E. Logothetis

Abstract

Heterotrimeric guanine nucleotide-binding proteins (G-proteins) consist of an alpha subunit (Gα) and the dimeric beta-gamma subunit (Gβγ). The first example of direct cell signaling by Gβγ was the discovery of its role in activating G-protein regulated inwardly rectifying K^+ (GIRK) channels which underlie the acetylcholine-induced K^+ current responsible for vagal inhibition of heart rate. Published crystal structures have provided important insights into the structures of the G-protein subunits and GIRK channels separately, but co-crystals of the channel and Gβγ together remain elusive and no specific reciprocal residue interactions between the two proteins are currently known.

Given the absence of direct structural evidence, we attempted to identify these functionally important channel-Gβγ interactions using a computational approach. We developed a multistage computational docking algorithm that combines several known methods in protein-protein docking. Application of the docking protocol to previously published structures of Gβγ and GIRK1 homomeric channels produced a clear signal of a favored binding mode. Analysis of this binding mode suggested a mechanism by which Gβγ promotes the open state of the channel. The channel-Gβγ interactions predicted by the model *in silico* could be disrupted *in vitro* by mutation of one protein and rescued by additional mutation of reciprocal residues in the other protein. These interactions were found to extend to agonist induced activation of the channels as well as to activation of the native heteromeric channels.

Currently, the structural mechanism by which Gβγ regulates the functional conformations of GIRK channels or of any of its membrane-associated effector proteins is not known. This work

shows the first evidence for specific reciprocal interactions between Gβγ and a GIRK channel and places these interactions in the context of a general model of intracellular regulation of GIRK gating.

Acknowledgements

I will always be indebted to Dr. Logothetis and I would like to thank him for his mentorship and care over the past few years.

I would sincerely like to thank Dr. Clive Baumgarten, Dr. Lou De Felice, Dr. Glen Kellogg, and Dr. Jason Chen for their patience with my development, critical feedback on my work and most of all for their example as excellent academic scientists and mentors.

I would also like to thank Sophia Gruszecki and Heikki Vaananen for oocyte preparation and technical assistance as well as Junghoon Ha, Meng Cui, Shobana Sundaram and other members of the Logothetis laboratory for their assistance. I would like to thank Dr. Neel Scarsdale and the VCU Center for High Performance Computing for vital assistance with RosettaDock setup and resources. I would also like to thank Dr. Brian Pierce for a helpful correspondence.

Finally, I am grateful to my family Dr. Satish Mahajan, Mrs. Neelam Mahajan, and Dr. Anshu Mahajan for being the foundation on which all my other endeavors rest.

Table of Contents:

List of Figures

Chapter 1

Introduction

1.1 Vagal Inhibition of Heart Rate

Heterotrimeric guanine nucleotide-binding proteins (G-proteins) comprise a fundamental cellular signal transduction mechanism employed ubiquitously throughout human physiology. They consist of an alpha subunit (Gα) and the dimeric beta-gamma subunits (Gβγ). The first example of direct cell signaling by Gβγ was the discovery of its role in activating G-protein regulated inwardly rectifying K^+ (GIRK or Kir3) channels [1]. These channels play diverse functional roles including regulation of cardiac, neuronal, endocrine, and smooth muscle physiology [2]. Prior to any knowledge of their regulation by Gβγ, these channels were first recognized for their role in cardiac physiology where they are today known to conduct the cardiac potassium current (IK_{ACh}) responsible for the negative chronotropic effects of vagus nerve acetylcholine (ACh) release.

The general inhibitory effect of the vagus nerve on the heart has been known since at least the 19th century when the brothers Eduard and Ernst Weber demonstrated their results to an Italian congress of scientists in 1845 [3], [4]. They showed that heart rate in a frog preparation could be

slowed and brought to a stop by direct electrical stimulation of the vagus nerves using a rotary galvano-magnetic apparatus. Early indications towards the possible chemical transmission of this signal and the nature of the myocardial electrical response came as early as 1886 from the work of Walter Gaskell who, using extracellular recordings, recognized the sensitivity of this vagal inhibition to atropine and its accompaniment by the hyperpolarization of the heart muscle [5], [6]. Although the role of potassium channels in inducing hyperpolarization was not yet known, through careful chemical quantitation of extracellular fluids, Howell and Duke had demonstrated by 1908 that vagal inhibition of the heart is accompanied by a small release of potassium into extracellular fluid [7].

Modern neuroscience was ushered in by Otto Loewi through his direct demonstration of chemical transmission of nervous impulses [8]. In his classic experiment, inhibition of a denervated frog heart was observed upon the application of extract from a second frog heart which had undergone vagal stimulation (see Figure 1.1). The inferred substance in the vagally stimulated frog heart extract responsible for inhibition of activity was deemed *Vagusstoff*, which was later confirmed to be acetylcholine [9]. For his demonstration of chemical nervous transmission, Loewi shared the 1936 Nobel Prize in Physiology or Medicine with the discoverer of acetylcholine, Sir Thomas Dale [10].

The later advent of intracellular microelectrodes and voltage-clamp techniques allowed for more rigorous exploration of these phenomena and led to the direct implication of hyperpolarization of the sinoatrial node by acetylcholine-sensitive potassium channel activity as underlying the negative cardiac chronotropy induced by vagus nerve stimulation. Burgen and Terroux revisited

the vagal induced hyperpolarization of heart muscle reported by Gaskell. Using microelectrodes, they confirmed that hyperpolarization is induced by ACh application [11]. Furthermore, by measuring the effect of external K+ concentration on resting potential in the absence and presence of ACh, they also demonstrated that an increased cell permeability to potassium may underlie hyperpolarization. Del Castillo and Katz used microelectrodes to directly show hyperpolarization of the sinus node upon vagal stimulation [12]. Voltage clamp allowed Trautwein and Dudel to measure K+ reversal potentials and thus directly confirm changes in cell potassium permeability in response to ACh [13]. With the role of changes in cell potassium permeability in inducing sinoatrial node hyperpolarization established, Noma and Trautwein studied activation kinetics of ACh-induced K+ currents and concluded that ACh binding activates a specific ion channel, K_{ACh} [14]. Finally, the introduction of the patch-clamp technique [15] led to the first single-channel recordings of K_{ACh} currents [16] which clearly demonstrated kinetic properties distinct from other background potassium channels (see Figure 1.2).

Thus, the negative chronotropic effect of vagal stimulation was shown to be underlain by the hyperpolarization of the sinus node due to the activation of a specific K+ channel in response to ACh released at the vagal termini. In subsequent years, the cloning of the molecular components underlying IK_{ACh} have revealed a heterotetramer comprised of GIRK1 and GIRK4 subunits [17], [18], [19]. In heterologous expression, GIRK1 alone yields no currents and GIRK4 alone yields very small currents compared to robust currents conducted by the heterotetramer. To aid their study individually, single point mutations have been introduced in the reentrant pore helix region of these channels to yield the widely studied GIRK1* (GIRK1 F137S) and GIRK4* (S143T)

channels. These mutant channels conduct robust currents even when expressed alone and thus have allowed for the study of functional homomeric channels [20], [21]. The other known GIRK isoforms are the GIRK2 and GIRK3 isoforms (reviewed in [2]). GIRK channels usually consist of a heterotetramer of GIRK1 with another isoform and have been found to be expressed in various other tissues outside the heart including brain, pancreas, and kidney [2]. The heterotetramer primarily found in cardiac tissue is the GIRK1/4 channel which underlies IK_{ACh}; the neuronal heterotetramer primarily consists of the GIRK1/2 channel. GIRK1/2 channels play important roles in neuronal function including pain perception and memory modulation [22] and the GIRK1/4 channel has been shown to play important roles in cardiac pathophysiology. *In vivo* loss of function of this current was shown to cause an almost complete loss of variability in the heart's beat to beat frequency and a large reduction in heart rate vagal response [23]. Loss of its function by mutations in GIRK subunits have also been associated with long QT syndrome in humans [24]. On the other hand, excessive GIRK1/4 activity is associated with atrial fibrillation in humans [25], [26].

1.2 Molecular Components of K_{ACh} Regulation

In order to examine the molecular regulators of IK_{ACh}, a brief discussion of G-proteins is necessary.

Heterotrimeric G-proteins consisting of alpha and beta-gamma subunits (Gα and Gβγ, respectively) are intracellular, membrane-bound proteins that couple to transmembrane G-protein coupled receptors (GPCRs) and act as molecular switches to help transduce extracellular signals to downstream effector proteins. Their activity is dependent on the binding of Gα to guanosine triphosphate (GTP) and terminates with hydrolysis of GTP to guanosine diphosphate (GDP) in a process known as the G-protein cycle (see Figure 1.3). Over 1000 GPCRs have been identified, constituting the largest class of membrane receptors and the most common targets for drugs on the market today [27]. The G-protein signaling mechanism underlies remarkably diverse physiological phenomena from sensory modalities such as sight and odor sensation to control of homeostasis through endocrine, adrenergic, and chemokine signaling to behavioral and mood regulation through neurotransmission and control of cellular excitability [27]. While the role of Gβγ in directly regulating the activity of downstream effector proteins is a more recent discovery, G-proteins have long been characterized by the activity of the Gα subunit, especially in relation to its regulation of adenylyl cyclases.

Work from Earl Sutherland in the 1950's had demonstrated that several hormones lead to stimulation of adenylyl cyclase and the production of cyclic adenosine monophosphate (cAMP) within cells where it acts as a soluble second messenger [28]. At first the GTP dependence of

this process was not known because the process of purifying adenosine triphosphate (ATP) used as a substrate for the generation of cAMP was imperfect and allowed for contamination by GTP (reviewed in [29]). Rodbell and colleagues showed that when supplying low concentrations of ATP, application of hormone or agonist became insufficient to stimulate cAMP production unless GTP was supplied [30]. This identified a GTP dependent step in the signaling process leading to stimulation of cAMP production, but the identity of the GTP dependent component was not known.

Gill and Meren showed that cholera toxin leads to sustained elevation of cAMP levels by ADP-ribosylation of some unidentified cellular protein component [31]. Haga and colleagues in Al Gilman's laboratory generated a cell line which failed to elevate cAMP levels in response to known agonists [32]. Yet, direct assessment of adenylyl cyclase function in this cell line showed that the activity of the cAMP producing enzyme was intact and thus the deficiency arose from a component in the transduction mechanism. Using cholera toxin and a radioactive ADP substrate, they demonstrated radioisotope incorporation into a 45kilodalton (kD) polypeptide occurred in normal cells but not in their deficient cell line. These advances eventually allowed Gilman's laboratory to purify the 45kD polypeptide identified as the alpha subunit of the adenylyl cyclase-stimulating GTP binding protein (Gs) [33]. This polypeptide co-purified with a 35kDa and an 8-10kDa identified as the beta and gamma subunits of heterotrimeric G-proteins.

Today, the G-protein family has been extended to include 3 more classes of Gα subunits: Gq/11, G12/13 the pertussis toxin sensitive Gi/o. Various isoforms of these Gα subunits heteromerize with one of 5 known Gβ isoforms and one of 12 known Gγ subunits to form the heterotrimeric

G-protein. Their coupling is promiscuous but not every combination of isoforms can be found physiologically (Reviewed in [29]). In addition to adenylyl cyclases, several downstream effectors have been identified that are regulated by either or both of Gα and Gβγ [27], [34].

Several lines of evidence implicated G-proteins in the signal transduction mechanism which allowed ACh to activate K_{ACh}. Soejima and Noma showed in 1984 that the mechanism of K_{ACh} activation is membrane delimited. Bath application of ACh did not activate K_{ACh} current in a cell attached patch but inclusion of ACh within the patch pipette solution could successfully activate the channels [35]. Thus the ACh had to be applied directly to the patch of membrane being recorded and no freely diffusible intracellular signaling mechanism could be responsible for activating the channel. Evidence from two groups implicated guanine nucleotide binding proteins (G-proteins) in the signaling mechanism. Breitwieser and Szabo used intracellular application of non-hydrolyzable GTP analogs to maximally activate IK_{ACh} such that it no longer responded to extracellular application of ACh [36]. This implied the channel was a distinct entity from the ACh receptor and that the GTP dependent activation mechanism likely involved G-proteins. Pfaffinger and colleagues demonstrated the sensitivity of the current to pertussis toxin and thus implicated G-proteins and specifically, the Gi/o family [37]. Finally, Logothetis et al demonstrated that it was the Gβγ subunits of heterotrimeric G-proteins that were responsible for channel activation [1]. Purified Gβγ but not Gα protein could be applied to the intracellular surface of an excised membrane patch to activate the channels (see Figure 1.4). Activation of IK_{ACh} was the first example of direct Gβγ signaling, but many Gβγ effectors are now known and their numbers rival Gα effectors (reviewed in [27], [34]).

Although it has now been shown that Gβγ activates GIRK channels, there is some evidence that Gα plays a modulatory role. Receptor activation of GIRK currents is selective to Gi coupled receptors. Because identical Gβγ subunits can bind to various receptors, the reason for this specificity is not known. It has been suggested that such specificity is achieve by co-localization of signaling components into preformed complexes. Chimeric analysis of different Gα subunits suggested that domains of Gα may play a role is conferring this specificity [38]. Several studies have shown biochemically that Gα can bind to various domains of GIRK [38], [39], [40], [41]. Fluorescent techniques also suggest that there is a basal interaction between Gα and GIRK channels even in the absence of receptor activation [42], [43].

In addition to G-proteins, other molecular entities can also directly regulate GIRK channel activity. Like all members of the Kir inward rectifying potassium channel family, GIRK (Kir3) channels require the presence of phosphatidylinositol 4,5 bisphosphate (PIP_2) for function [44], [45], [46]. PIP_2 is necessary for channel activation but is not sufficient; an additional gating molecule such as Gβγ is required for channel activation [44]. Another gating molecule which can activate GIRK channels is intracellular Na^+. Both Gβγ and Na^+ appear to stabilize channel PIP_2 interactions [45], [46] . Other activators include alcohols such as ethanol [47] and strongly reducing intracellular environments [48].

1.3 Structural Insights

The first crystal structure of a potassium ion channel revealed a tetramer of four identical subunits and confirmed many features predicted by functional experiments [49]. Among these were the presence of pore constrictions comprising the selectivity filter at the extracellular end of the ion permeation pathway and the helix bundle crossing (HBC) gate towards the intracellular end. Inward rectifier potassium channels (Kir channels) contain an intracellular domain which extends the ion permeation pore well beyond the membrane into the intracellular environment and serves to interact with several intracellular regulators of channel activity. The first structures of GIRK channels only crystallized the intracellular domain and consisted of a fusion construct of the intracellular N- and C- termini of the channel. The transmembrane regions were not included and the termini were connected with an artificial linker region [50], [51]. These structures revealed the presence of a third putative gate at the apex of the intracellular region, the G-loop gate. A more recent GIRK structure is of a GIRK1 (Kir3.1) chimera between a mammalian and prokaryotic channel [52]. Substitution of the top three-fourths of the transmembrane region of GIRK1 with prokaryotic residues allowed the crystallization of a full length channel which places the intracellular termini in the proper context of a transmembrane region. The structure of the GIRK intracellular domains are organized through the cascading arrangement of secondary structure elements (see Figure 1.5). Beginning most centrally near the pore is the G-loop which comprises a gate in the channel structure. Moving outwards and downwards along a subunit surface are the CD loop, the N-terminus of the adjacent subunit, the LM loop, and the DE loop of the adjacent subunit. Although even more recent structures of full-length GIRK2 channels exist [53], the GIRK1 chimera crystal structure uniquely captures the G-

loop gate in two distinct conformations such that the G-loop gate is dilated "open" in one and constricted or "closed" in the other. The secondary structure elements also show reorganization between the two conformations.

A previous study from our lab conducted molecular dynamics simulations of these differing conformations of the GIRK1 chimera structure in the absence and presence of PIP_2 to study the interactions of the channel which allow for PIP_2 stabilization of the "open" conformation [54]. The conclusions of the detailed channel motions observed in the study can be summarized in terms of movements of the secondary structure elements (see Figure 1.6). Transition to the "open" conformation of the channel stabilized by PIP_2 saw a dramatic upward movement of the LM loop causing it to interact strongly with N-terminus. The LM thus moves up and acts as a "sink" for the N-term so that the N-term switches its interactions from the CD loop to the LM. This frees the CD loop to interact with G-loop to stabilize its open state. PIP_2 interacts directly with the CD loop and parts of the N-terminus to stabilize this open G-loop conformation.

Several lines of evidence suggest that the movements of the putative channel gates are not independent but that the gates likely undergo correlated movements. Clarke and colleagues examined 11 crystal structures of bacterial Kir channels and concluded that changes in intracellular domain orientations were correlated with changes in the selectivity filter gate [55]. Xiao and colleagues examined the state-dependence of accessibility of intracellular cationic modifiers to a cysteine modified pore residue in an inward rectifier potassium channel [56]. Although they call into question the function of the helix bundle crossing as a gate, they conclude that motions at the intracellular membrane interface correlate with changes in

conduction through the selectivity filter at the extracellular end of the ion permeation pore. Finally, by determining multiple crystal structures of the full length GIRK2 channel in the presence and absence of PIP_2, Whorton and MacKinnon suggest that PIP_2 acts to couple opening of the G-loop gate to movements of the transmembrane helices to cause opening of the HBC gate [53].

Unlike channel structures which have only arrived within the last decade, G-protein structures have existed since the mid-1990's. Structures of the inactive GDP bound heterotrimer revealed that Gα consists of an upper GTPase domain and a helical domain. Its interaction surface with Gβγ consists of loops in the GTPase domain called the switch regions as well as its long N-terminal helix [57], [58] (See Figure 1.7). This N-terminal helix is disordered when Gα is not bound to Gβγ (reviewed in [59]).

The Gβγ structure consists of a 7-blade beta-propeller structure. It has been crystallized alone [60] or together with regulatory proteins such as beta adrenergic receptor kinase (BARK), phosducin [61], [62], or of course, Gα. Comparisons of the various Gβγ structures do not reveal any major conformational changes although small changes in inter-strand loops and sidechain positions are observable. The exception is the co-crystal of Gβγ with phosducin where a separation of blades 6 and 7 is observed [62]. This conformation may be unique to the effect of phosducin. The farnesyl moiety which normally anchors the C-terminus of Gγ1 to the membrane is observed to occupy the cleft created between the propeller blades. Phosducin has the particular ability to dissociate Gβγ from the membrane and cause it to translocate to the

cytoplasm. The opening of a cleft in the protein to bind the lipid anchor would be consistent with this function.

Numerous studies have addressed GIRK-Gβγ interactions. Biochemical binding studies employ different strategies for choosing fragments of the channel and testing their ability to bind Gβγ [18], [40], [41], [63], [64], [65], [66], [67], [68]. Other studies have focused on making chimeras between GIRK channels and the closely related but G-protein insensitive IRK channels [69], [70], [71], [72]. Chimeras are then functionally characterized. Some studies have used the chimeric analysis to suggest a functionally critical region and then created specific point mutants within the region. Such a previous study from our lab identified a residue in the LM loop at position L333 of GIRK1 to play a critical role in activation by Gβγ [71]. Mutation of GIRK1* L333 to the corresponding glutamate residue in IRK1 produced a phenotype such that the mutant channel showed intact basal activity but was not activated by Gβγ co-expression or agonist induced receptor activation. While by no means exhaustive, results from many of these studies are summarized in Figure 1.8.

Similarly, studies have also attempted to identify regions of Gβγ important for channel interaction. Ford et al performed an alanine scan of all residues which comprised the Gα binding site on Gβγ [73]. These mutants were tested for their ability to regulate various Gβγ effectors including their ability to activate GIRK channels upon co-expression. Albsoul-Younes and colleagues preformed a chimeric analysis between mammalian Gβ and a yeast Gβ which is deficient in activating GIRK channels[74]. They identified blades 1 and 2 as the critical regions

for channel interaction. Several other studies also identify mutants with reduced ability to activate GIRK channels [75], [76], [77].

1.4 Approach

Our study is motivated by the general hypothesis that the stimulatory effect of Gβγ on the GIRK1 channel is mediated by specific interactions of the two proteins. Understanding these interactions is critical to a structural understanding of GIRK activation and also informs questions regarding regulation of effector proteins by Gβγ. As discussed above, past studies addressing Gβγ-GIRK interactions have used various experimental techniques: biochemical binding, peptide competition, truncation, chimeric analysis, and point mutation. The designs of these past studies have been informed by increasing amounts of information. Initial studies simply analyzed primary sequence information. Comparing primary sequences appears to lend itself to chimeric analysis but it provides little information to inform the choosing of boundaries of chimeric regions within a protein. The advent of relevant crystal structures allowed more structurally informed designs such as a chimeric analysis of Gβγ which swapped specific propeller blades or specific surface exposed strands within blades of the Gβγ structure rather than arbitrary regions [75]. Similarly, crystal structures allowed studies of the GIRK channel to focus on particular exposed secondary structure elements [70].

Unlike previously published studies addressing Gβγ-GIRK interactions, our study aimed to utilize information from structures of *both* proteins together. Rather than simply identifying likely regions of interaction on one protein or the other, we used computational docking to predict *reciprocal* interactions between the two proteins. The favorable complexes resulting from docking required further interpretation and analysis to generate secondary hypotheses

regarding specific interactions within the binding surface which may contribute to channel activation. These hypotheses were then tested experimentally in mammalian proteins *in vitro*. Thus although hypotheses were generated using input structures that were chimeric or otherwise differed from the mammalian protein, evidence for our model of GIRK activation is been based on results from experiments in the mammalian proteins.

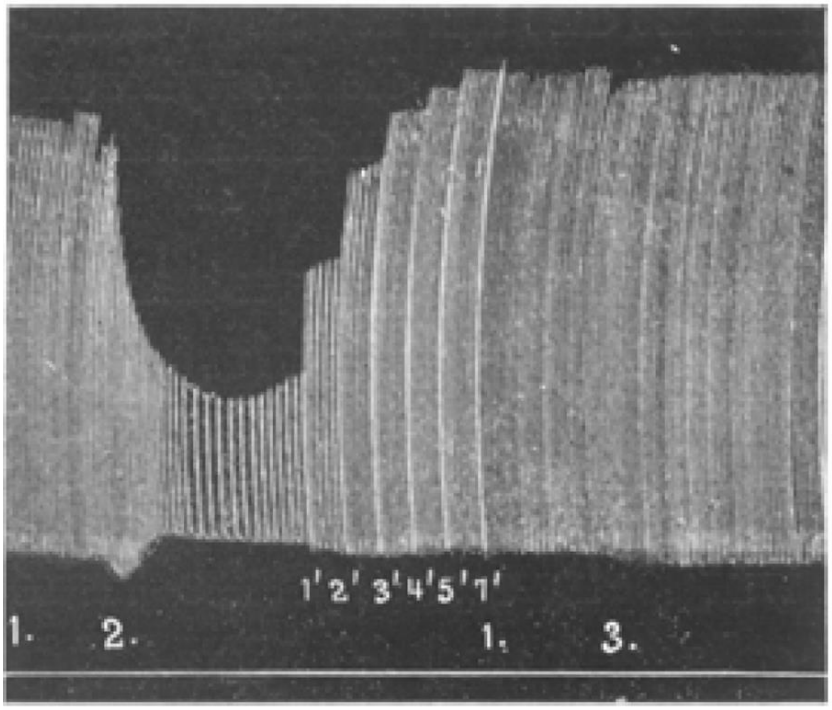

Figure 1.1 Adopted from [9]. Frog heart contractions in a perfused frog heart, measured by suspension-lever. (1.) Marks application of Ringer's solution. (2.) Marks the application of *Vagusstoff* (extract from a separate heart after 15 minutes of vagal stimulation). Negative ionotropic (vertical amplitude) and chronotropic (horizontal frequency) effects can be seen. (1'-7') represent increasing dilution of the applied heart extract in Ringer's solution demonstrating the concentration dependence of the effects.

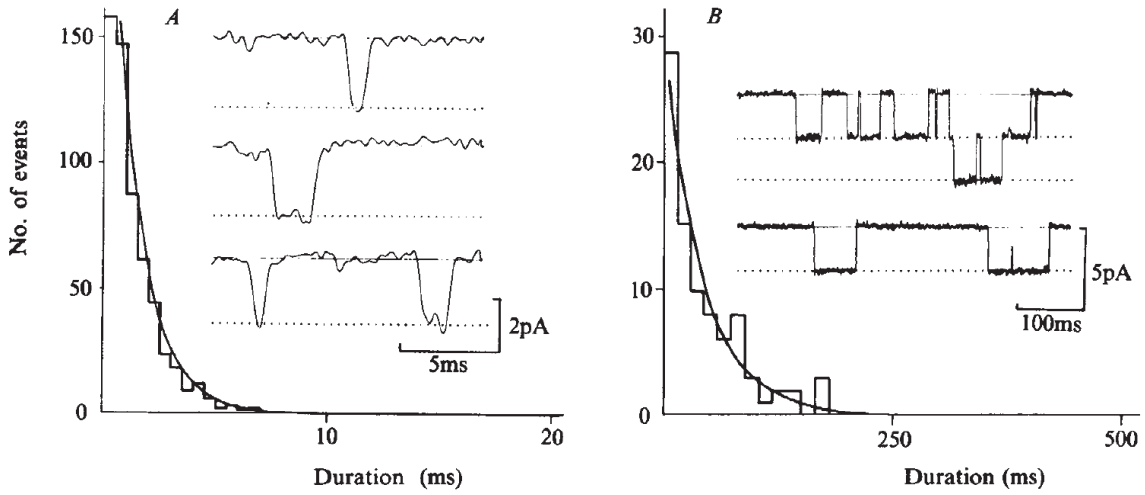

Figure 1.2 Adopted from [16]. Single channel recordings were performed on dispersed non-beating AV nodal cells under identical conditions in (A) and (B). Frequency histograms of observed channel opening durations are displayed. Although the single channel conductance did not vary much between (A) and (B) (see inset traces), the kinetics clearly differentiated the two classes of potassium channels. The channels in (A) were shown to be ACh sensitive and correspond to IK_{ACh} while those in (B) are ACh insensitive and correspond to background IK_1 channels.

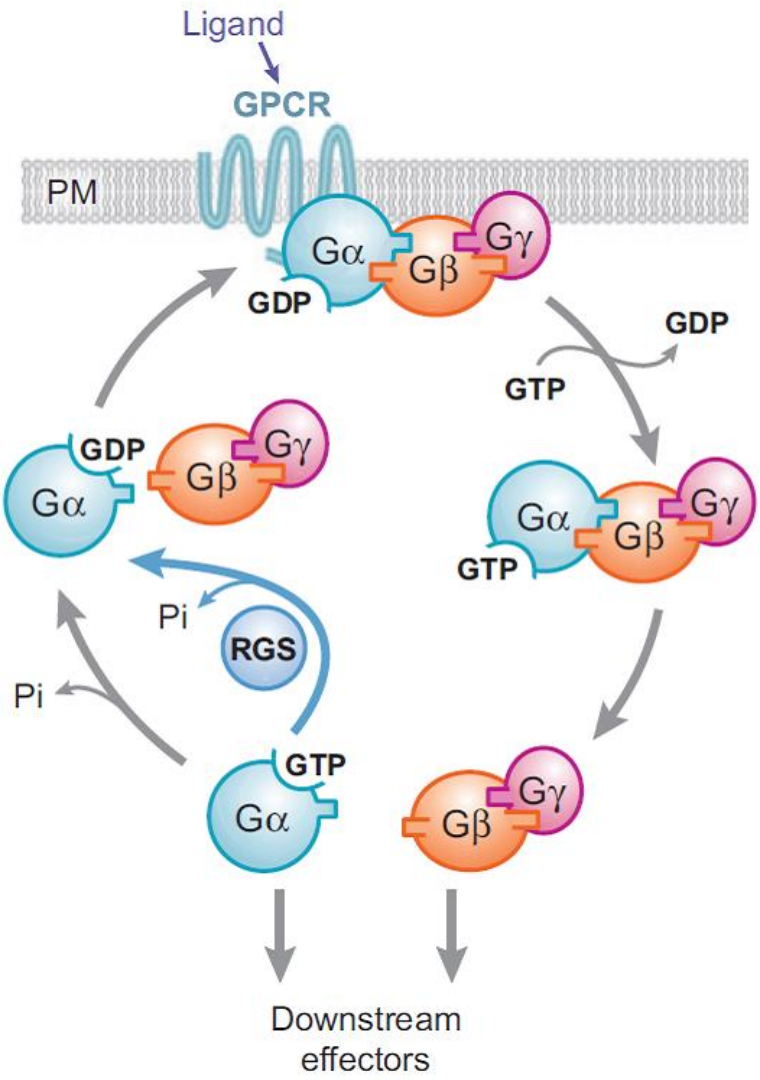

Figure 1.3 Adopted from [78]. The G-protein cycle. In the inactive state, G-proteins exist as heterotrimers. Gα is bound to GDP and thus stabilized in a conformation with high affinity for Gβγ. Agonist binding to the G-protein coupled receptor (GPCR) elicits a conformational change in the receptor allowing it to catalyze the exchange of GTP for GDP on the Gα subunit. Binding of GTP to Gα reduces its affinity for Gβγ but complete dissociation of the two may or may not occur [79]. This represents the active form of both G-protein subunits and each of Gα and Gβγ may interact with various downstream effector proteins to modulate their activity. Gα has intrinsic GTPase activity which causes it to hydrolyze the GTP back into GDP, releasing a pyrophosphate. Alternately, association of a regulator of G-protein signaling (RGS) molecule with Gα may accelerate its GTPase activity. The conversion of GTP to GDP returns alpha to a conformation with high affinity for Gβγ and the inactive heterotrimer is re-formed.

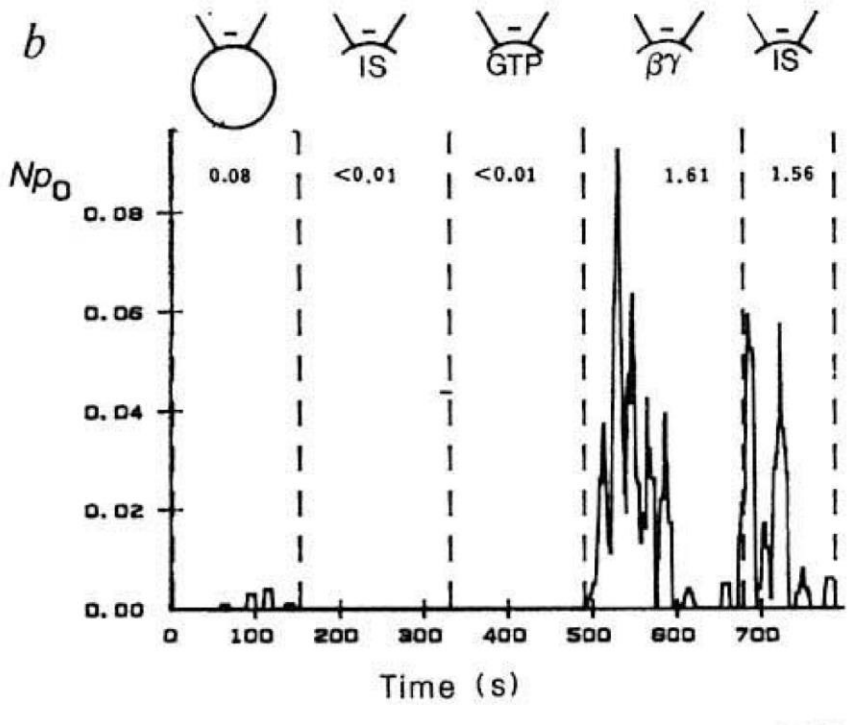

Figure 1.4 Adopted from [1]. Np_o is plotted for observed potassium channel activity in a recording from cell-attached (first section) and inside-out patch (remaining sections) configurations of chick atrial myocytes. Application of purified Gβγ protein to the intracellular surface of the patch causes robust activation even in the absence of ACh in the pipette. The perfused Gβγ protein is not readily washed out.

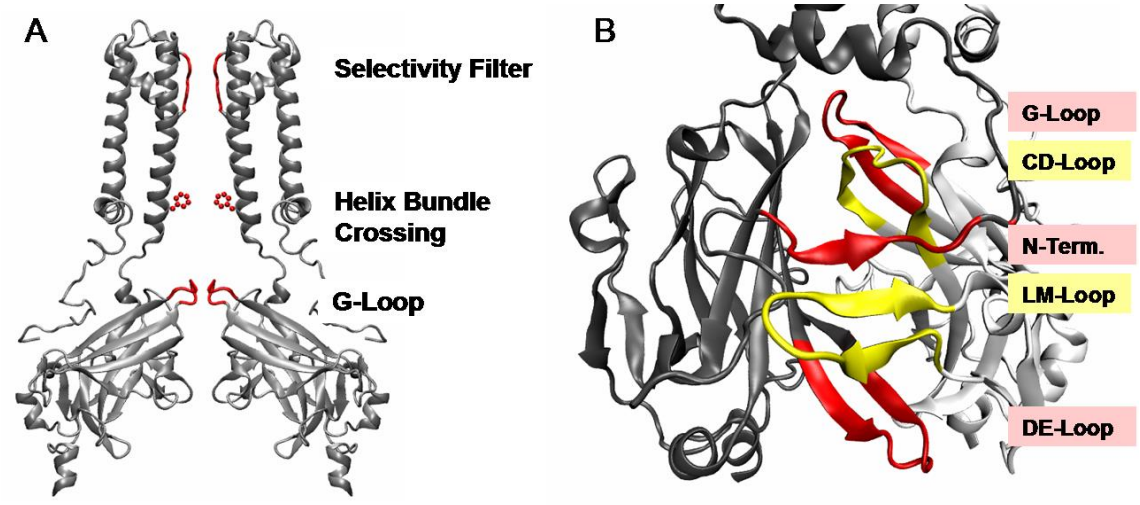

Figure 1.5 Summary of some structural features of GIRK1channels. The structure depicted is the Kir3.1 Chimera [52]. (A) shows a cartoon depiction of two opposite subunits of the channel. Putative gates along the potassium permeation pathway are highlighted in red and labeled. (B) shows a magnified view of a cartoon depiction of the intracellular region of two adjacent subunits of the channel. Secondary structure elements that play important roles in gating are highlighted alternately in red and yellow and labeled. The configuration depicted corresponds to the "open" conformation of the crystal structure and thus shows the LM loop in the "raised" conformation interacting closely with the N-terminus while the CD loop interacts closely with the G-loop.

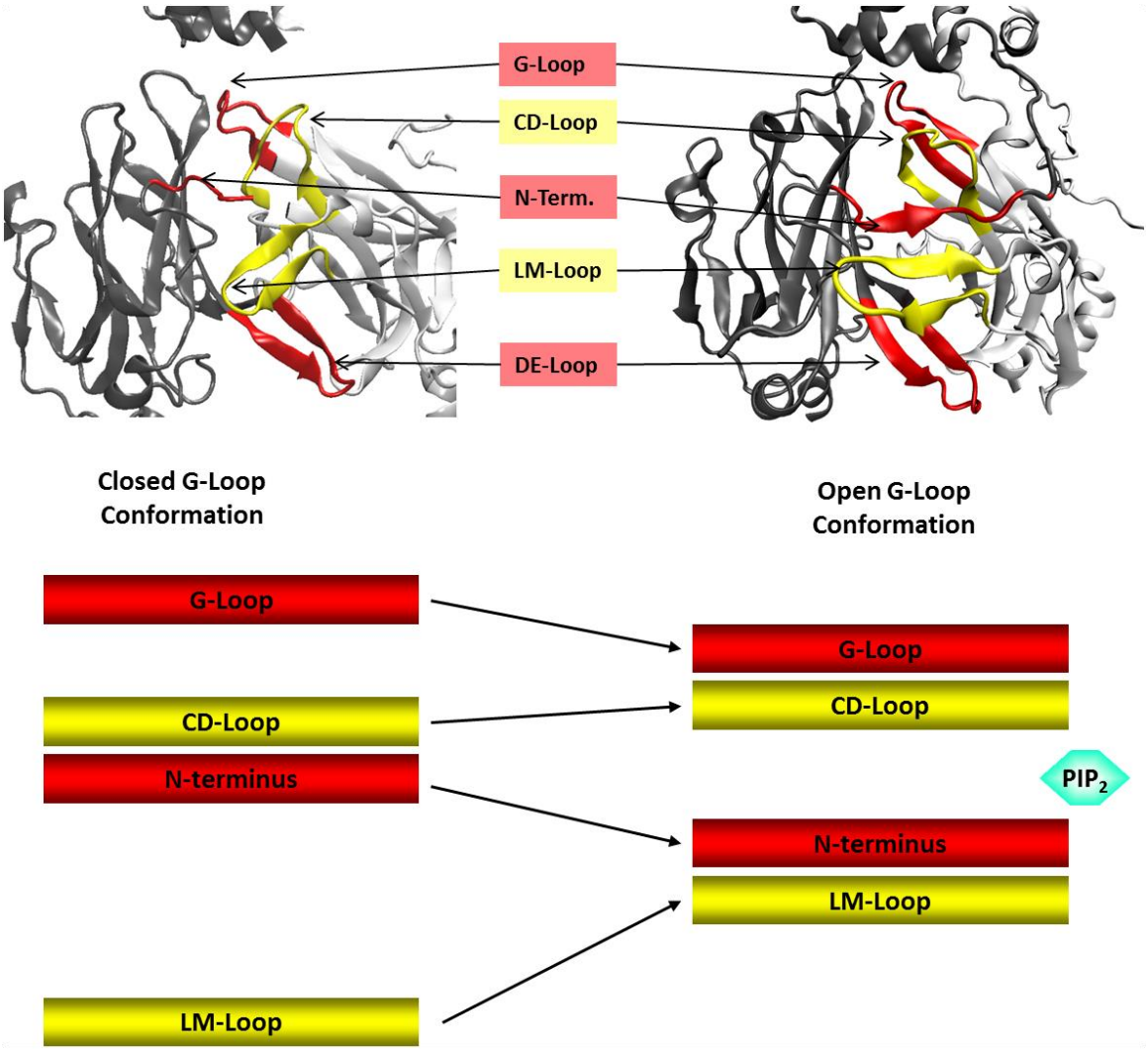

Figure 1.6 Summary of results of Meng et al. to show changes in internal conformation of the channel stabilized by PIP_2 [54]. As the channel transitions from the closed G-loop conformation (Left) to the open (Right), the LM loop makes a dramatic upward change in conformation and the N-terminus switches its interactions from the CD loop to the LM-loop. The CD loop no longer closely associates with the N-terminus and switches its interactions to the G-loop to stabilize it in its open conformation. PIP_2 interacts in a pocket near the CD loop and N-terminus and acts to stabilize the open G-loop conformation.

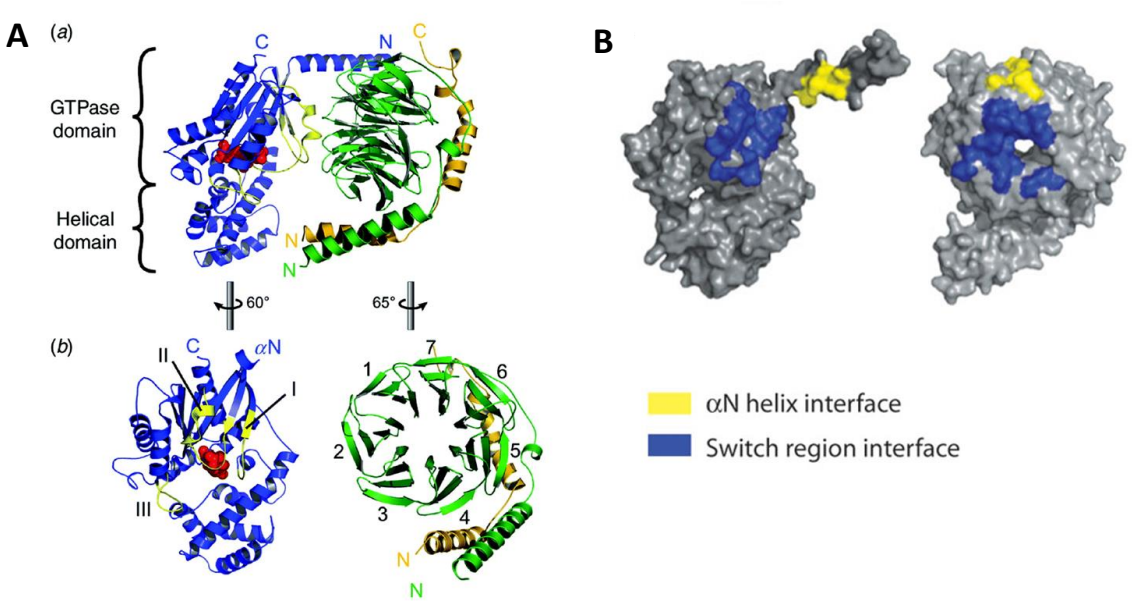

Figure 1.7 (A) is adopted from [59] and (B) is adopted from [79]. (A) (a) The inactive heterotrimeric configuration is depicted as a cartoon (Gα, blue; Gβ, green; Gγ, yellow). The domains of Gα are labelled. (b) shows a separated view of Gα and Gβγ in order to label the individual switch regions of Gα (I, II, III) and the individual propeller blades of Gβγ (1-7). (B) Surface depiction of Gα (left) and Gβγ (right). The binding site of Gα on Gβγ can be separated into two regions: the regions contacting Gα switch regions (blue) or the Gα N-terminal helix (yellow).

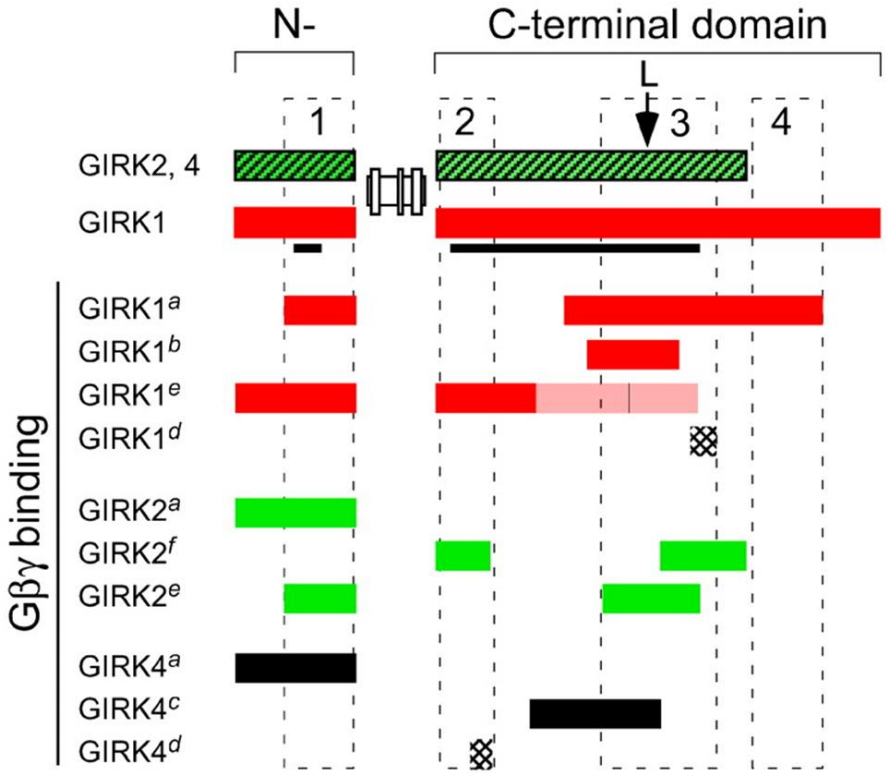

Figure 1.8 Adopted from [70]. Critical regions of the GIRK channel for Gβγ binding as determined by 8 different studies (designated by a-f superscript labels) of biochemical binding of fragments of channel protein to Gβγ. The position marked "L" at the top represents the critical leucine reside (position 333 in GIRK1) discovered by He et al 1999. This residue was shown to be critical for both channel activation by Gβγ co-expression and by agonist induced stimulation. While no obvious consensus region emerges from the data, the LM loop area which contains the highlighted leucine residue overlaps with the critical regions identified by 4 of the six studies. (Studies depicted are a: [40], [63] b: [65] c: [71], [72] d: [66] e: [67] f: [70])

Chapter 2

Computational Docking

2.1 Introduction to Computational Protein-protein Docking

Biomolecular docking is the process of computationally combining separate molecular structures to predict preferred binding modes of their complex (Reviewed in [80]). While sources of the individual structures could include electron microscopy (EM), nuclear magnetic resonance (NMR) spectroscopy, or even homology modeling, we restrict our discussion to the most common case of coordinates determined by x-ray crystallography. Docking typically consists of a larger protein molecule called the "Receptor" and a smaller interacting molecule called the "Ligand", which may be another protein, a nucleic acid, or a small drug molecule. While specific techniques differ depending on the type of ligand molecule, the general docking problem can be subdivided into optimization of two processes: searching conformational space and recognizing favorable binding modes by scoring/ranking of models.

Full-atom simulation methods such as molecular dynamics (MD) can follow the temporal evolution of a system of atoms and can provide detailed information about conformational space, equilibrium properties, and protein dynamics (reviewed in [81]). Advanced techniques also exist

to extract interaction energies from simulations of a given configuration [82], [83]. However, limits on computational power prevent their direct application as a protein-protein docking algorithm: conventional simulations tend to explore limited local energy minima and currently feasible timescales of simulation are inadequate to sufficiently sample the rotational, translational, and internal conformational space. Calculation of interaction energies from simulations is also prohibitively computationally expensive for more than a handful of configurations. These shortcomings are magnified when the ligand molecule itself is also a large macromolecule, as is the case in protein-protein docking.

Current approaches to protein-protein docking thus must rely on application of "scoring functions" of varying complexity rather than calculation of explicit energies (reviewed in [84], [85], [86]). These scoring functions attempt to approximate binding free energy with varying treatments and combinations of factors including shape complementarity, long and short range electrostatics, solvation, van der Waals interactions etc. Computational time is a product of scoring function complexity and conformational search size and thus individual docking programs naturally subdivide into categories reflecting the factor they maximize: those which thoroughly search through a large region of conformational space at the expense of a detailed scoring function versus those which calculate an extensive scoring function while performing a more localized search.

Docking programs of the first variety tend to explore large regions of conformational space through displacements in the translational and rotational degrees of freedom by performing global rigid body docking. Specific implementations include systematic searches using fast

Fourier transform (FFT) correlation or geometric hashing, and stochastic searches using pseudo-Brownian dynamics. The associated scoring functions tend to emphasize geometric complementarity and protein interactions which occur over relatively long distances such as electrostatics and solvation effects. They also usually incorporate some method of "softening" which reduces the penalty for small overlaps or clashes which could be expected to resolve by sidechain repacking or small movements of the backbone that are otherwise precluded in rigid docking. Other docking methods perform a more local search in rotational and translational space but allow for greater degrees of freedom in the internal conformations. These often include sidechain flexibility or even small movements of the backbone and incorporate a more extensive scoring function which can include van der Waals interactions, hydrogen bonding, pairwise potentials and many other terms attempting to capture enthalpic and entropic components of free energy.

A final category consists of restraint-based docking primarily exemplified by the program HADDOCK [87]. While many docking programs allow for limited inclusion of experimental knowledge, the scoring function of HADDOCK is primarily driven by restraints based on experimental or bioinformatic data. Restraints can directly be directly generated from sequence conservation and from various NMR data or they can reflect interface residue predictions from any other source including mutagenesis, deuterium exchange, electron microscopy etc. Besides experimental data, interface residues can also be predicted by methods which compare regions of each protein surface to the characteristics of known protein interfaces, methods based on sequence conservation, and methods based on statistical analysis of independent protein-protein docking runs. These interface prediction methods do not predict a particular binding mode of the

two proteins together but rather predict interface residues for each protein individually. Although other docking programs may not explicitly accommodate experimental knowledge, this information can still be included in any docking schema by introducing filters which reject potential conformations inconsistent with experimental data.

While restraint-based docking can give excellent results when adequate amounts of reliable experimental data are available, this is often not the case. Comparing global versus flexible docking, the differing strengths of each approach are evident. The paradigm of multistage docking attempts to combine these strengths by using a docking algorithm which combines programs from different categories [84], [86]. The CAPRI (Critical Assessment of Prediction of Interactions) experiment brings together developers of docking software to predict the binding modes of target protein complexes before experimentally determined structures are released by structural biologists [88]. Parallel efforts representing each of the docking categories are represented among the most successful approaches [84]. Multistage algorithms, at first designed within individual laboratories, and more recently combining the efforts of different groups have yielded significant improvements in performance. The typical phases of a multistage algorithm are illustrated in Figure 2.1. Global search by rigid body docking discards billions of relative orientations of the two proteins to retain a few thousand poses. Regions of interest can then be identified through the application of a more detailed scoring function on the retained poses and/or by clustering. Structures representing these regions of interest can then undergo flexible docking with a detailed scoring function to refine the docked poses. Re-scoring the refined structures with detailed scoring functions can then suggest final models. Experimental data can be incorporated at any level.

2.2 Design of Docking Protocol

Choice of software for each phase of multistage docking was driven by its past performance in the CAPRI assessment and availability in a free and downloadable form. Recognizing that the small number of targets thus far evaluated in the CAPRI assessment (less than 100) prevents assigning significance to small differences in performance between different protocols, the assessment nonetheless is the clearest comparison of the latest versions of each protocol to an equivalent dataset using identical assessment criteria. Downloadable software was favored over webserver implementations because webservers often limit the options for full control of individual phases of docking and often restrict the size of the input proteins.

The structure selected to represent the GIRK channel was the crystal structure of a GIRK1 (Kir3.1) chimera (PDB code: 2QKS) consisting of mouse Kir3.1 (intracellular and proximal transmembrane regions) and the prokaryotic KirBac1.3 (middle and distal transmembrane regions) [52]. The upper three-fourths of the transmembrane regions in this structure may be prokaryotic, but the intracellular regions, where Gβγ binding is expected to occur, are completely mammalian in origin. How the intracellular binding of Gβγ may induce changes in transmembrane regions and the gates therein is not addressed by docking as any docking procedure will only yield a binding mode. However, as previously discussed, evidence exists to suggest that there may be some correlation to the function of the multiple channel gates and that they do not gate independently [53], [55], [56]. Thus the stabilization of the G-loop gate in an open conformation may be expected to correlate with increased opening of other gates and increased current. The first 40 amino terminal residues and the long, unique distal carboxy

terminus of GIRK1 (residues 365 to 501) are both missing from the crystal structure. However, previous experimental results suggest that activation of the channel or its binding to Gβγ can be preserved even with loss or alteration of large parts of these regions [67], [71]. A short loop linking the N-terminus to the first transmembrane domain is unresolved in the crystal structure. This region and any unresolved side-chains were modeled using the loop modeling routine in Modeller [89].

In addition to the GIRK1 chimera structure discussed above, a structure of a mammalian GIRK2 channel in various conditions including in the absence and presence of PIP2 also exists. Although GIRK isoforms may differ depending on the organ and physiological system, a GIRK1 structure holds special interest as most native GIRK channels are heterotetramers that necessarily include GIRK1 subunits. Furthermore, the intracellular domains are captured in two distinct conformations in the GIRK1 chimera crystal structure. The G-loop gate located at the apex of the intracellular domain is dilated one conformation ("open") and is constricted in the other conformation ("closed"). The ability compare these two conformations is a unique feature of this structure and presents the opportunity for insights into gating related changes in the channel's intracellular domains. As most protein docking methods do not allow for changes in backbone conformations, selection of an appropriate starting conformation is essential. We began our docking experiments using the "open" structure of the GIRK1 chimera channel.

The Gβγ structure used in our study was extracted from a co-crystal of $G\alpha_q$, GRK2, and Gβγ (PDB code: 2BCJ) [90]. This structure represents the most complete structure of $G\beta_1\gamma_2$ with the least residues missing from the termini (3 and 1 from the N- and C- termini respectively of $G\gamma_2$).

ZDock was the best performing global rigid body docking program in rounds 1-11 of the CAPRI assessment ([91], [92], reviewed in [84]). It is an FFT correlation based method with a scoring function that incorporates shape complementarity, electrostatics, and pairwise statistical potential [93]. Only the intracellular N and C termini of two adjacent subunits of the channel were included in the docking due to restraints placed by the membrane and redundancy of 4x symmetry. Including intracellular regions of two adjacent subunits still retains some redundant regions but this strategy ensures the inclusion of one complete inter-subunit interface. 54,000 poses were retained and these were then subject to a filter which excluded any poses containing any Gβγ atoms protruding more than 8 angstroms above the expected plane of the membrane at the interfacial helix of the channel. Similarly, the filter also excluded any poses where the C-terminus of Gγ was more than 30Å from the expected plane of the membrane. The first constraint reflects exclusion of the protein by the lipid bilayer and the second constraint reflects the expected prenylation (geranyl-geranylation) of the Gγ2 C-terminus which would anchor it to the lipid bilayer. These passing poses were rescored and re-ranked using ZRank. ZRank is a more detailed scoring function developed by the same group that developed ZDock [94]. It computes a score based on detailed electrostatics, van der Waals, and desolvation. The top 2000 ZRank scored poses which passed the filter were retained for further processing. Figure 2.2 illustrates this reduction in the number of retained poses.

Before continuing with the docking protocol to predict the binding mode of Gβγ and the channel, the 2000 structures were subject to statistical analysis to predict interface residues for each protein. There is evidence from several groups that analysis of residues which occur most often

in the predicted interfaces of a top fraction of docking poses from a global search can predict hot-spot residues which are important contributors to the free energy of binding [95], [96], [97], [98]. The prediction of these interface residues does not predict a specific binding mode and thus provides less information than a docking pose but the positive predictive value of these calculations can be significant [98]. The atomic contact frequency (ACF) method of Hwang et al. can be directly calculated from the top 2000 retained poses [96]. Our implementation is a slight modification of ACF in order to search for interface residues rather than specific hotspot residues (See methods).

Having completed the interface residue prediction, we continued the algorithm to predict the specific binding mode of Gβγ and the channel. The Cluspro 1.0 webserver [99] is motivated by the observation that true docking energy minima are distinguished from other local energy minima by the broad energy attractor which surrounds them [100], [101], [102], [103]. The number of such distinct broad energy basins is small and tends to correlate to actual binding modes [104]. Thus the Cluspro 1.0 algorithm uses the output of a rigid docking algorithm (such as ZDock) to sample the energy landscape and looks for broad energy minima by simple hierarchical clustering. Clustering is done based on interface RMSD and we employed the 9Å clustering radius recommended for average-sized protein complexes. This clustering approach has been shown to be superior to intrinsic energy functions and was able to retain at least one <10Å rmsd structure among its top 30 predictions in 93% of cases in a test benchmark [99]. Structures representing the centers of the 30 largest clusters were retained for further analysis.

Refinement via flexible docking was performed for each of these 30 structures using the local refinement module of RosettaDock, a freely downloadable flexible docking method that was among the best performers in rounds 1-11 of the CAPRI assessment ([105], reviewed in [103]). RosettaDock performs a Monte Carlo based search including small rigid body displacements of the ligand protein with simultaneous sidechain repacking. Unlike the "softened" potentials used during rigid docking, the RosettaDock scoring function is sensitive to clashes and employs a detailed scoring function which includes terms for: attractive and repulsive vdW, implicit solvation, surface-area based solvation, hydrogen bonding, rotamer probability, residue pair probability, and simple attractive and repulsive short and long range electrostatics. Although the search space is limited in terms of global rotation and translation, RosettaDock also performs extensive iterative side-chain repacking and thus the energy function still must be effective enough to score a large number of potential conformations. 1000 models were calculated to sample the energy landscape around each of the 30 starting structures.

In addition to scoring using the RosettaDock internal scoring function (Rscore), each of the models was also scored using ZRank2.0 (Zscore). ZRank2.0 is a scoring function similar to the original ZRank described earlier, except the weights of the individual components of the scoring function were specifically optimized for scoring models that originated from ZDock but that have undergone flexible sidechain refinement [106]. The global docking in our algorithm was performed using rigid docking in ZDock, not using RosettaDock's internal global search method. The RosettaDock internal global docking method attempts to maintain incorporation of its detailed scoring function and thus its Monte Carlo based search of global rotational/translational space is not as thorough as ZDock's systematic search. This causes our input structures to

contain small clashes which were acceptable to ZDock's "softened" energy function in the initial stages. Unlike the Rscore, the Zscore has a reduced weight for the van der Waals repulsive term and thus maintains a degree of "softness" although this softness is reduced compared to the original ZRank. Although our algorithm is unique, examples already exist in the literature where one or more of the component (ZDock, ZRank, ClusPro, RosettaDock, ZRank2.0) have been used in combination [99], [101], [106].

Initial RosettaDock results from this stage were equivocal in their suggestion of a particular binding mode (See Figure 2.3). As opposed to a diffuse cloud, the presence of an "energy funnel" can be expected around a favorable conformation. Unfortunately, models from several different clusters organized into funnel shapes using either energy function. The results show that different information is encoded in the Rscore versus Zscore evidenced by the very different pattern and relative distributions of scores for the same RosettaDock models. However, multiple clusters achieve relatively low (favorable) values for both scores and no particular cluster or model could clearly be distinguished as the best prediction. A few modifications to our docking schema eventually allowed for greater discrimination.

The first such modification was the development of a composite score. The composite score was developed in the context of a separate but related project which involved the docking of a bee venom toxin (tertiapin) to the extracellular pore of the GIRK2 crystal structure. In the tertiapin-GIRK2 docking project, we used the same docking protocol described above for the Gβγ-GIRK1 project with very few modifications. Briefly, rigid docking was performed using ZDock to dock the crystal structure of tertiapin [107] to the external two thirds of the transmembrane regions of

all four subunits of the GIRK2 [53]. The top 54,000 models from ZDock were rescored with ZRank and the top 2000 were retained. No filtering step equivalent to the membrane based distance constraints used in the channel-Gβγ docking was performed for the toxin docking. Clustering was performed in the same manner using ClusPro 1.0 except the clustering radius was reduced to 5Å. The structures representing the top 30 cluster centers were subject to local refinement in RosettaDock and the 500 models produced for each initial structure were scored using the Rscore and Zscore (see Figure 2.4). Using the Rscore, the best scoring models (far right with high RMSD values in Figure 2.4A) were actually located at non-physiologic sites outside the channel pore on the outside of the transmembrane helices in an area that would physiologically within the lipid bilayer. This again likely reflects the Rscore's sensitivity to clashes as placing the toxin outside the central pore would likely resolve many of its potential clashes with the channel. The Zscore fails to identify any one cluster as most favorable and at least 4 clusters representing very different orientations of the toxin were all equivalently scored.

A composite score combing the Rscore and Zscore was calculated to combine the information coded in both scoring functions and to facilitate identification of models of the tertiapin-GIRK2 complex which are robust to both scores. Rscores and Zscores for all models were normalized on a scale from 0 (least favorable) to -1 (most favorable). Outlier models that were extremely unfavorably scored compared to the vast majority of other unfavorable models were excluded prior to normalization. The composite score for each model ($Cscore_i$) was computed as the simple mean of its normalized Rscore and Zscore values:

$$Cscore_i = \frac{1}{2}({}_{norm}Rscore_i + {}_{norm}Zscore_i)$$

where Xscore representing either Rscore or Zscore is normalized by:

$$_{norm}Xscore_i = \frac{Xscore_i - MAX(Xscore)}{MAX(Xscore) - MIN(Xscore)}$$

Scoring with the Cscore (see Figure 2.5) allowed for identification of a single cluster as most favorable and pointed to a particular binding mode of the toxin and channel which could be further analyzed or tested with experiments. The interface residues of the channel and tertiapin identified by this binding mode correlated very well with equivalent residues from previously published data from extensive alanine scanning and mutant cycle analysis of tertiapin with a channel closely related to GIRK2 [108], [109].

Returning to Gβγ-GIRK1 docking, the application of the composite score unfortunately was not sufficient in similarly distinguishing a single dominant binding mode of Gβγ and the channel (see Figure 2.6). The final necessary modification to the docking protocol turned out to be the removal of the ZRank step prior to clustering. The training of weights of the components of the ZRank scoring function optimized the rank of a hit (very near-native structure) among ZDock output structures [94]. While such an optimization scheme will lead to improved ranking among the top hits, it may lead to some decrease in the number of near-native structures retained in the top 2000 (Dr. Brian Pierce, personal communication). ZRank thus appears to be designed for specificity, increasing the chances that a near-native structure will be ranked among the highest ranking structures but perhaps at some expense to sensitivity by reducing the total number of near-native structures retained in the top 2000. Furthermore, if our motivation for clustering is to

identify the broad energy basin dominated by long range intermolecular forces expected to surround the native binding site, then it is not appropriate to pre-process the data with a scoring function optimized for specificity that includes short range van der Waals forces. Such pre-processing would both decrease true positives among the top 2000 (by excluding poses within the broad energy attractor which have favorable long-range interactions but are not "hits" as they have not established optimal packing and van der Waals contacts) and increase false positives (by increasing the number of poses with favorable van der Waals interactions but which may not possess an accompanying broad energy attractor). Thus the appropriate use of ZRank would be as a replacement for clustering, in helping choose the top 10-30 poses for further processing, not as a pre-processing step. The elimination of the ZRank allowed the Cscored RosettaDock results to develop a single deep energy well indicating a strong signal for a particular binding mode (see Figure 2.7). The final version of the docking protocol used to obtain our best scoring model of Gβγ docked to the channel is summarized in Figure 2.8.

2.3 Gβγ-Channel Binding Mode and Gating Model

To summarize, the input structures for RosettaDock were the 30 structures representing the centers of the 30 largest clusters of orientations retained from ZDock rigid docking. Each of these 30 structures represented the center of a large number of nearby structures representing orientations favored by the ZDock scoring function which emphasizes longer range interactions such as electrostatics and desolvation. These 30 structures were used as inputs to RosettaDock where each then underwent small rigid body perturbations and repacking of sidechains resulting in 1000 new structures for each of the initial orientations. These orientations were scored using the Cscore, as discussed above and shown in Figures 2.7, where the deep energy well (pink) containing the final model is observed.

Confidence in the best scoring model is supported by intrinsic features of the model and by comparison to previously published data. Analysis of the energy landscape explored by RosettaDock models suggests the existence of a broad energy basin surrounding the best scoring model, a feature discriminative of native binding sites [100], [101], [102], [103], [104]. The results of Figure 2.7, showing Cscored RosettaDock results after elimination of ZRank pre-processing, are re-plotted in Figure 2.9 with the x-axis now representing interface RMSD relative to the best scoring model instead of relative to an arbitrary model. Furthermore, due to some redundancy introduced by the channel's 4-way symmetry, prior to computation of interface RMSDs, structures were rotated by 90° increments as needed along the channel's axis of symmetry to bring all structures together relative to a single channel subunit. The resulting figure again demonstrates the best scoring model residing in a steep energy well (blue) consisting

of structures produced by RosettaDock from the input structure representing the center of one of the smaller clusters. Interestingly, this energy well appeared to connect to the group of orientations produced from the structure representing the center of the very largest cluster (see Figure 2.9, green). The existence of a large cluster of favorable conformations near the final model suggests the existence of a broad energy minimum near the final steep energy well. A wider search of conformational space around the center of the largest cluster may have allowed it to produce decoys that also descended down the steep energy well leading to the final model.

It is important to note that the docking was conducted blindly in that the binding mode is predicted purely on the basis of energy functions and no experimental evidence was used in the docking procedure except for the membrane based distance filtering. This allows us to use published data to help validate the binding mode since it was derived independent of any such data. The channel residues predicted to be a part of the Gβγ interface by our best scoring model correlate well with results of the statistical interface residue prediction. Furthermore, this interface matches closely the interface predicted by experimental work in a recent NMR study examining the binding of Gβγ to the intracellular regions of mammalian GIRK1 [110] (see Figure 2.10). The implicated region of the channel includes the leucine residue (GIRK1 L333) previously identified as critical for Gβγ-mediated activation [71]. Similarly, the interface on Gβγ from the best scoring model includes regions previously implicated by experiments (see Figure 2.11). This includes the two propeller blades implicated by chimeric analysis of Gβγ [74], specific mutations on the side of the propeller blades [75], and part of the Gβγ interface with Gα [73]. The binding mode of the best scoring model is further illustrated in Figure 2.12.

Any computational results thus far discussed have reflected the docking of Gβγ to the "open" structure of the channel. We repeated the docking procedure using the "closed" state of the channel. Comparison of the interface residue prediction results for the two conformations revealed interesting differences which helped to highlight areas of the channel which may be involved in mediating Gβγ-induced gating (see Figure 2.13). The open state interface is predicted to include the LM loop, the K and N strands as well as the DE loop. The closed results highlight a similar region except the DE loop is completely excluded. This may indicate that the availability of the DE loop may play a role in the Gβγ mediated channel gating. Interface prediction results of Gβγ showed highlighted residues from the same propeller blades (6, 7, 1, and 2) for docking with either conformation of the channel, although local differences did exist in terms the specific regions of the propeller blades.

Further focusing on the DE loop, we discovered that multiple residues of the DE and nearby LM loop are completely conserved in all human isoforms of GIRK channels but not in isoforms of the closely related (but G-protein insensitive) IRK (Kir2) channels (see Figure 2.13). Among these residues, a large conformational difference between the open and closed conformations was noted for L333 (LM loop) and F243 (DE loop). These resides go from close vdW radius contact in the closed conformation to opening a significant pocket between them as they separate in the open conformation (see Figure 2.14).

Analyzing the binding mode of the best scoring model, we discovered that the model predicts L55 of Gβ1 to protrude into the pocket formed between the channel's L333 and F243 (see Figure 2.14). This observation gives rise to a hypothesis about how Gβγ interaction may promote the

open conformation of the channel. As the LM loop undergoes a large movement downwards in transitioning from the open to closed channel conformation, it brings L333 into contact with F243 and abolishes the pocket in between them. The presence of L55 in between these residues or other interactions between the channel and Gβγ may serve to prevent this downward movement of the LM loop seen in the closed conformation and stabilize its "raised" conformation seen in the open state. Stabilizing the "raised" conformation of the LM loop would also be expected to promote its close interaction with the N-terminus where it plays a role in gating of the channel by PIP_2 [54].

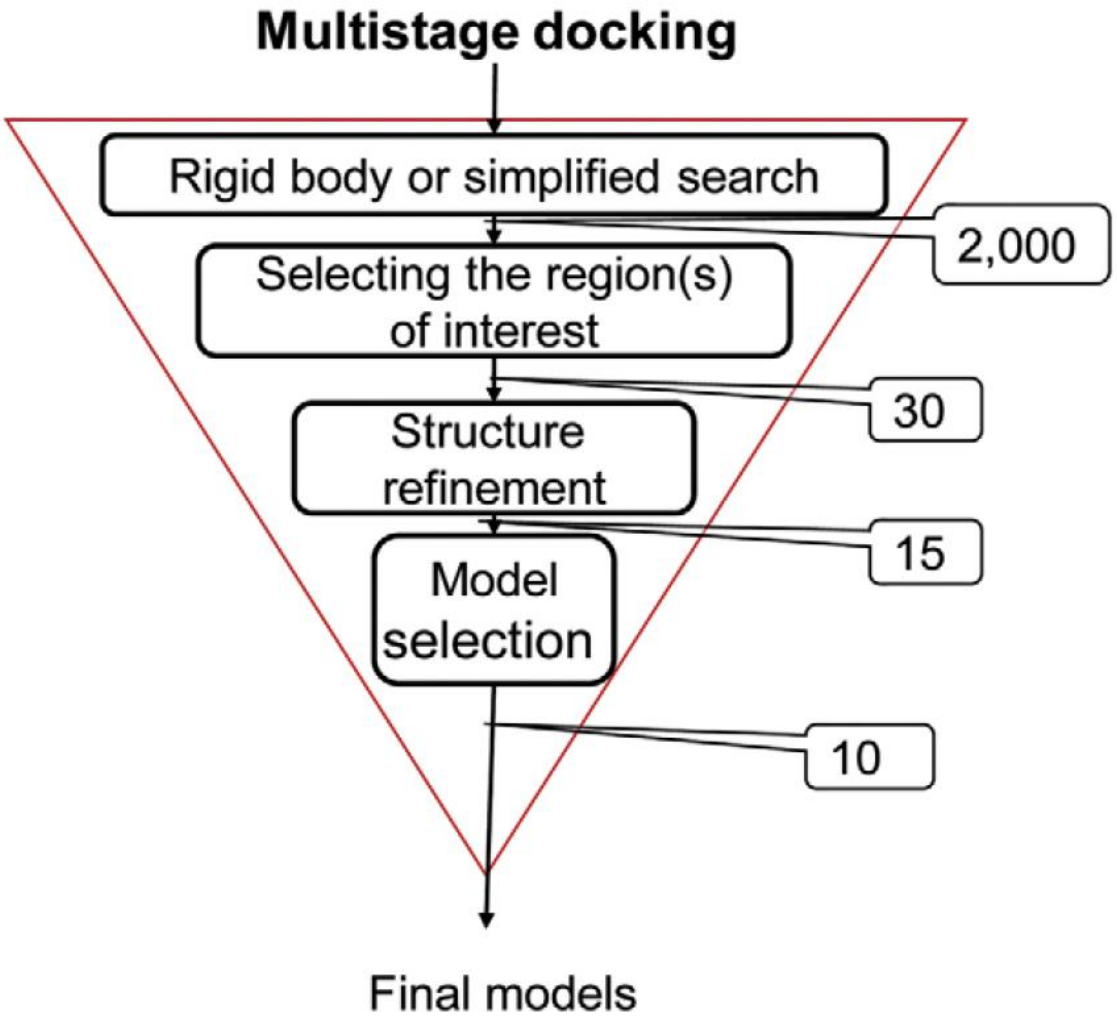

Fig. 2.1 Adopted from [84]. A suggested generalized approach to multistage protein-protein docking. Numbers in bubbles indicate approximate number of poses retained at the end of each phase. A similar scheme is suggested by [80], [86].

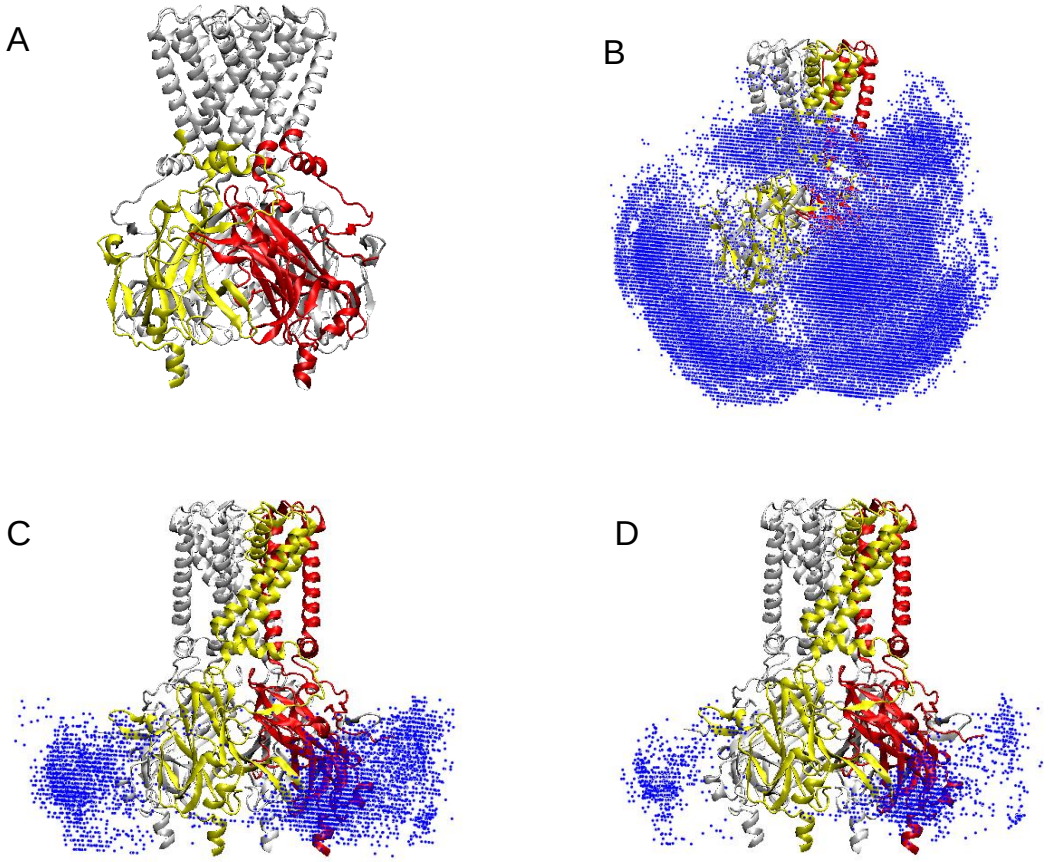

Fig. 2.2 Cartoon representation of the channel structure. Red and yellow colors highlight two adjacent subunits. (A) The intracellular region of two adjacent subunits are highlighted reflecting the regions of the channel that were included in the ZDock phase. (B-C) Blue dots represent the centers of mass of individual retained poses at the end of the ZDock phase (54,000 poses) (B), Filtering (~5000 poses) (C), and ZRank phase (2000 poses) (D).

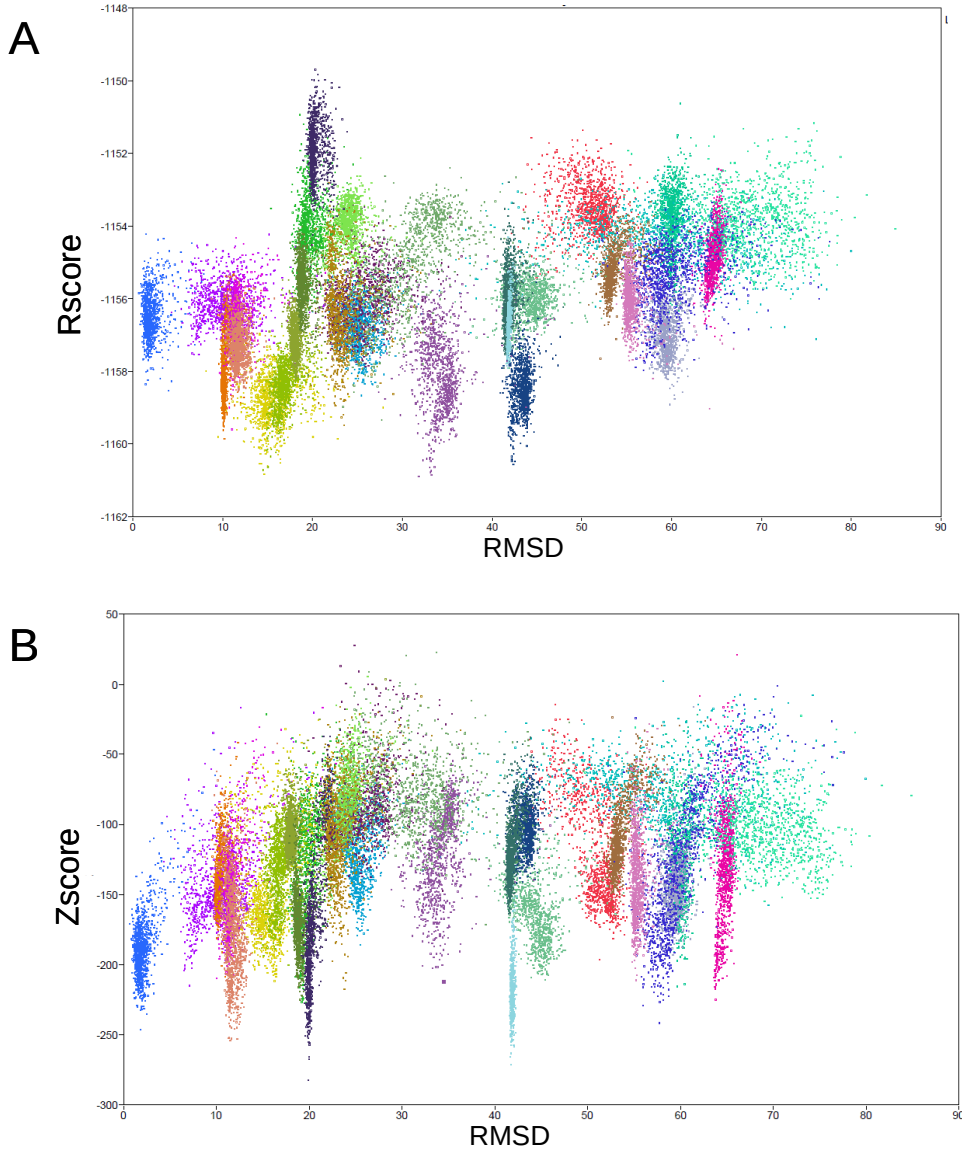

Fig. 2.3 Scoring of RosettaDock models of the channel and Gβγ using two different scores. Rscore (A) or Zscore (B) are plotted versus interface RMSD from an arbitrary model (Model 1 of the first cluster). There are 1000 points for each color representing the scores of each of the refined models derived from one of the 30 original cluster centers. Lower values for both scores represent more favorable scoring.

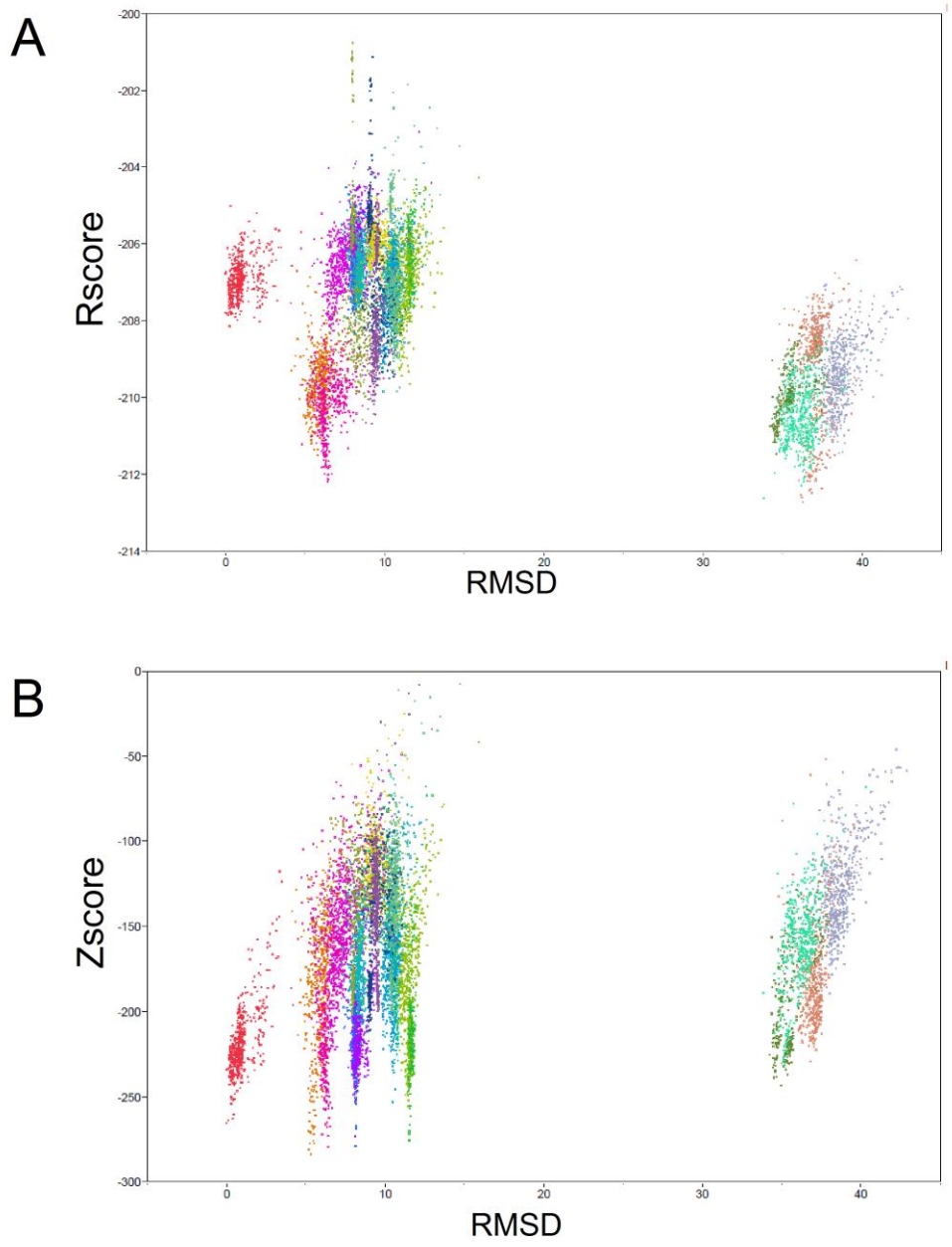

Fig. 2.4 Scoring of RosettaDock models of tertiapin and GIRK2 using two different scores. Rscore (A) or Zscore (B) are plotted versus interface RMSD from an arbitrary model (Model 1 of the first cluster). There are 500 points for each color representing the scores of each of the refined models derived from one of the 30 original cluster centers. Lower values for both scores represent more favorable scoring.

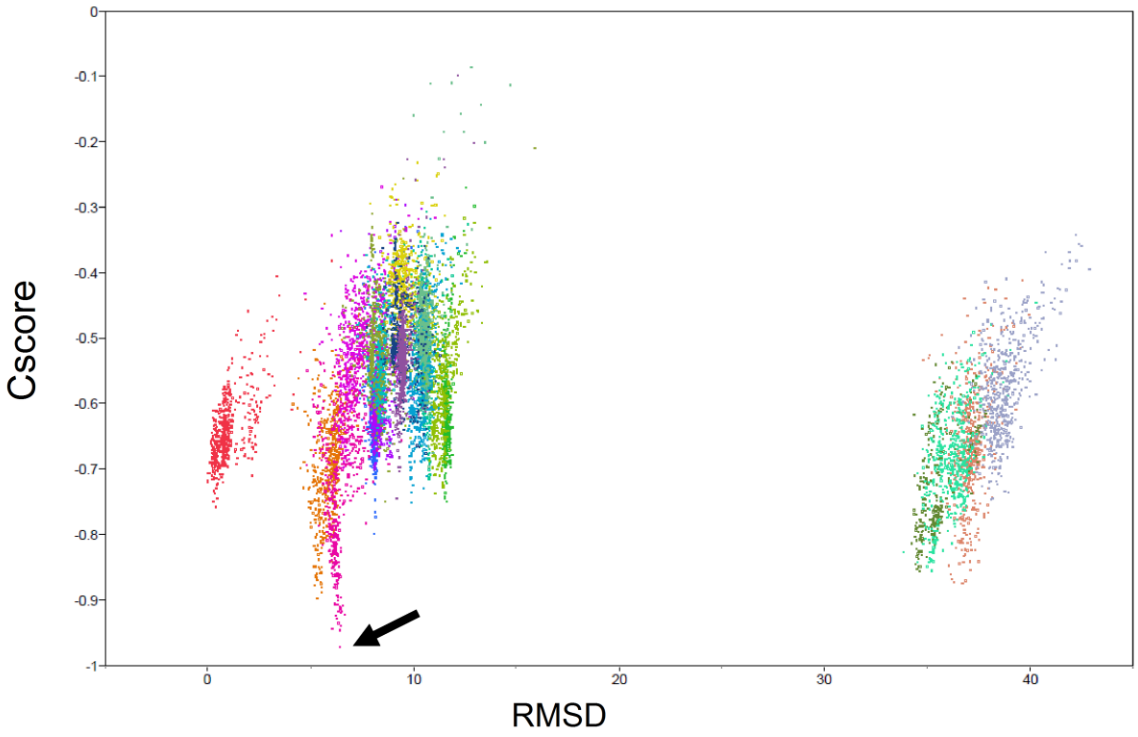

Fig. 2.5 Scoring of RosettaDock models of tertiapin and GIRK2 using the Cscore. Scores are plotted versus interface RMSD from an arbitrary model (Model 1 of the first cluster). There are 500 points for each color representing the scores of each of the refined models derived from one of the 30 original cluster centers. Lower values represent more favorable scoring and the black arrow points to the most favorably scored model from the most favorable cluster.

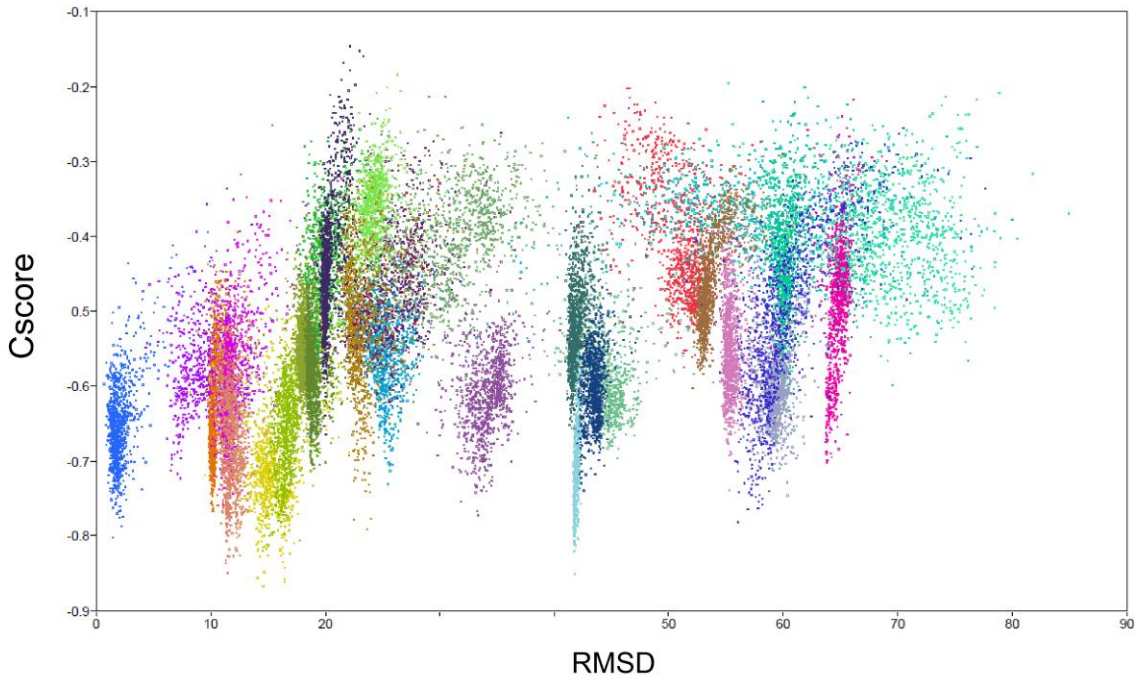

Fig. 2.6 Scoring of RosettaDock models of the channel and Gβγ using the Cscore. Scores are plotted versus interface RMSD from an arbitrary model (Model 1 of the first cluster). There are 1000 points for each color representing the scores of each of the refined models derived from one of the 30 original cluster centers. Lower values represent more favorable scoring.

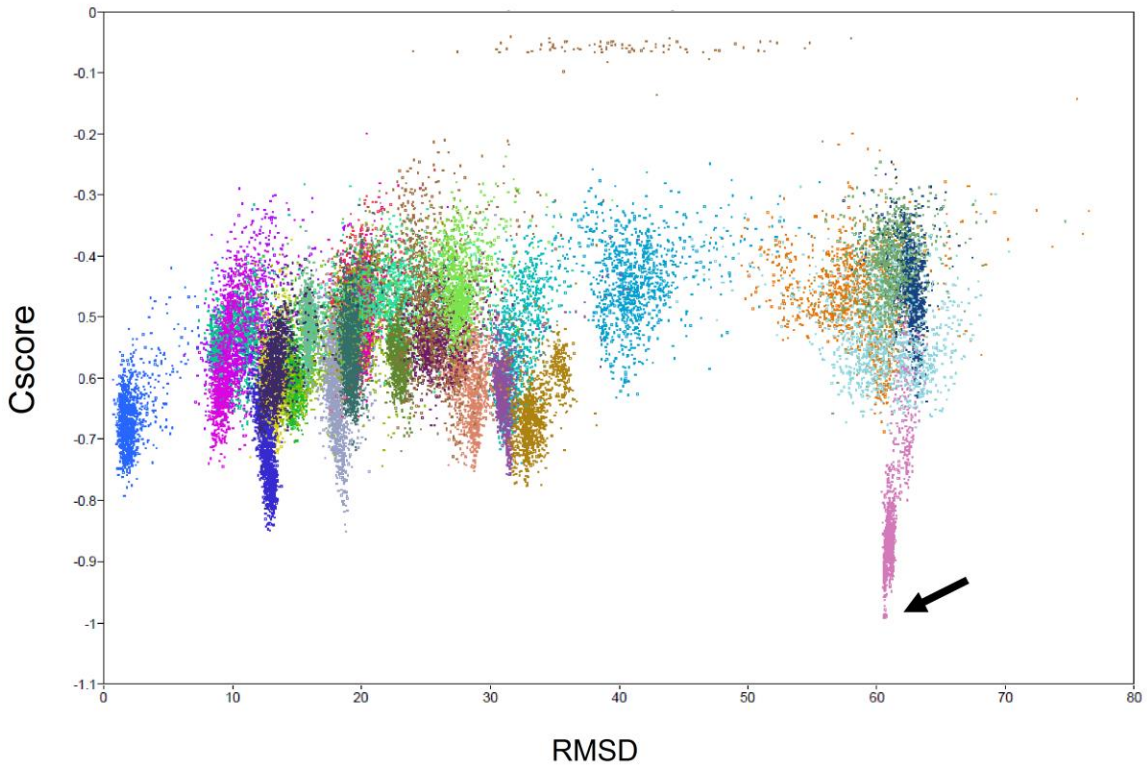

Fig. 2.7 Scoring of RosettaDock models of the channel and Gβγ using the Cscore after elimination of the ZRank pre-processing step. Scores are plotted versus interface RMSD from an arbitrary model (Model 1 of the first cluster). There are 1000 points for each color representing the scores of each of the refined models derived from one of the 30 original cluster centers. Lower values represent more favorable scoring and the black arrow points to the most favorably scored model from the most favorable cluster.

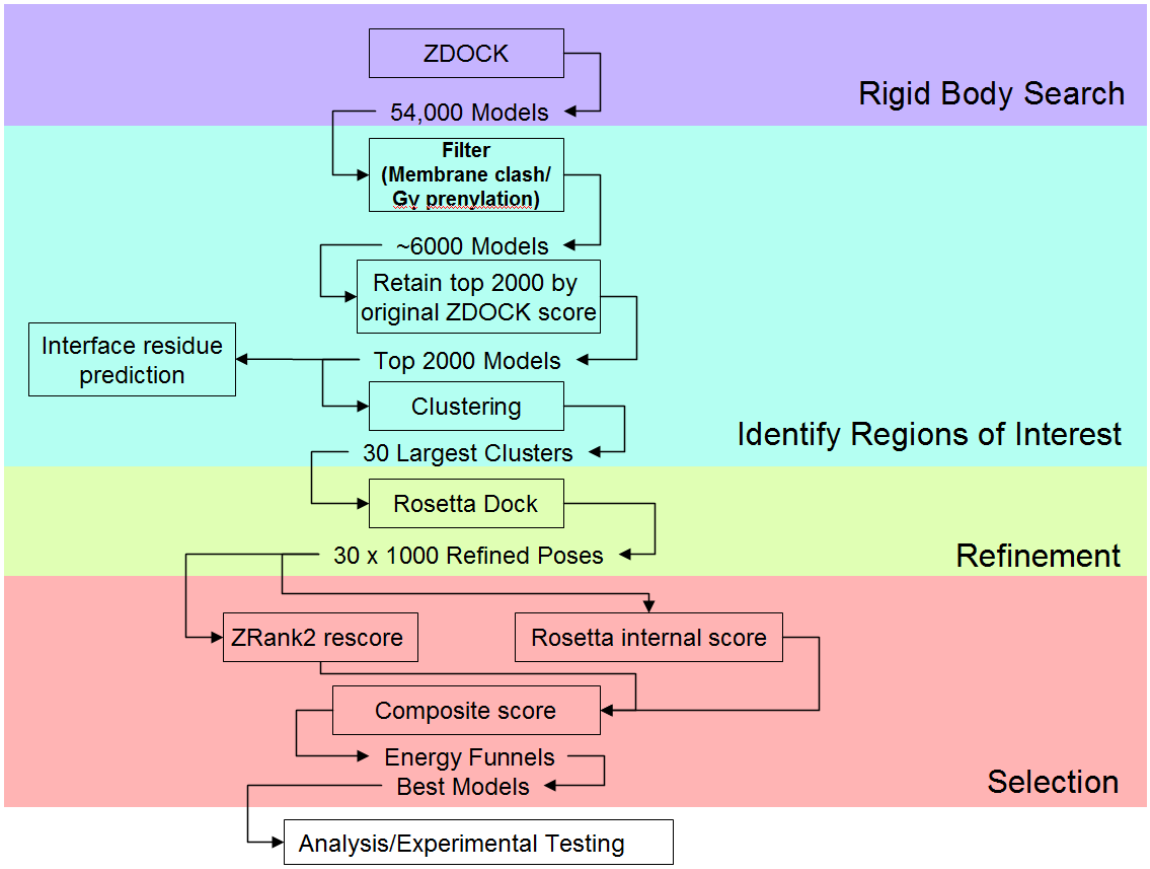

Fig. 2.8 Summary of docking protocol used to predict the channel-Gβγ binding mode.

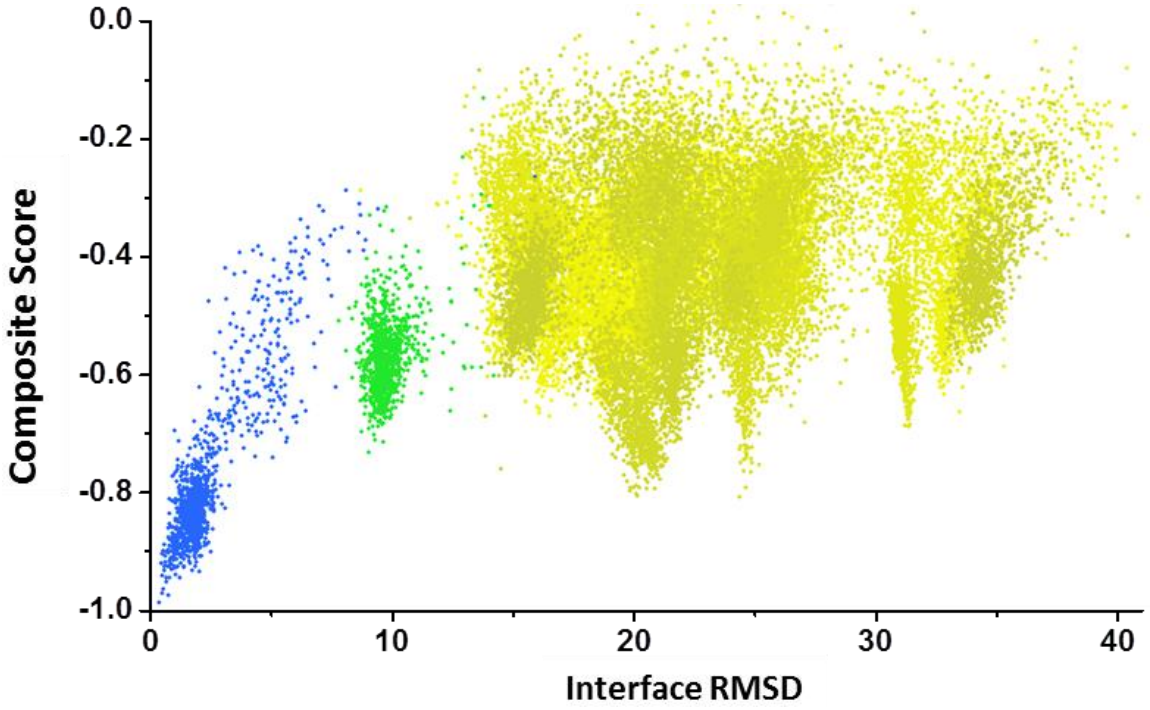

Fig. 2.9 Scoring of RosettaDock models of the channel and Gβγ using the Cscore after elimination of the ZRank pre-processing step. Scores are plotted versus interface RMSD from the best scoring model. All models have been rotated around the channel's 4-way axis of symmetry to superimpose their positions relative to the same channel subunit. There are 1000 points for each of the input 30 structures representing the largest cluster centers. Blue highlights RosettaDock models produced from the same input structure which yielded the best scoring model. Green highlights models produced from the input structure which was the center of the largest of the 30 clusters. Lower values represent more favorable scoring.

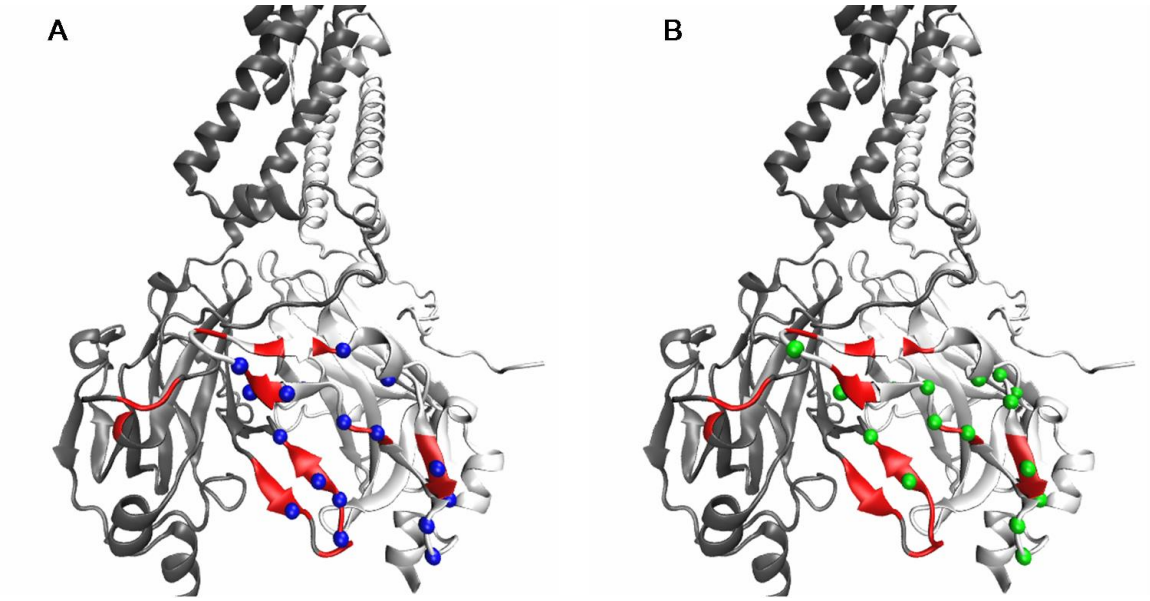

Fig. 2.10 Two adjacent subunits of the channel are shown as cartoons in each panel. The red highlight reflects the residues predicted to be in the interface by the NMR work of [110]. Blue spheres (A) show the interface residues predicted by our interface residue prediction method. Green spheres (B) show the interface residues of the best scoring model.

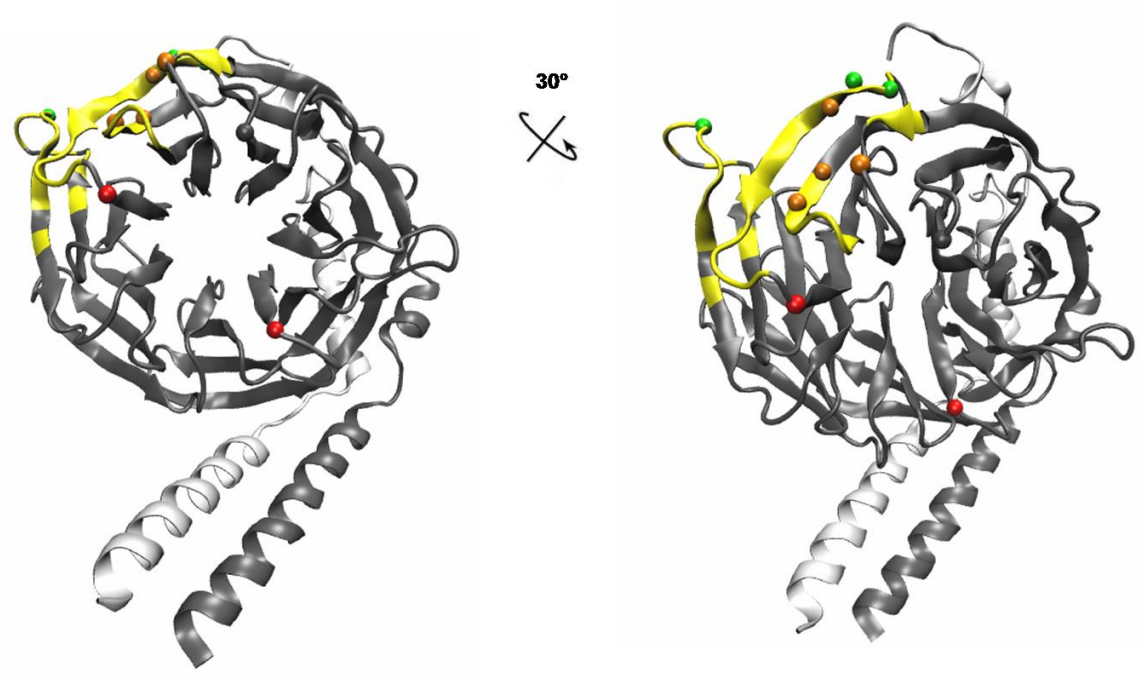

Figure 2.11 Cartoon depiction of Gβ1(gray) and Gγ2(white). The yellow highlight represents the interface residues predicted by the best scoring model. Green spheres are residues implicated in channel activation by mutagenesis work in [75]. The remaining spheres reflect residues implicated by alanine scanning mutagenesis in [73]. Residues represented by orange spheres overlap with the model predicted interface, red spheres do not.

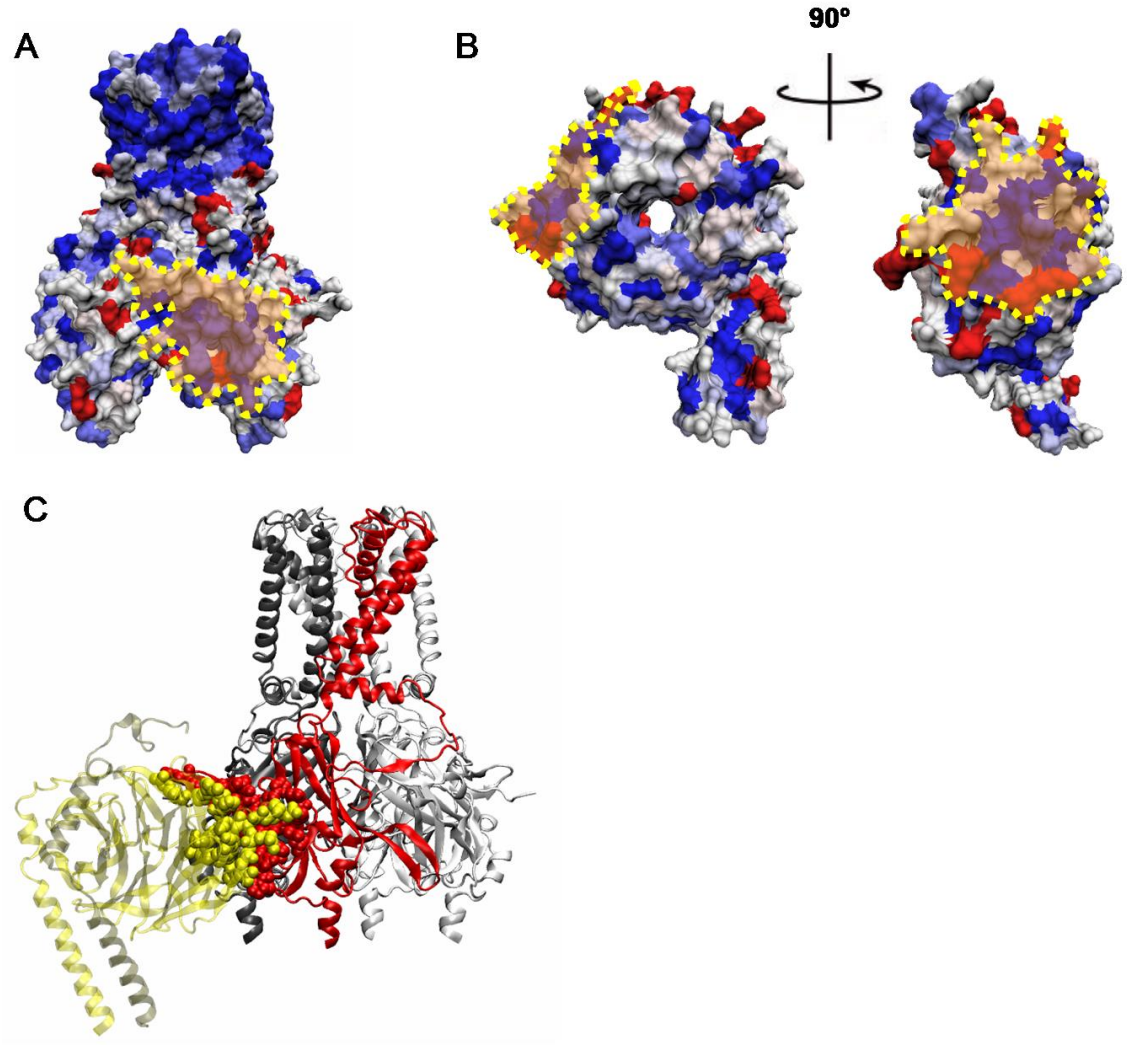

Fig. 2.12 Surface representations of the channel and Gβγ (A and B respectively) are colored by residue hydrophobicity [111]: blue is most hydrophobic, white is intermediate, and red is least hydrophobic. Interface regions found in the best scoring model are highlighted in yellow. (C) Cartoon illustration of the two proteins together: two adjacent subunits of the channel are highlighted in red and gray while the Gβ1 is yellow (transparent), Gγ2 is tan (transparent). Interface residues of the channel (red/gray) and the corresponding residues of Gβγ (yellow) are illustrated as spheres.

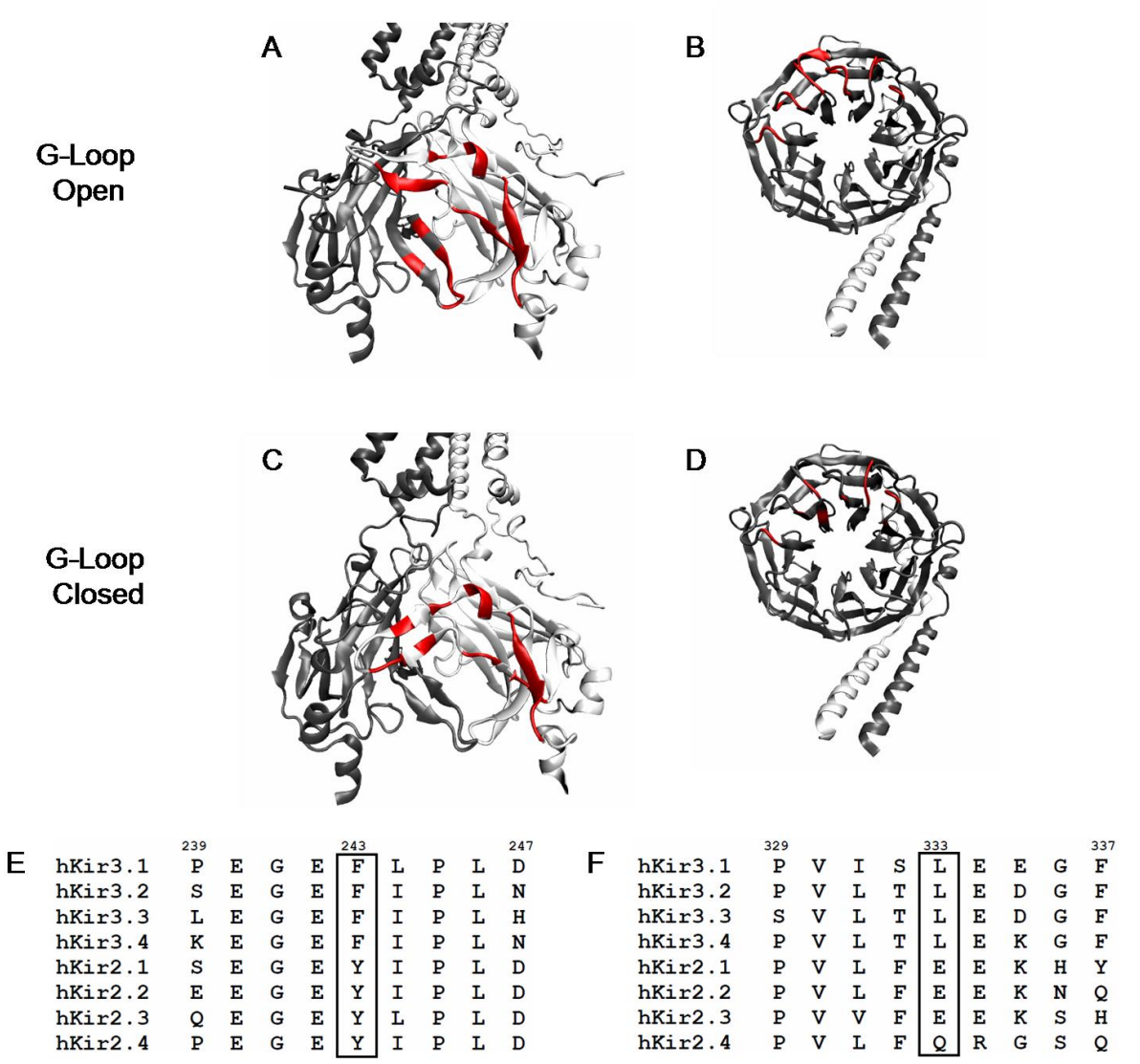

Fig. 2.13 Cartoon depiction of interface residue prediction results are illustrated in (A-D). (A) and (C) show two adjacent subunits of the channel with red highlighting the predicted interface residues for the G-loop open conformation (A) and closed conformation (C). The predicted interface residues of Gβγ are highlighted in red for the open conformation (B) and closed (D). Sequence alignment of the human GIRK (Kir3) and IRK (Kir2) channel sequences in the DE loop area (E) and the LM loop (F). Numbering at top follows GIRK1 residue positions and the positions corresponding to GIRK1 F243 and L333 highlighted with a boxed outline.

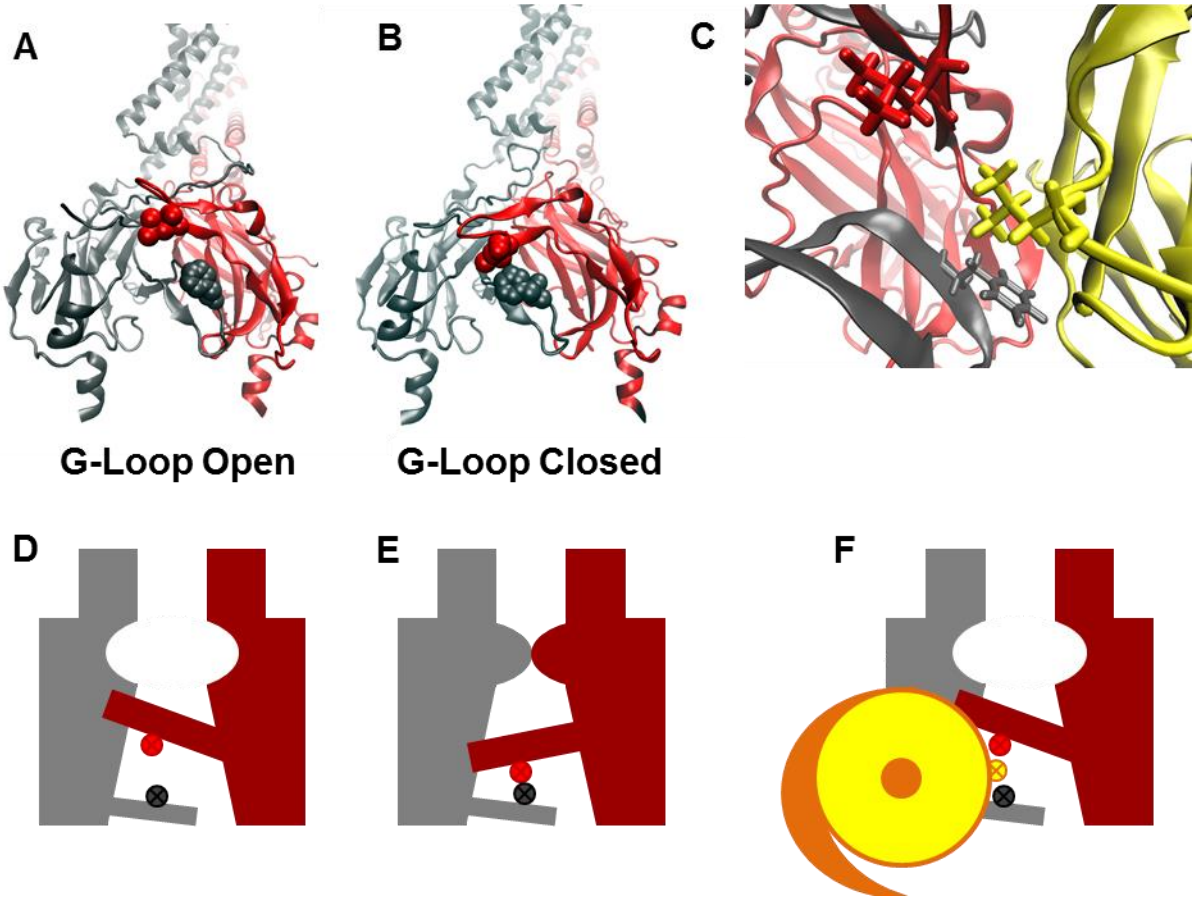

Fig. 2.14 (A) and (B) show cartoon depictions of two adjacent subunits of the channel in the G-loop open and closed conformations respectively. GIRK1 residues F243 (gray) and L333 (red) are depicted as spheres in both panels. (C) Close up view of the cleft between LM and DE loops in the best scoring model. Cartoon depictions of two adjacent channel subunits are in red and gray while the Gβ1 is yellow. Specific residues are highlighted in stick representation: GIRK1 L333 (red), GIRK1 F243 (gray), Gβ1 L55 (yellow). (D-F) Schematized versions of (A-C), respectively. Adjacent channel subunits are illustrated in gray and dark red. Gβγ is yellow and orange in (F). G-loop state is illustrated as open or closed by state of constriction in the central pore. Specific residues (crossed circles) of GIRK1 L333 (red), F243 (black), and Gβ L55 (yellow) are drawn along with conformation of LM loop and the DE-LM loop cleft.

Chapter 3

Electrophysiological Testing of the Gating Model

3.1 Experimental Design

Our computational approach allowed us to predict a specific binding mode of Gβγ with the channel and suggested a mechanism by which this binding mode may promote the conformation of the channel consistent with an open G-loop gate. We used site directed mutagenesis and electrophysiological recordings to test the functional role of channel-Gβγ interactions proposed by these predictions. Wild-type and mutant constructs of GIRK1* channels and Gβ1γ2 were expressed in *Xenopus laevis* oocytes. Total barium sensitive current were measured after 2-3 days of expression using two-electrode voltage clamp (TEVC) (see methods section). Each of the channel mutations was expressed alone or co-expressed with wild-type Gβγ and the fold change between the two groups was calculated for each mutant. This Gβγ-induced fold change in mutant channel current was compared to the Gβγ-induced fold change of wild-type GIRK1* currents. Likewise, wild-type GIRK1* channels were expressed alone or co-expressed with each of the Gβγ mutants and a fold change was computed. Again, this fold change was compared to the fold change in GIRK1* channel currents caused by wild-type Gβγ. To facilitate comparisons across experiments, the data were normalized such that, when present, the control group

reflecting the fold change in wild-type GIRK1* channel currents caused by wild-type Gβγ co-expression, was set to 1.

There are several important advantages of using Gβγ co-expression to activate the channel. For channel mutations, focusing on the fold change in current caused by Gβγ co-expression rather than raw currents allows isolation of the Gβγ-induced effect rather any changes in intrinsic gating of the channel. Furthermore, for Gβγ mutants, examining activation of channels by Gβγ co-expression rather by agonist-induced GPCR activation avoids the influence of any confounding changes in Gβγ coupling to Gα or in the ability of the GPCR to activate the mutant heterotrimer.

3.2 Sidechain Volume Substitutions

We first examined if the predicted insertion of Gβ1 L55 into the cleft between GIRK1 F243 and L333 was critical to Gβγ-induced channel activation. The sidechain volume of each of the residues was varied and the ability of the mutant protein to recapitulate Gβγ-induced channel activation was examined. Figure 3.1 shows the effect of substituting sidechains of various volumes at residue position 243 in the GIRK1* channel. Large or bulky substitutions at GIRK1 F243 allow for Gβγ-induced activation but small substitutions such as alanine or cysteine show deficient activation. For GIRK1 L333, larger or bulkier mutations of the channel show an increasing ability to be activated by Gβγ while smaller sidechain mutations do not show any such enhancement (see Figure 3.2). Changes in sidechain volume of Gβγ L55 show a similar effect: substitution of small sidechains causes deficient activation of the channel, while larger sidechains allow activation (see Figure 3.3). The phenylalanine substitution is somewhat anomalous in that it causes quite weak activation of GIRK1*. However, the level of activation achieved remains significantly higher than activation by the smaller alanine or cysteine substitutions.

Having tested the effects of sidechain volume changes in Gβγ or the channel individually, we next tested if we could rescue defective mutants of one protein by co-expression with functional mutants of the other protein. The small volume L55C mutation of Gβγ was defective in its ability to activate the wild-type GIRK1* channel (see Figure 3.3). Yet, it is successfully able to activate the channel if a bulky tryptophan mutation is introduced at L333 of the channel (see Figure 3.4). Similarly, the small volume F243C channel mutation was deficient in its ability to

be activated by wild-type Gβγ (see Figure 3.1). Yet this mutant is successfully activated by the L55W mutant of Gβγ (see Figure 3.4).

We have thus demonstrated that small sidechain substitutions at residue positions 243 or 333 of GIRK1* corresponding to the DE – LM loop cleft or at position 55 of Gβ1 corresponding to the residue predicted to occupy the cleft all cause deficient activation by Gβγ. Furthermore we show that small volume mutants, defective in Gβγ activation can be rescued by co-expression of large volume mutants of the interacting protein.

3.3 Electrostatic Interactions and Crosslinking

Experiments varying the sidechain volumes at the DE – LM loop cleft suggest a mechanism by which Gβ1 L55 sterically prevents closure of the cleft. Adjacent to the critical GIRK1* L333 residue are two consecutive glutamate residues (E334 and E335). We hypothesized that another means to stabilize the "raised" conformation of the LM loop is to electrostatically (rather than sterically) repel LM loop residues to prevent closure of the cleft. Figure 3.5 shows that the L55E mutation of Gβγ strongly activates the channel. However, neutralization of the negative charges at positions 334 and 335 of GIRK1* make it resistant to activation by Gβγ L55E. The neutralization mutations have little effect on the ability of the wild-type leucine sidechain of Gβγ at position 55 to activate the channels.

In addition to steric or electrostatic repulsion from within the cleft, the "raised" conformation of the LM loop could also be expected to be stabilized by appropriately positioned attractive interactions. Figure 3.6 illustrates a predicted salt-bridge interaction between GIRK1* E334 and Gβγ K89 which seems appropriately positioned to prevent downward movement of the LM loop. Figure 3.7 shows the effect of charge reversing mutations at these residues. The K89E mutant of Gβγ is defective in its ability to activate the wild type channel. However, this deficiency of the negatively charged Gβγ mutant can be reversed and activation actually enhanced by the simultaneous positively-charged mutation of GIRK1* at position E334. The positively charged E334K channel mutant is not significantly affected in its sensitivity to wild-type Gβγ.

With several experiments suggesting that the L55 residue of Gβγ closely interacts with the DE – LM loop cleft area, we tested if it was possible to crosslink Gβγ to the channel by simultaneous introduction of cysteine mutations. Perfusion of 10mM H_2O_2 was used to was used to oxidize the intracellular oocyte environment to allow for disulfide bond formation [112]. GIRK channels are inherently sensitive to intracellular redox potential such that reducing environments cause activation while oxidizing environments inhibit [48]. Consistent with this, panel A and subpanels i-ii of panel B of Figure 3.8 demonstrate that the introduction of a single cysteine mutation on either the channel at position L333 or Gβγ at position L55 does not alter the effect of oxidation and the current continues to show inhibition by H_2O_2. However, when cysteine residues are simultaneously introduced in the channel and Gβγ at these positions, the effect of H_2O_2 reverses and causes channel activation (see subpanel iii of panel B, and summary data in panel C of Figure 3.8). The introduction of a cysteine residue at a different channel position, F243, showed inhibition by H_2O_2 but could not recapitulate reversal of the effect upon simultaneous cysteine mutation of Gβγ L55 (data not shown). That the activation by H_2O_2 only occurs when cysteines are simultaneously present at both GIRK1 L333 and Gβ1 L55 strongly suggests that these residues approach each other closely and a disulfide bond is formed under oxidizing conditions which causes channel activation. Confirmation of disulfide bond formation will require biochemical evidence of crosslinking and this work is actively being pursued in our lab.

3.4 Extension of the Gating Model to Physiologic Signaling

Analysis of the computationally predicted binding mode suggested a gating mechanism whereby key interactions of Gβγ with the channel can stabilize the LM Loop in its "raised" conformation and allow it to make important intramolecular interactions to stabilize the open state of the channel. While testing predicted interactions for their ability to be confirmed eletrophysiologically, we used Gβγ co-expression as a simplified and less confounded method for channel activation. Having identified Gβγ-channel interactions that are confirmed by the co-expression assay, we sought to test interactions using agonist-induced G_i signaling. TEVC recordings were done as earlier, but co-expression of a G_i coupled GPCR in all groups allowed for monitoring of agonist-induced currents. We chose to co-express the type 2 metabotropic glutamate receptor as the GPCR rather than the muscarinic type 2 receptor found in atrial cells to avoid perfusion of acetylcholine which can activate muscarinic type 1 receptors endogenous to *Xenopus* oocytes. Activation of the G_q coupled M1Rs can cause activation of phospholipases, PIP_2 hydrolysis, and thus GIRK current inhibition.

Figure 3.9 shows raw agonist-induced currents associated with the mutations used to check the GIRK1* E334 – GβγK89 salt-bridge interaction. The basal currents show the same trends seen in the absence of receptor co-expression (see Figure 3.7). Wild-type GIRK1* channel basal currents are successfully increased with wild-type Gβγ co-expression but not by the K89E mutant Gβγ. The GIRK1*E334K mutant channels show a different behavior such that wild-type Gβγ modestly increases their basal currents but the K89E mutant increases them maximally. The maximal current upon agonist-stimulation closely follows the same trends: K89E co-expression

causes defective total activation of wild-type GIRK1* but enhanced activation of the GIRK1* E334K mutant.

In addition to extending our findings to agonist-induced signaling, we also sought to test their relevance to the GIRK4 channel which heteromerizes with GIRK1 to form the GIRK1/GIRK4 (G1/4) heteromeric channel that comprises the physiological IK_{ACh} channel. Homomeric GIRK4* channels were tested for their sensitivity to the sidechain volume of Gβγ L55. In contrast to the results obtained for GIRK1* (see Figure 3.3), GIRK4* showed no sensitivity to the sidechain volume of Gβγ L55: any mutation which deviated from the wild-type leucine sidechain caused defective activation of the channel (see Figure 3.10). This result suggests that important differences exist between GIRK1 and GIRK4 channels regarding the mechanism of activation by Gβγ L55. Having seen differences between homomers of either channel, we next tested the sensitivity of wild type GIRK1/GIRK4 heteromeric channels to changes in Gβ1 L55 sidechain volume. Figure 3.11 shows that the effect observed in the heteromeric channels is very similar to that observed in GIRK1* channels. It appears that upon co-expression of GIRK1 and GIRK4, the GIRK1 effect dominates and sensitivity to Gβ1 L55 sidechain volume is restored.

We thus have demonstrated that key effects discovered in the context of GIRK1* channels with Gβγ co-expression can be extended to GIRK1/GIRK4 heteromeric channels and agonist-induced activation. Studies that can provide further confirmation including the introduction of equivalent mutations in GIRK4*, GIRK1, and GIRK4 are being carried out in our lab.

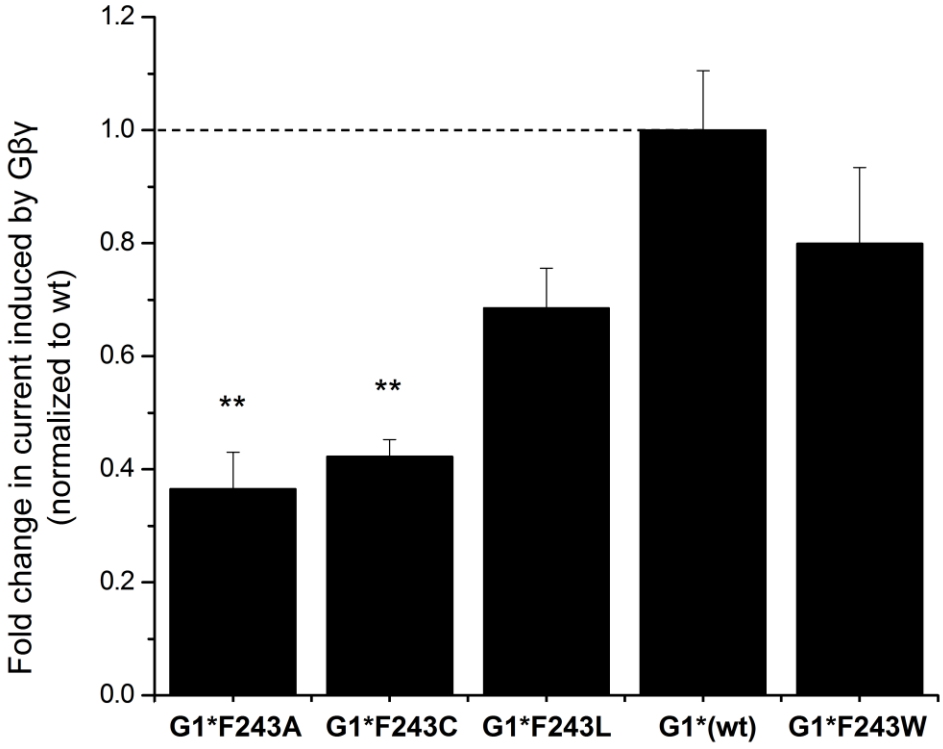

Figure 3.1 The effect of sidechain volume substitutions at GIRK1* F243 on fold induction of total GIRK current by wild-type Gβγ co-expression in *Xenopus* oocytes (mean ± SEM). Channels containing the indicated mutations were expressed alone or co-expressed with wild-type Gβγ and the fold activation for each mutation was computed. Fold-activation of wild-type GIRK1* channels by wild-type Gβγ was normalized to 1. (** indicates 95% confidence interval does not overlap with that of wild-type; estimated p-value < 0.01. See methods section)

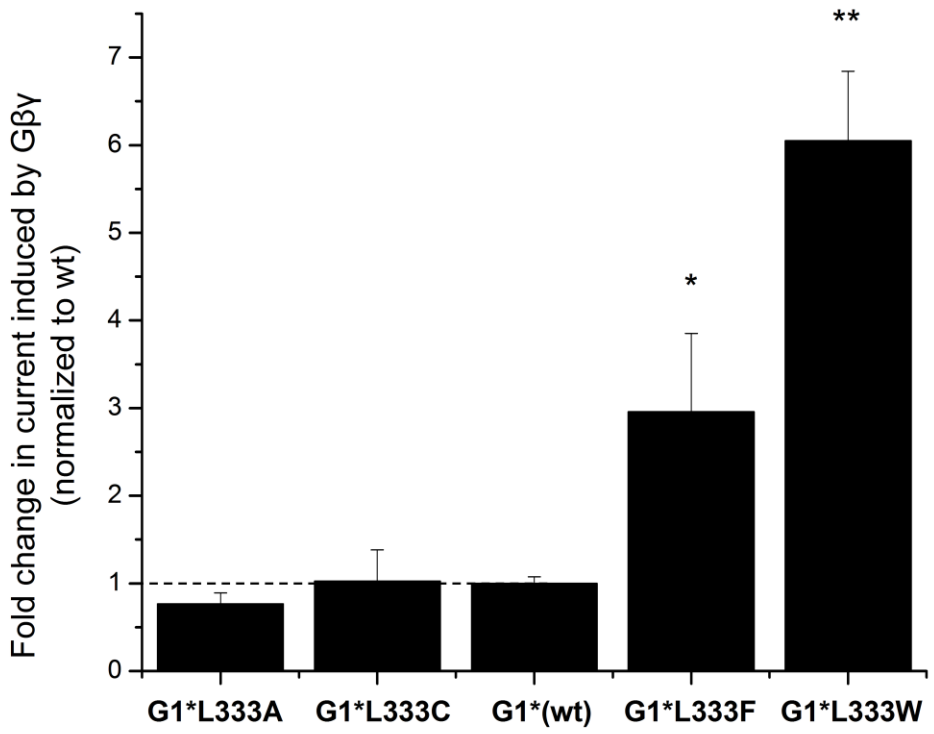

Figure 3.2 The effect of sidechain volume substitutions at GIRK1* L333 on fold induction of total GIRK current by wild-type Gβγ co-expression in *Xenopus* oocytes (mean ± SEM). Channels containing the indicated mutations were expressed alone or co-expressed with wild-type Gβγ and the fold activation for each mutation was computed. Fold-activation of wild-type GIRK1* channels by wild-type Gβγ was normalized to 1. (** indicates 95% confidence interval does not overlap with that of wild-type; estimated p-value < 0.01. * indicates 90% confidence interval does not overlap with that of wild-type; estimated p-value < 0.05. See methods section.)

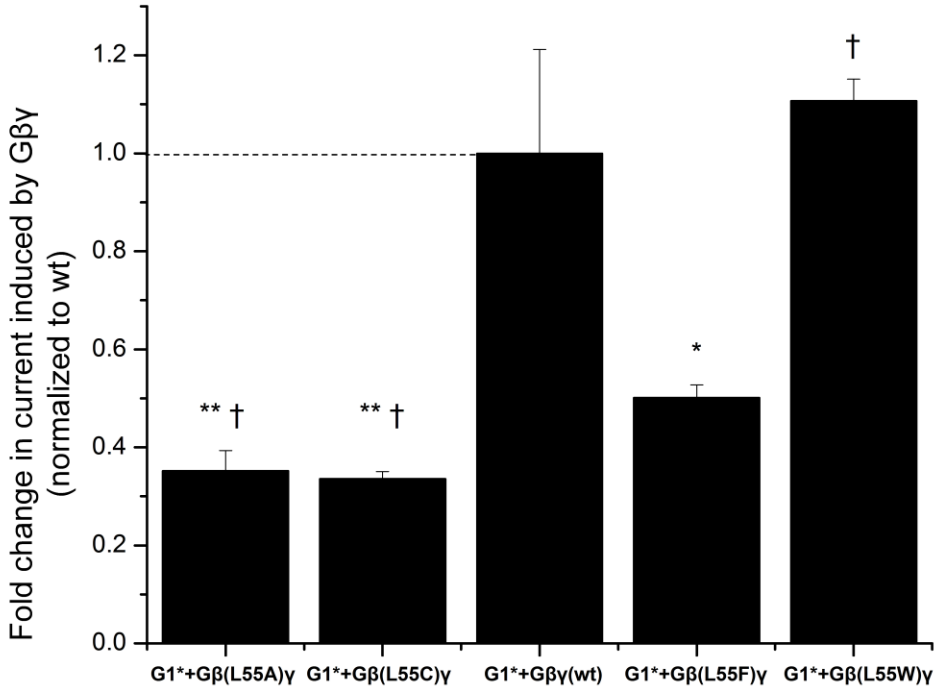

Figure 3.3 The effect of sidechain volume substitutions at Gβ1 L55 on fold induction of total GIRK current by Gβγ co-expression in *Xenopus* oocytes (mean ± SEM). Wild-type GIRK1* channels were expressed alone or co-expressed with the indicated Gβγ mutations and the fold activation for each mutation was computed. Fold-activation of wild-type GIRK1* channels by wild-type Gβγ was normalized to 1. (** indicates 95% confidence interval does not overlap with that of wild-type; estimated p-value < 0.01. * indicates 90% confidence interval does not overlap with that of wild-type; estimated p-value < 0.05. † indicates 90% confidence interval does not overlap with that of Gβ(L55F)γ; estimated p-value < 0.05. See methods section.)

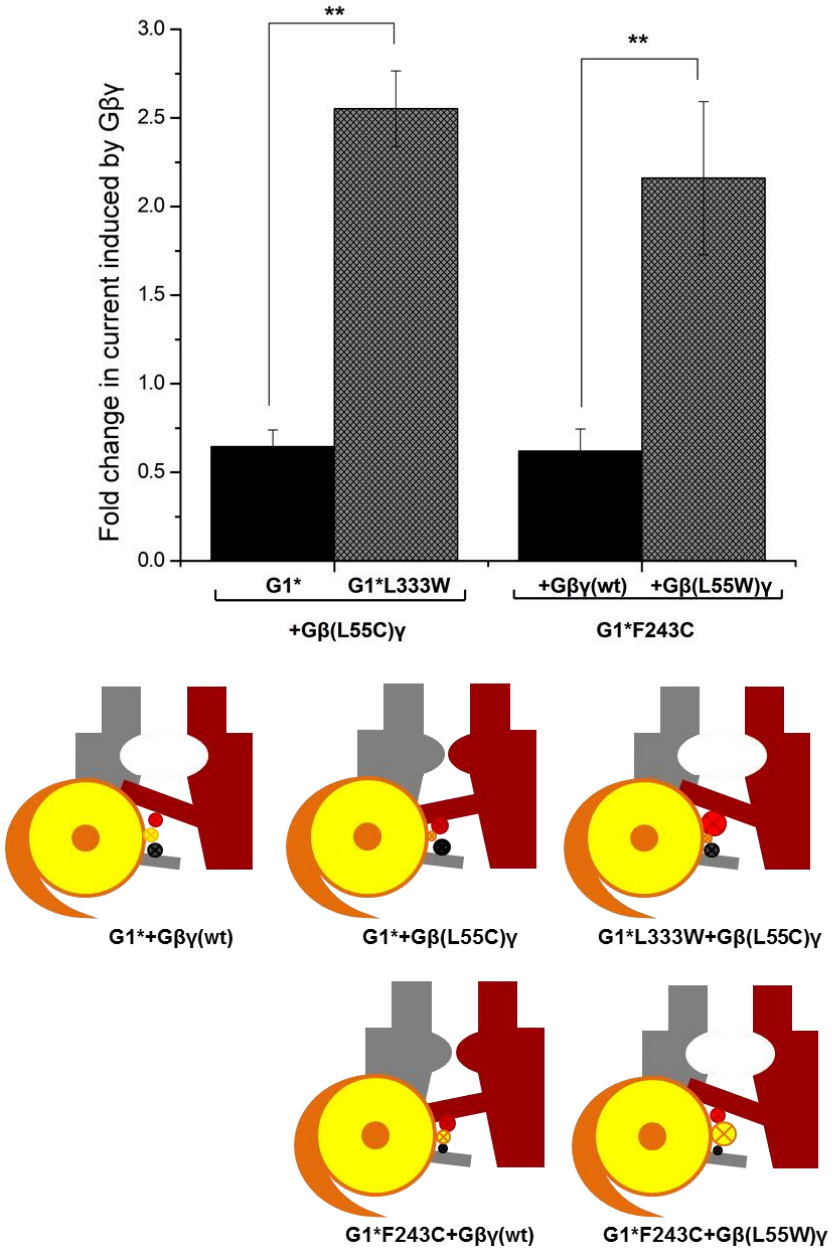

Figure 3.4 (A) The effect of combining sidechain volume altering mutations in GIRK1* and Gβγ on fold induction of total GIRK current by Gβγ co-expression in Xenopus oocytes (mean ± SEM). (Left) The effect of Gβ1 L55C mutation was tested on wild-type GIRK1* channels versus G1*L333W mutant channels. (Right) The ability of GIRK1*F243C mutant channel to be activated by wild-type versus Gβ(L55W)γ was tested. Indicated channels were expressed alone or co-expressed with the indicated Gβγ mutations and the fold activation was computed. (** indicates 95% confidence interval do not overlap; estimated p-value < 0.01. See methods section.) (B) Schematized drawings as in Figure 2.14 demonstrate inability of cysteine mutations within the DE-LM loop cleft to change the LM loop conformation and open the G-loop gate. Introduction of tryptophan mutations within the cleft successfully compensate for the small cysteines.

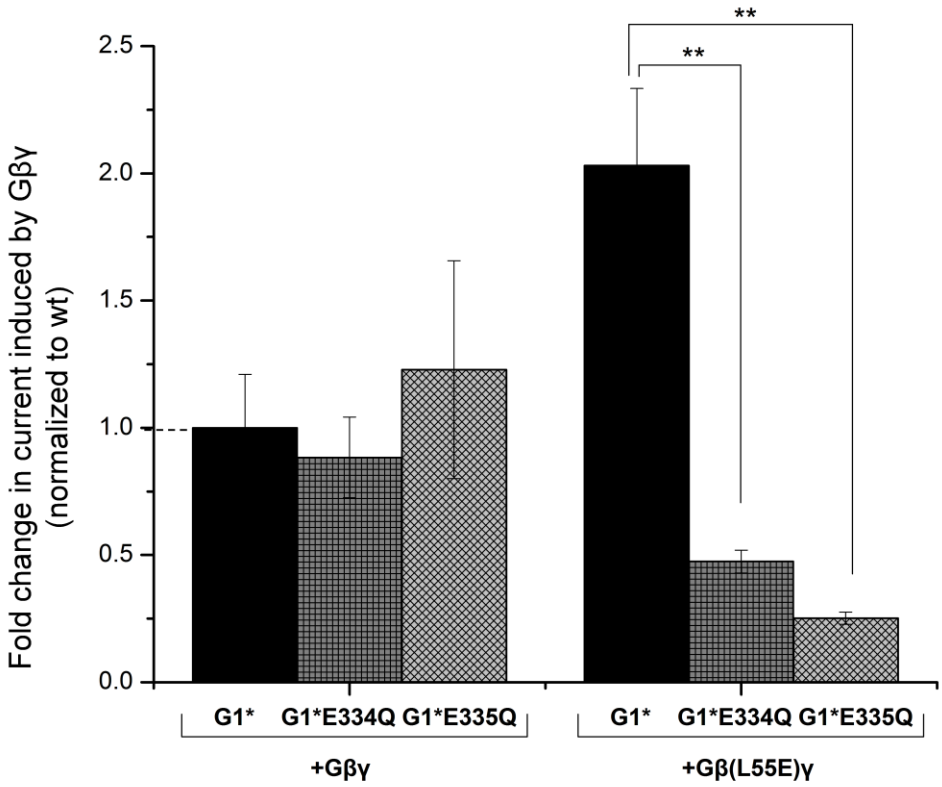

Figure 3.5 The effect of neutralizing negative charges at the channel LM loop on the ability of Gβ(L55E)γ to activate the channel. Summary data showing fold induction of total GIRK current by Gβγ co-expression in *Xenopus* oocytes (mean ± SEM). Wild-type GIRK1* or its indicated mutants were expressed alone, co-expressed with wild-type Gβγ, or co-expressed with Gβ(L55E)γ and the fold activation by each Gβγ co-expression was computed. Fold-activation of wild-type GIRK1* channels by wild-type Gβγ was normalized to 1. (** indicates 95% confidence intervals do not overlap; estimated p-value < 0.01. See methods section.)

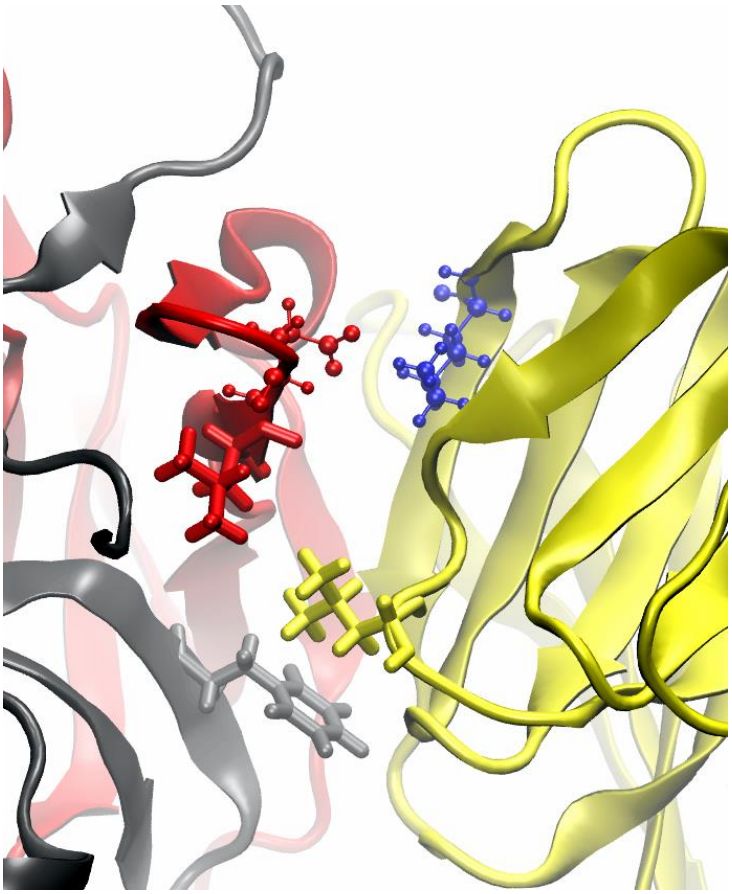

Fig. 3.6 Close up view of the cleft between LM and DE loops in the best scoring model. Cartoon depictions of two adjacent channel subunits are in red and gray while the Gβ1 is yellow. The residues comprising a predicted salt bridge interaction are depicted as red (GIRK1* L334) or blue (Gβ1 K89) spheres. Residues predicted to be involved in the LM – DE loop cleft interaction are highlighted for reference in stick representation: GIRK1 L333 (red), GIRK1 F243 (gray), Gβ1 L55 (yellow).

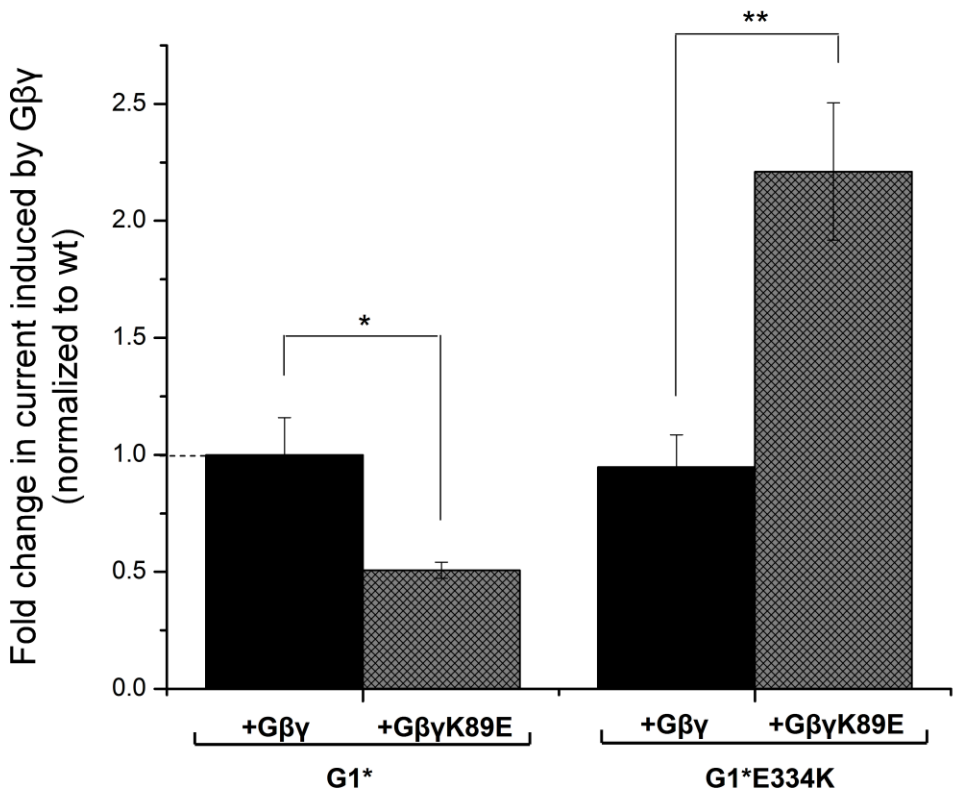

Figure 3.7 The effect of charge-reversing mutations of residues predicted to participate in an intermolecular salt-bridge interaction. Summary data showing fold induction of total GIRK current by Gβγ co-expression in *Xenopus* oocytes (mean ± SEM). Indicated channels were expressed alone or co-expressed with the indicated Gβγ mutations and the fold activation was computed. Fold-activation of wild-type GIRK1* channels by wild-type Gβγ was normalized to 1. (** indicates 95% confidence intervals do not overlap; estimated p-value < 0.01. * indicates 90% confidence intervals do not overlap; estimated p-value < 0.05. See methods section.)

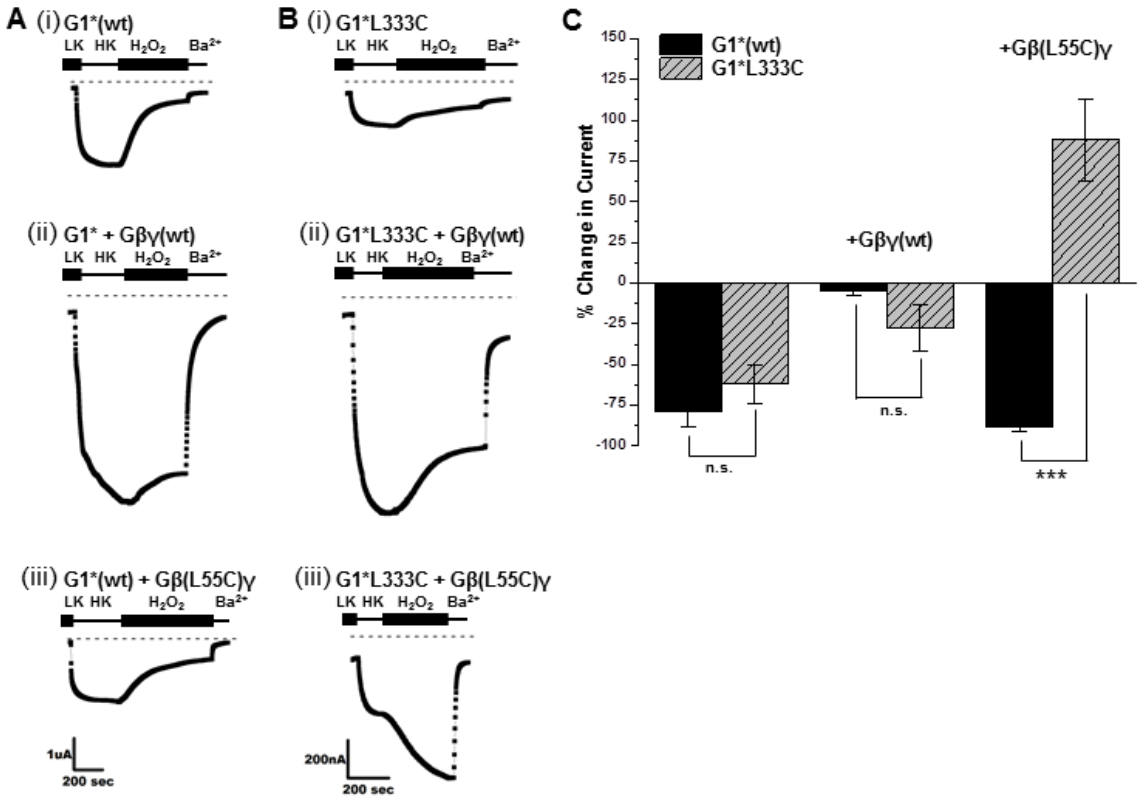

Figure 3.8 The effect of cysteine mutations of GIRK1* L333 or Gβγ L55 on current sensitivity to H_2O_2. (A-B) Representative TEVC traces showing effect of H_2O_2 on cysteine mutants expressed in *Xenopus* oocytes. Abbreviations: LK, Low potassium Solution; HK, High potassium solution; Ba^{2+}, High potassium solution containing 3mM $BaCl_2$. See Methods section. (C) Summary data showing % change in current due to H_2O_2 perfusion (mean ± SEM). (n.s. indicates not significant, *** indicates $p<0.0001$ using one-way ANOVA with Tukey's HSD post-hoc test.)

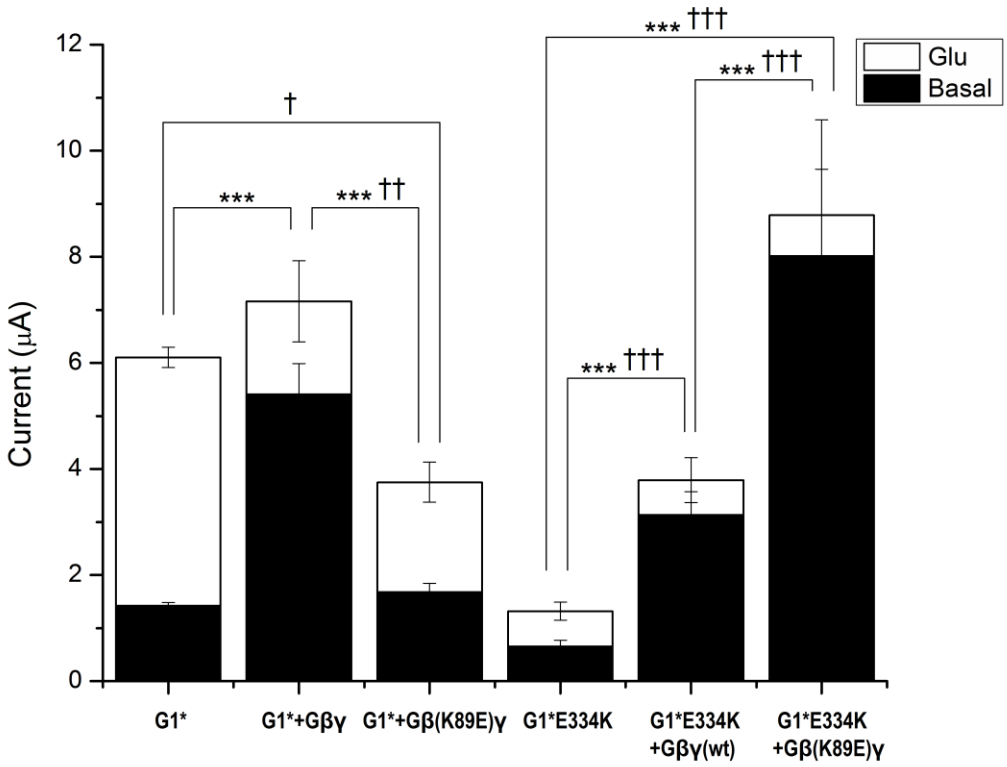

Figure 3.9 The effect of charge-reversing mutations of residues predicted to participate in an intermolecular salt-bridge interaction on agonist-induced currents. Summary data showing mean basal and agonist-induced currents measured in *Xenopus* oocytes (mean ± SEM). Indicated channel and Gβγ constructs were co-expressed with mGluR2 and stimulated with 10μM glutamate to induce activation. (*** indicates $p<0.0001$ for basal current comparison. † indicates $p<0.05$, †† indicates $p<0.001$, ††† indicates $p<0.0001$ for total maximal current comparison. Comparisons by oneway ANOVA with Dunnet's post-hoc test).

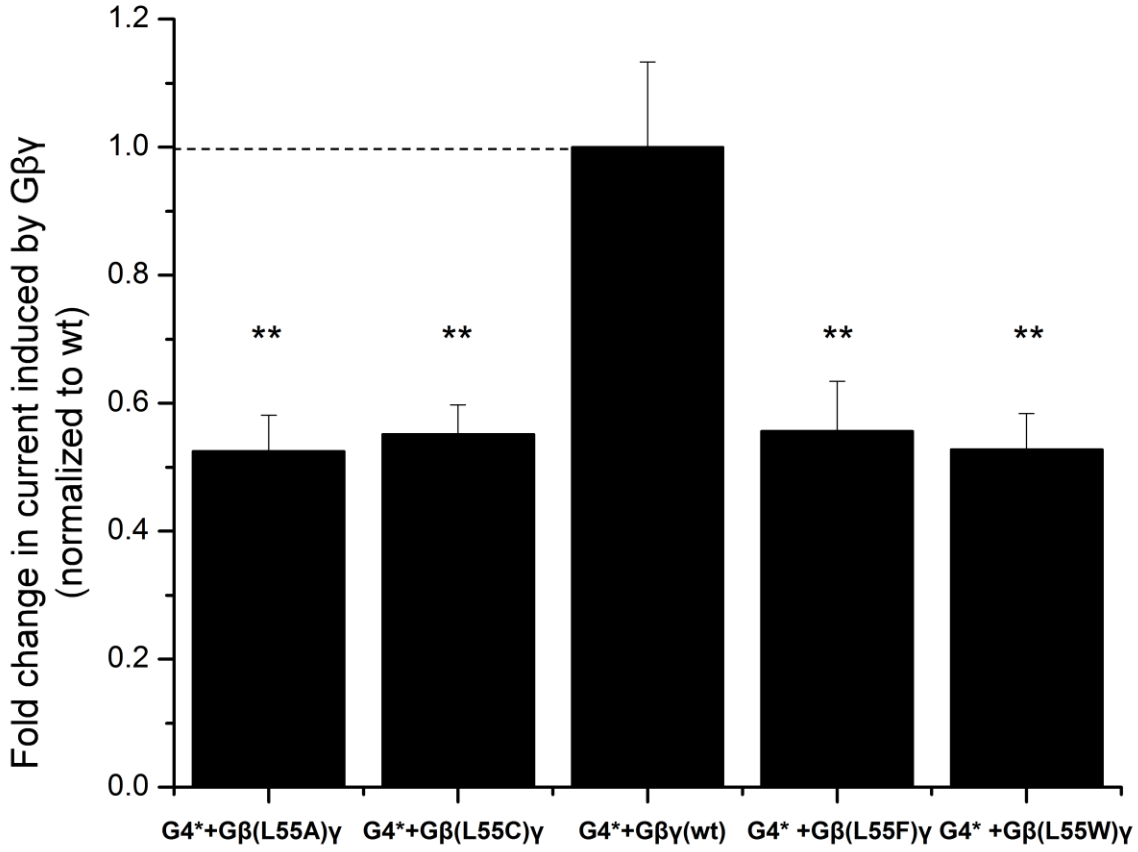

Figure 3.10 The effect of sidechain volume substitutions at Gβ1 L55 on fold induction of total GIRK current by Gβγ co-expression in *Xenopus* oocytes (mean ± SEM). Wild-type GIRK4* channels were expressed alone or co-expressed with the indicated Gβγ mutations and the fold activation for each mutation was computed. Fold-activation of wild-type GIRK4* channels by wild-type Gβγ was normalized to 1. (** indicates 95% confidence interval does not overlap with that of wild-type; estimated p-value < 0.01. See methods section.) The electrophysiological data in this experiment were recorded and analyzed by my colleague Mr. Junghoon Ha.

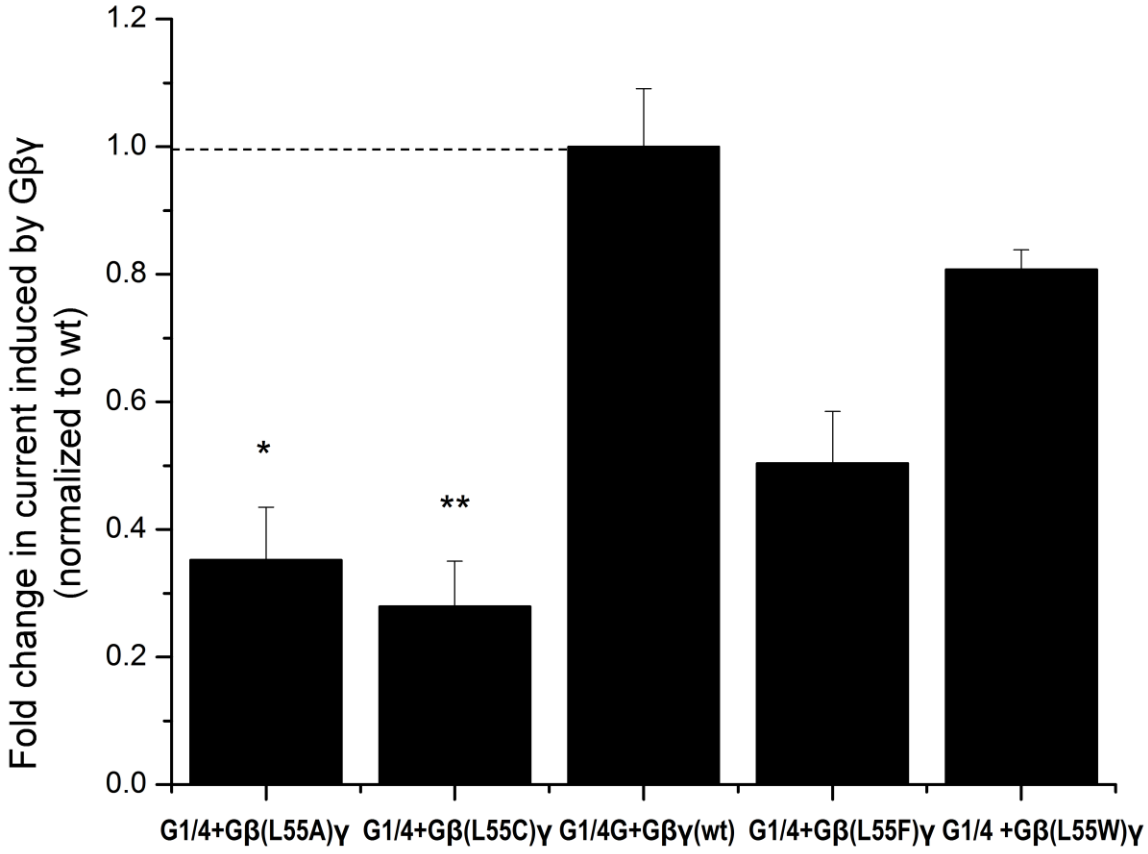

Figure 3.11 The effect of sidechain volume substitutions at Gβ1 L55 on fold induction of total GIRK current by Gβγ co-expression in *Xenopus* oocytes (mean ± SEM). GIRK1/GIRK4 (G1/4) heteromeric channels were expressed alone or co-expressed with the indicated Gβγ mutations and the fold activation for each mutation was computed. Fold-activation of GIRK1/GIRK4 channels by wild-type Gβγ was normalized to 1. (** indicates 95% confidence interval does not overlap with that of wild-type; estimated p-value < 0.01. * indicates 90% confidence interval does not overlap with that of wild-type; estimated p-value < 0.05. See methods section.) The electrophysiological data in this experiment were recorded and analyzed by my colleague Mr. Junghoon Ha.

Chapter 4

Gα Interactions

Both active and inactive forms of Gα have been shown biochemically to bind to GIRK channels [41], [63], [68] and emerging evidence suggests Gα may play a modulatory role in channel activity. Although the direct modulatory role of role of the active form Gα(GTP) still remains unclear [39], [113] the binding site for Gα(GTP) on GIRK channels has recently and directly been addressed by an NMR study [110]. Binding interfaces on both the channel and Gα were determined and the results were used in restraint-based docking to generate a model. While the study represents a major advance, an important consideration is that the experiments were performed with solubilized proteins. The absence of a membrane may allow the complex to adopt conformations that would be unfavorable in a native environment. Furthermore, the experiments are conducted in the absence of Gβγ. Gα has only been shown to play a modulatory role on channel activity which depends on Gβγ and the functional significance of any Gα-channel interactions in the absence of Gβγ has not been demonstrated for mammalian GIRK channels.

The role of Gα(GDP) in associating with Gβγ to form an activatable heterotrimer is much more established. Insights into regions of the channel which may specifically mediate heterotrimer

interactions can come from modifications to the channel which abrogate agonist-induced currents but spare direct activation by Gβγ. Such modifications presumably prevent effective heterotrimer association with the channel but retain the Gβγ activation site. Slesinger and colleagues demonstrated such behavior in IGC4, a chimera of IRK1 containing most of C-terminus of GIRK1 from position 325 onward [69]. This chimera shows robust activation by Gβγ co-expression but a complete lack of activation by agonist stimulation with receptor co-expression. This implicates the GIRK region prior to residue 325 in heterotrimer interactions. The paper goes on to implicate the N-terminus as playing a role in receptor coupling by studying effects of N-terminal chimeras on activation kinetics. More recently, Clancy et al showed that a series of mutations in GIRK2 corresponding to positions 307-319 in GIRK1 cause loss of binding to Gα(GTP) as well as to the Gα(GDP)βγ heterotrimer [39]. A point mutant from this region shows the expected behavior of reduced agonist-induced currents but intact Gβγ co-expression-induced currents.

Our work screening various channel mutants led to the discovery of another mutation whose behavior is consistent with a role in heterotrimer coupling. Figure 4.1 shows that the GIRK1* R286E mutation leads to a complete loss of agonist induced currents but shows enhanced activation by Gβγ co-expression. Furthermore, Figure 4.2 shows that co-expression of Gα along with Gβγ leads to complete restoration of basal and agonist-induced currents. This may suggest that the R286E mutation causes a weakening of the channel's ability to associate with functional endogenous heterotrimers while leaving the Gβγ activation site intact. The weakened affinity for endogenous heterotrimers could thus be overcome by over-expression of the G-proteins. Mapping of regions implicated in heterotrimer interaction onto the channel structure identify an

area of the channel where such implicated regions approach one another (see Figure 4.3). This area is adjacent to the predicted Gβγ binding site. The Gα binding critical region of the N-terminus has only been narrowed to the region between residues 32-86 [68]. It is not currently clear how much of this 54 residue region is needed for binding to the heterotrimer. Residues 32-40 of this critical region are missing from the Kir3.1 chimera structure and thus the heterotrimer's binding site may be incomplete in the structure.

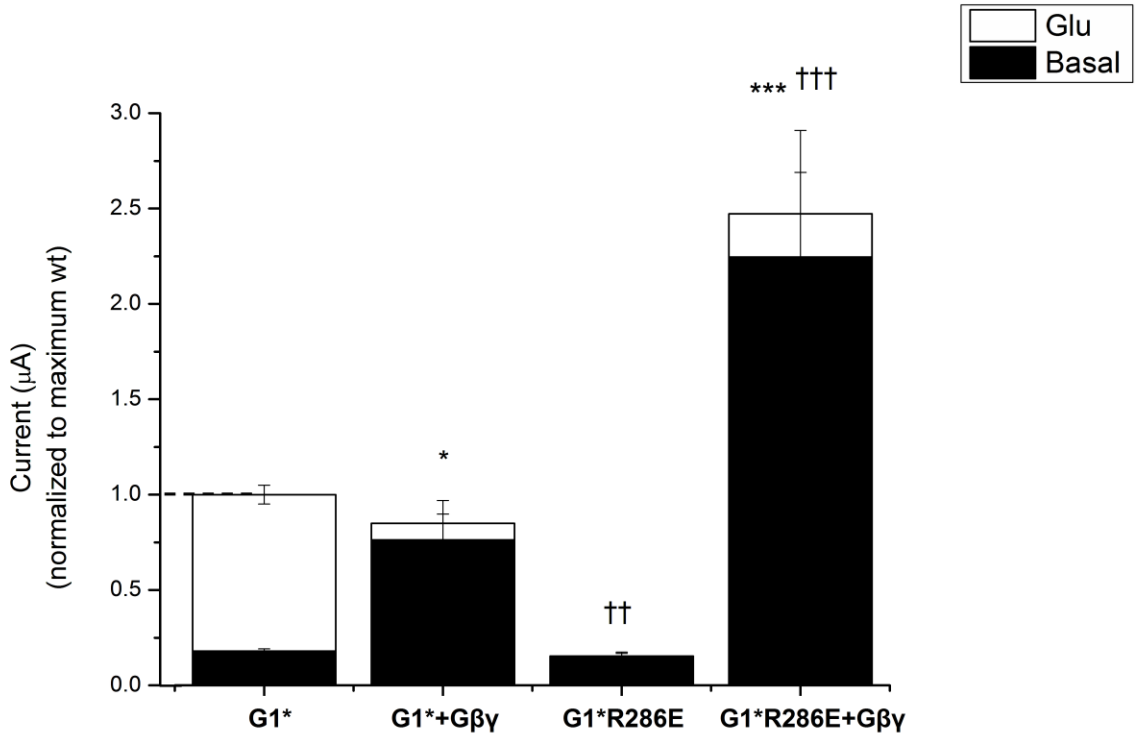

Figure 4.1 Effects of R286E mutation. Summary data showing mean basal and agonist-induced currents measured in *Xenopus* oocytes (mean ± SEM). Indicated channel and Gβγ constructs were co-expressed with mGluR2 and stimulated with 10μM glutamate to induce activation. All currents were normalized to the maximal GIRK1* current. (*** indicates $p<0.0001$, ** indicates $p<0.001$ for basal current comparison to GIRK1*. †† indicates $p<0.001$, ††† indicates $p<0.0001$ for total maximal current comparison to GIRK1*. Comparisons by oneway ANOVA with Dunnet's post-hoc test).

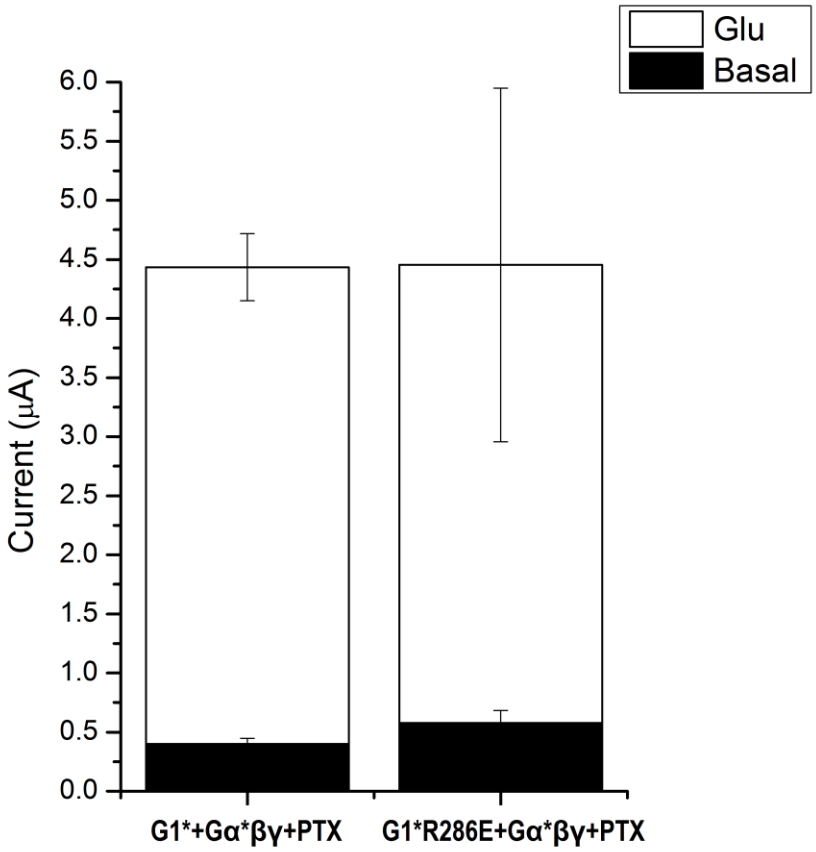

Figure 4.2 Effects of R286E mutation with G-protein over-expression. Summary data showing mean basal and agonist-induced currents measured in *Xenopus* oocytes (mean ± SEM). GIRK1* versus GIRK1*R286E mutant channel were co-expressed with mGluR2, Gα*, Gβγ, and pertussis toxin (PTX). Gα* is Ga_i1 containing the Gα(C351A) mutation making it resistant to the action of PTX. Thus co-expression of the toxin can prevent activation of endogenous Gα while allowing activation of expressed Gα. Indicated channel and Gβγ constructs were co-expressed with mGluR2 and stimulated with 10μM glutamate to induce activation. (Comparisons by student's t-test found no significant differences in basal or total current).

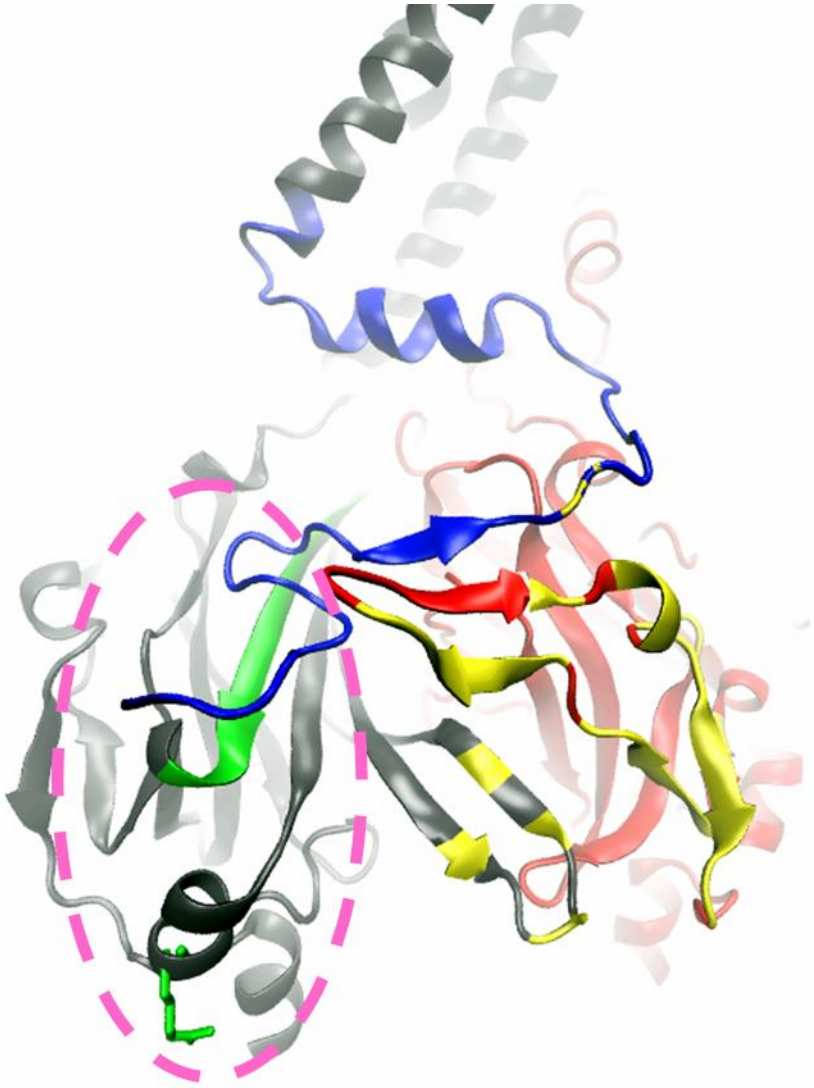

Figure 4.3 Regions of GIRK channels implicated in heterotrimer association. Cartoon depiction of two adjacent subunits of the channel are shown in gray and red. Green represents the region implicated in Clancy et al.[39] Blue represents the N-terminus implicated by multiple studies (Slesinger et al, Ivanina et al [68], [69]). Green sticks represent the GIRK1* R286 residue implicated in our lab. Yellow highlights the predicted Gβγ interface from our computational results. Dashed pink circle highlights a possible consensus region for heterotrimer association.

Chapter 5

Discussion

5.1 Mechanism of the G-protein Activation of GIRK channels

This study confirms our original hypothesis that specific reciprocal interactions between Gβγ and the GIRK1 channel mediate G-protein activation of the channel. Using computational docking to take advantage of crystal structures of both Gβγ and the GIRK channel, we were also able to test and experimentally confirm secondary hypotheses regarding binding sites, gating mechanisms, and specific interactions. These findings give a detailed understanding of molecular mechanisms underlying GIRK activation as well as informing mechanisms by which Gβγ regulates effector proteins.

Beyond simply predicting the binding mode, we develop a model for how the specific Gβγ-channel interactions identified by the binding mode promote the open state of the channel's G-loop gate: by stabilizing the "raised" conformation of the LM loop to allow it to interact strongly with the N-terminus. Our current work extends the gating mechanism proposed in Meng et al. [54] to now include the role of the DE loop and the LM - DE loop cleft (see Figure 5.1). Meng and colleagues had proposed (see Figure 1.6) that when the G-loop is in the closed state, the CD loop and N-terminus are closely interacting while the LM loop assumes a downward

conformation away from the N-terminus. Introduction of PIP_2 stabilizes a different conformation of these secondary structure elements such that each element switches its close interactions from adjacent elements on one side to those on the other. Thus, the open G-loop conformation is stabilized by its interactions with the CD loop which no longer closely interacts with the N-terminus. The N-terminus in turn, switches its close interactions from the CD loop to the LM loop which has assumed a "raised" conformation.

Our current work proposes that this cascade of switching interactions continues farther down to include the DE-LM loop cleft (see Figure 5.1). In the closed state, the LM loop in its downward conformation closely interacts with the adjacent DE loop but this interaction switches in the open state so the LM loop instead interacts closely with the adjacent N-terminus. Thus we propose that PIP_2 and Gβγ modulate a similar cascade of switching interactions but their sites of action are distinct. PIP_2 acts close to the pore and G-loop gate by directly interacting with residues of the CD-loop and N-terminus. On the other hand, Gβγ acts at the level of the LM and DE loops. Ethanol, which activates the channel, also interacts with the channel at the LM – DE loop cleft [47], supporting the importance of this cleft in channel activation.

The Gβγ residues implicated in channel activation by our model are part of the Gα binding site on Gβγ. Specifically, these residues including L55 and K89 are among the residues which interact with the N-terminal helix of Gα [57], [73] (see Figure 1.7). Thus we may speculate that, although our model and experiments provide no information about the interactions of Gα, agonist-induced activation involves the unbinding of the Gα-N-terminal helix from Gβγ to reveal these important Gβ residues to allow them to interact with and activate the channel. As it is

known that the N-terminal helix adopts a disordered conformation upon Gβγ unbinding from Gα [59], even a partial unbinding of the two proteins may be enough to uncover these critical Gβ residues from behind the Gα N-terminal helix.

We further identified a GIRK1 mutation R286E which appears to weaken channel coupling to activatable heterotrimers. The localization of this residue directly adjacent to our predicted Gβγ binding site (see Figure 4.3) further tempts speculation that the region surrounding the R286 residue may bind Gα(GDP) in the inactive heterotrimeric form such that it orients Gβγ near its activation site on the channel. Purely based on space restraints, such a site on the channel for association with heterotrimeric G-proteins would be consistent with accommodating up to 4 heterotrimers. Such a stoichiometry is supported by previously published studies [114]. Agonist stimulation would then cause partial unbinding of Gα and Gβγ leading to a disordered conformation of the Gα N-terminal helix and rapid association of important Gβγ residues with the appropriate channel site to activate the channel by triggering a stereotyped cascade of changes in conformations of secondary structure channel elements.

This study further reports the development of a docking algorithm which was able to produce a strong and clear signal upon identification of a favored binding mode of our complex. We propose the use of such a multistage docking algorithm as a valuable tool in the analysis of protein complexes otherwise intractable to traditional experimental structure determination techniques. Although the algorithm yielded a clear signal in the case of our Gβγ-GIRK1 complex, success with other proteins will vary depending on the nature of the protein binding and will always depend critically on selection of starting structures in appropriate conformations.

Regardless, even without clear identification of a single binding mode, computational docking can serve as an important tool for generating or narrowing hypotheses to pursue experimentally.

5.2 Future Experiments

The binding mode and gating model were predicted and largely tested in the context of the GIRK1* channel. GIRK4* channels behaved differently in their sensitivity to sidechain volume of Gβγ L55. On one hand this may reflect differences in gating mechanisms of GIRK4 versus GIRK1. GIRK4 is after all closer in homology to GIRK2 than it is to GIRK1. While no GIRK4 structures exist, no GIRK2 structures (even those with closed G-loop gates) have shown the dramatic downward movement of the LM loop. The LM loop remains in a "raised conformation" in all GIRK2 structures. Thus perhaps Gβγ mediated activation of GIRK4 occurs by some other mechanism. However, our preliminary experiments with GIRK4* only ascertained the role of Gβγ L55 in steric stabilization of the "raised" LM loop conformation. GIRK4* star channels may very well use a similar overall gating mechanism as GIRK1* but perhaps due to small local differences in the channel structures, a different Gβγ residue plays the same role. Further studies which would attempt to extend all of our current findings to GIRK4* would be needed to compare the gating mechanisms thoroughly. Similarly, the work could more thoroughly be extended to heteromeric GIRK1/4 channels.

Extension to GIRK2* and eventually GIRK1/GIRK2 would also be of interest in order to explore the neuronal implications of the current work. If the lack of heterogeneity in LM-loop conformations seen in different crystal structures of GIRK2 reflects an actual lack of such protein dynamics then we can expect differences in the behavior of GIRK2 compared to what we observed in GIRK1. However, since the crystal structures of GIRK2 are available, it would then be possible to try to repeat the docking procedure for GIRK2 to find its distinct binding mode

and gating mechanism. Since the docking procedure does not produce movements in backbone atoms, the success of such an endeavor would strongly depend on the availability of a crystal structure of GIRK2 where the conformation of its intracellular domains approaches the conformation stabilized by Gβγ binding.

While our electrophysiological results regarding response to H_2O_2 strongly suggest the formation of a functionally active disulfide bond, confirmation will require biochemical testing. Confirmation of the crosslink would open the door to possible attempts to co-crystallize the channel and Gβγ as difficulties due to their low relative affinities outside of a membrane environment would no longer be a concern. Biochemical means could also be used to characterize residues of our predicted binding site in terms of their contribution to binding versus activation.

Finally, while our docking procedure eventually produced a clear signal and a plausible binding mode for the case at hand, it will be important to benchmark its performance for a larger group of proteins with known binding modes in order to make generalizations about its performance.

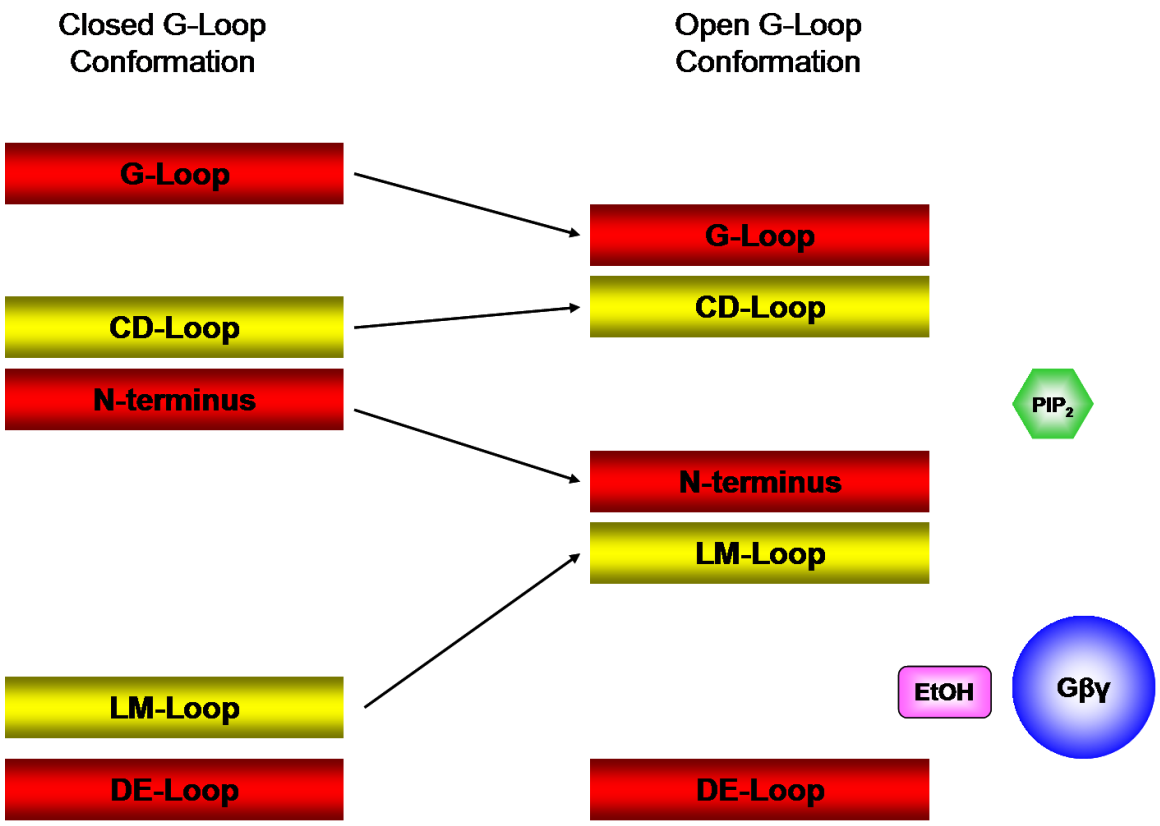

Figure 5.1 Summary of the major results of Meng et al. and their extension to include the DE loop and LM-DE loop cleft [54]. Transitioning from the closed to open, the secondary structure elements switch their close interactions from the adjacent element on one side to the element on the other side. PIP_2 stabilizes the conformation on the right by direct interactions with the CD loop and N-terminus. We propose that Gβγ works through a similar mechanism by stabilizing the same overall conformation but by direct interactions with a different part of the channel. Its proposed site of action at the DE-LM loop cleft is shared with the site of ethanol (EtOH) action.

Appendix

Methods

A.1 Docking

Missing sidechains and N-terminal linker region residues of the Kir3.1 chimera structure [52] (PDB code: 2QKS) were built using the loopmodeling routine of Modeller [89]. Residues in the structure were renumbered to correspond to the equivalent GIRK1 residue. All references to channel residue numbering are relative to GIRK1 unless otherwise stated. The dense 6° sampling option N=54000 of ZDock3.0.1 was used to perform rigid docking [93]. All channel residues except for the intracellular regions of two adjacent subunits were blocked form the binding site using the ZDock provided script.

In-house scripts were used to filter the results by rejecting any ZDock output model containing any atoms more than 8Å above the plane of the membrane or with the C-alpha atom of the C-terminal Gγ more than 30Å below the plane of the membrane. The plane of the membrane was defined as the plane defined by the C-alpha atoms of L75 in the interfacial helix.

ZRank was initially used to re-rank the remaining poses, but this step was eventually abandoned [94].

The top 2000 remaining poses were subject to clustering using the ClusPro1.0 webserver (http://nrc.bu.edu/cluster/cluspro_v1.cgi) [99]. Clustering was performed at a 9Å clustering radius using otherwise default parameters of ClusPro.

Structures representing the centers of the 30 largest clusters were used as inputs for RosettaDock3.1 [105]. 1000 models for each input structure were produced using the local refinement protocol of Rosetta dock. Input sidechain rotamers as well as extra chi1 rotamers and chi2 aromatic rotamers were included in the side chain search.

All the poses produced by RosettaDock were rescored using the ZRank2.0 scoring function [106]. The composite score was computed as described in Chapter 2.2.

Interface residue prediction was carried out using the top 2000 models prior to clustering using a method similar to [96]. For a given model, each residue was assigned a binary score of 0 if it was not a contact residue or a 1 if it was a contact residue. Contact residues were defined using a 6Å cutoff. These scores were summed over all the models such that the maximum score a residue could achieve would be 2000 (it was included in the interface in 100% of the models). The summed scores were divided by the maximum score achieved by any residue in order to normalize the values. Residues achieving a final score of 0.7 or above were predicted to be interface residues.

A.2 Mutagenesis

cDNAs of GIRK1*, GIRK4*, GIRK1, GIRK4, Gβ1, Gγ2, Ga_i1, mGluR2, and PTX had already each been subcloned into an oocyte expression vector (pGEMHE) by previous efforts in our lab. Desired mutations were introduced by the commercial Quickchange (Agilent Technologies) method. Briefly, complimentary primers containing and centered about the desired mutation were designed. PCR was carried out using the pfu polymerase and was allowed to cycle only 18 times to avoid errors. All mutants were confirmed by DNA sequencing (Genewiz).

A.3 *Xenopus* oocyte expression

All constructs were linearized using NheI restriction enzyme and *in vitro* transcribed using the "message machine" (Ambion) commercial kit. cRNA concentrations were quantified by optical density. *Xenopus* oocytes were surgically extracted, dissociated and defolliculated by collagenase treatment, and microinjected with 50 nl of a water solution containing the desired cRNAs. All constructs used in this study were injected to achieve 2ng/oocyte. Oocytes were incubated for 2-4 days at 18 °C.

A.4 Electrophysiology

Whole-oocyte currents were measured by conventional two-electrode voltage clamp with a GeneClamp 500 amplifier (Axon Instruments). Agarose-cushion microelectrodes were used with resistances between 0.1 and 1.0 MΩ. Oocytes were held at 0mv and currents were assessed by 800ms ramps from -80 to +80mv. Current at -80mv was recorded. Barium-sensitive basal currents were defined as the difference between the steady state currents while perfusing High potassium (ND96K or HK) solution or Barium solution. 10μM Glutamate dissolved in ND96K was used to stimulate agonist-induced currents. These were also defined as the difference in steady-state currents between perfusion of the Glutamate or the Barium solution. ND96K solution contained: 91mM KCl, 1mM NaCl, 1mM MgCl2, 5mM KOH/HEPES, pH 7.4. Barium solution consisted of ND96K + 3mM $BaCl_2$.

5-10 oocytes from the same batch were recorded for each group and the experiments were repeated in at least two groups.

A.5 Statistical Analysis

The quantity of interest in many of the experiments was the fold-change in basal current induced by co-expression of Gβγ. Thus this fold-change represents the ratio of two unpaired means where each mean carries its individual degree of uncertainty. The mean current observed with Gβγ co-expression for a particular channel mutation is divided by the mean current observed for that channel expressed alone. Simply rescaling the individual observations of the numerator

(channel + Gβγ) by the mean value of the denominator (channel alone) and then proceeding with a traditional comparison such as a t-test or ANOVA is not a valid solution because it ignores the uncertainty associated with the denominator's mean. A rigorous treatment to this problem is provided by Fieller's Theorem ([115], [116]). Application of Fieller's theorem allows for rigorous construction of confidence intervals and calculation of standard error but it does not provide p-values for hypothesis testing. Non-overlap of confidence intervals does certainly confirm statistical significance, but it is a very conservative test and actual associated error rate would be much lower than the 0.05 implied by a single 95% confidence interval. Assuming an adequate sample, equal variance, and independence, the chance of finding non-overlapping 95% confidence intervals for the same mean purely due to chance (i.e. under the null hypothesis that the means are equal) can be calculated to be close to 0.0056 [117]. Thus, we use Fieller's theorem to construct 95% confidence intervals for the fold-change values and we conservatively report $p<0.01$ when we find non-overlapping 95% confidence intervals for our data. For 90% confidence intervals, that value is calculated to be 0.02 which we conservatively report as $p<0.05$.

Other conventional statistical tests were employed in experiments reporting raw current values or within-oocyte % changes in current. These statistical tests used are identified within the appropriate figure legends

References:

[1] D. E. Logothetis, Y. Kurachi, J. Galper, E. J. Neer, and D. E. Clapham, "The beta gamma subunits of GTP-binding proteins activate the muscarinic K+ channel in heart," *Nature*, vol. 325, no. 6102, pp. 321–326, Jan. 1987.

[2] H. Hibino, A. Inanobe, K. Furutani, S. Murakami, I. Findlay, and Y. Kurachi, "Inwardly Rectifying Potassium Channels: Their Structure, Function, and Physiological Roles," *Physiol Rev*, vol. 90, no. 1, pp. 291–366, Jan. 2010.

[3] J. F. Fulton and L. G. Wilson, *Selected readings in the history of physiology*. C.C. Thomas, 1966.

[4] J. F. Jones, "Vagal control of the rat heart," *Exp. Physiol.*, vol. 86, no. 6, pp. 797–801, Nov. 2001.

[5] W. H. Gaskell, "The Electrical changes in the Quiescent Cardiac Muscle which accompany Stimulation of the Vagus Nerve," *J Physiol*, vol. 7, no. 5–6, pp. 451–452, Nov. 1886.

[6] W. H. Gaskell, "On the Action of Muscarin upon the Heart, and on the Electrical Changes in the non-beating Cardiac Muscle brought about by Stimulation of the Inhibitory and Augmentor Nerves," *J Physiol*, vol. 8, no. 6, pp. 404–i8, Dec. 1887.

[7] W. H. Howell and W. W. Duke, "The Effect of Vagus Inhibition on the Output of Potassium from the Heart," *Am J Physiol*, vol. 21, no. 1, pp. 51–63, Feb. 1908.

[8] O. Loewi, "Über humorale übertragbarkeit der Herznervenwirkung," *Pflügers Archiv European Journal of Physiology*, vol. 189, no. 1, pp. 239–242, 1921.

[9] O. Loewi and E. Navratil, "Über humorale Übertragbarkeit der Herznervenwirkung," *Pflügers Archiv European Journal of Physiology*, vol. 214, no. 1, pp. 678–688, 1926.

[10] "The Nobel Prize in Physiology or Medicine 1936," *Nobelprize.org*, Nobel Media AB-2012. [Online]. Available: http://www.nobelprize.org/nobel_prizes/medicine/laureates/1936/. [Accessed: 02-Oct-2012].

[11] A. S. V. Burgen and K. G. Terroux, "On the negative inotropic effect in the cat's auricle," *J Physiol*, vol. 120, no. 4, pp. 449–464, Jun. 1953.

[12] J. D. Castillo and B. Katz, "Production of Membrane Potential Changes in the Frog's Heart by Inhibitory Nerve Impulses," *, Published online: 11 June 1955; | doi:10.1038/1751035a0*, vol. 175, no. 4467, pp. 1035–1035, Jun. 1955.

[13] W. Trautwein and J. Dudel, "Zum Mechanismus der Membranwirkung des Acetylcholin an der Herzmuskelfaser," *Pflügers Archiv European Journal of Physiology*, vol. 266, no. 3, pp. 324–334, 1958.

[14] A. Noma and W. Trautwein, "Relaxation of the ACh-induced potassium current in the rabbit sinoatrial node cell," *Pflugers Archiv European Journal of Physiology*, vol. 377, no. 3, pp. 193–200, 1978.

[15] E. Neher and B. Sakmann, "Single-channel currents recorded from membrane of denervated frog muscle fibres," *, Published online: 29 April 1976; | doi:10.1038/260799a0*, vol. 260, no. 5554, pp. 799–802, Apr. 1976.

[16] B. Sakmann, A. Noma, and W. Trautwein, “Acetylcholine activation of single muscarinic K+ channels in isolated pacemaker cells of the mammalian heart,” *Nature*, vol. 303, no. 5914, pp. 250–253, May 1983.
[17] Y. Kubo, E. Reuveny, P. A. Slesinger, Y. N. Jan, and L. Y. Jan, “Primary structure and functional expression of a rat G-protein-coupled muscarinic potassium channel,” *Nature*, vol. 364, no. 6440, pp. 802–806, Aug. 1993.
[18] G. Krapivinsky, E. A. Gordon, K. Wickman, B. Velimirović, L. Krapivinsky, and D. E. Clapham, “The G-protein-gated atrial K+ channel IKACh is a heteromultimer of two inwardly rectifying K(+)-channel proteins,” *Nature*, vol. 374, no. 6518, pp. 135–141, Mar. 1995.
[19] N. Dascal, W. Schreibmayer, N. F. Lim, W. Wang, C. Chavkin, L. DiMagno, C. Labarca, B. L. Kieffer, C. Gaveriaux-Ruff, and D. Trollinger, “Atrial G protein-activated K+ channel: expression cloning and molecular properties.,” *Proc Natl Acad Sci U S A*, vol. 90, no. 21, pp. 10235–10239, Nov. 1993.
[20] K. W. Chan, J.-L. Sui, M. Vivaudou, and D. E. Logothetis, “Control of channel activity through a unique amino acid residue of a G protein-gated inwardly rectifying K+ channel subunit,” *Proc Natl Acad Sci USA*, vol. 93, no. 24, pp. 14193–14198, Nov. 1996.
[21] M. Vivaudou, K. W. Chan, J. L. Sui, L. Y. Jan, E. Reuveny, and D. E. Logothetis, “Probing the G-protein regulation of GIRK1 and GIRK4, the two subunits of the KACh channel, using functional homomeric mutants,” *J. Biol. Chem.*, vol. 272, no. 50, pp. 31553–31560, Dec. 1997.
[22] C. Lüscher and P. A. Slesinger, “Emerging roles for G protein-gated inwardly rectifying potassium (GIRK) channels in health and disease,” *Nat. Rev. Neurosci.*, vol. 11, no. 5, pp. 301–315, May 2010.
[23] K. Wickman, J. Nemec, S. J. Gendler, and D. E. Clapham, “Abnormal Heart Rate Regulation in GIRK4 Knockout Mice,” *Neuron*, vol. 20, no. 1, pp. 103–114, Jan. 1998.
[24] Y. Yang, Y. Yang, B. Liang, J. Liu, J. Li, M. Grunnet, S.-P. Olesen, H. B. Rasmussen, P. T. Ellinor, L. Gao, X. Lin, L. Li, L. Wang, J. Xiao, Y. Liu, Y. Liu, S. Zhang, D. Liang, L. Peng, T. Jespersen, and Y.-H. Chen, “Identification of a Kir3.4 Mutation in Congenital Long QT Syndrome,” *The American Journal of Human Genetics*, vol. 86, no. 6, pp. 872–880, Jun. 2010.
[25] L. Carlsson, G. Duker, and I. Jacobson, “New pharmacological targets and treatments for atrial fibrillation,” *Trends in Pharmacological Sciences*, vol. 31, no. 8, pp. 364–371, Aug. 2010.
[26] P. Kovoor, K. Wickman, C. T. Maguire, W. Pu, J. Gehrmann, C. I. Berul, and D. E. Clapham, “Evaluation of the role of IKACh in atrial fibrillation using a mouse knockout model,” *Journal of the American College of Cardiology*, vol. 37, no. 8, pp. 2136–2143, Jun. 2001.
[27] K. L. Pierce, R. T. Premont, and R. J. Lefkowitz, “Seven-transmembrane receptors,” *Nat. Rev. Mol. Cell Biol.*, vol. 3, no. 9, pp. 639–650, Sep. 2002.
[28] J. Berthet, T. W. Rall, and E. W. Sutherland, “The relationship of epinephrine and glucagon to liver phosphorylase. IV. Effect of epinephrine and glucagon on the reactivation of phosphorylase in liver homogenates,” *J. Biol. Chem.*, vol. 224, no. 1, pp. 463–475, Jan. 1957.
[29] G. Milligan and E. Kostenis, “Heterotrimeric G-proteins: a short history,” *Br. J. Pharmacol.*, vol. 147 Suppl 1, pp. S46–55, Jan. 2006.

[30] M. Rodbell, L. Birnbaumer, and S. L. Pohl, “Characteristics of glucagon action on the hepatic adenylate cyclase system.,” *Biochem J*, vol. 125, no. 3, p. 58P–59P, Dec. 1971.
[31] D. M. Gill and R. Meren, “ADP-ribosylation of membrane proteins catalyzed by cholera toxin: basis of the activation of adenylate cyclase,” *PNAS*, vol. 75, no. 7, pp. 3050–3054, Jul. 1978.
[32] T. Haga, E. M. Ross, H. J. Anderson, and A. G. Gilman, “Adenylate cyclase permanently uncoupled from hormone receptors in a novel variant of S49 mouse lymphoma cells,” *Proc. Natl. Acad. Sci. U.S.A.*, vol. 74, no. 5, pp. 2016–2020, May 1977.
[33] J. K. Northup, P. C. Sternweis, M. D. Smigel, L. S. Schleifer, E. M. Ross, and A. G. Gilman, “Purification of the regulatory component of adenylate cyclase.,” *Proc Natl Acad Sci U S A*, vol. 77, no. 11, pp. 6516–6520, Nov. 1980.
[34] T. M. Cabrera-Vera, J. Vanhauwe, T. O. Thomas, M. Medkova, A. Preininger, M. R. Mazzoni, and H. E. Hamm, “Insights into G Protein Structure, Function, and Regulation,” *Endocrine Reviews*, vol. 24, no. 6, pp. 765–781, Dec. 2003.
[35] M. Soejima and A. Noma, “Mode of regulation of the ACh-sensitive K-channel by the muscarinic receptor in rabbit atrial cells,” *Pflügers Archiv European Journal of Physiology*, vol. 400, no. 4, pp. 424–431, 1984.
[36] G. E. Breitwieser and G. Szabo, “Uncoupling of cardiac muscarinic and beta-adrenergic receptors from ion channels by a guanine nucleotide analogue,” *Nature*, vol. 317, no. 6037, pp. 538–540, Oct. 1985.
[37] P. J. Pfaffinger, J. M. Martin, D. D. Hunter, N. M. Nathanson, and B. Hille, “GTP-binding proteins couple cardiac muscarinic receptors to a K channel,” *Nature*, vol. 317, no. 6037, pp. 536–538, Oct. 1985.
[38] R. Rusinova, T. Mirshahi, and D. E. Logothetis, “Specificity of Gbetagamma signaling to Kir3 channels depends on the helical domain of pertussis toxin-sensitive Galpha subunits,” *J. Biol. Chem.*, vol. 282, no. 47, pp. 34019–34030, Nov. 2007.
[39] S. M. Clancy, C. E. Fowler, M. Finley, K. F. Suen, C. Arrabit, F. Berton, T. Kosaza, P. J. Casey, and P. A. Slesinger, “Pertussis-toxin-sensitive Galpha subunits selectively bind to C-terminal domain of neuronal GIRK channels: evidence for a heterotrimeric G-protein-channel complex,” *Mol. Cell. Neurosci.*, vol. 28, no. 2, pp. 375–389, Feb. 2005.
[40] C. L. Huang, Y. N. Jan, and L. Y. Jan, “Binding of the G protein betagamma subunit to multiple regions of G protein-gated inward-rectifying K+ channels,” *FEBS Lett.*, vol. 405, no. 3, pp. 291–298, Apr. 1997.
[41] N. A. Cohen, Q. Sha, E. N. Makhina, A. N. Lopatin, M. E. Linder, S. H. Snyder, and C. G. Nichols, “Inhibition of an inward rectifier potassium channel (Kir2.3) by G-protein betagamma subunits,” *J. Biol. Chem.*, vol. 271, no. 50, pp. 32301–32305, Dec. 1996.
[42] I. Riven, S. Iwanir, and E. Reuveny, “GIRK Channel Activation Involves a Local Rearrangement of a Preformed G Protein Channel Complex,” *Neuron*, vol. 51, no. 5, pp. 561–573, Sep. 2006.
[43] S. Berlin, T. Keren-Raifman, R. Castel, M. Rubinstein, C. W. Dessauer, T. Ivanina, and N. Dascal, “Gαi and Gβγ Jointly Regulate the Conformations of a Gβγ Effector, the Neuronal G Protein-activated K+ Channel (GIRK),” *J. Biol. Chem.*, vol. 285, no. 9, pp. 6179–6185, Feb. 2010.
[44] H. Zhang, C. He, X. Yan, T. Mirshahi, and D. E. Logothetis, “Activation of inwardly rectifying K+ channels by distinct PtdIns(4,5)P2 interactions,” *Nat. Cell Biol.*, vol. 1, no. 3, pp. 183–188, Jul. 1999.

[45] J. L. Sui, J. Petit-Jacques, and D. E. Logothetis, “Activation of the atrial KACh channel by the betagamma subunits of G proteins or intracellular Na+ ions depends on the presence of phosphatidylinositol phosphates,” *Proc. Natl. Acad. Sci. U.S.A.*, vol. 95, no. 3, pp. 1307–1312, Feb. 1998.
[46] C. L. Huang, S. Feng, and D. W. Hilgemann, “Direct activation of inward rectifier potassium channels by PIP2 and its stabilization by Gbetagamma,” *Nature*, vol. 391, no. 6669, pp. 803–806, Feb. 1998.
[47] P. Aryal, H. Dvir, S. Choe, and P. A. Slesinger, “A discrete alcohol pocket involved in GIRK channel activation,” *Nat Neurosci*, vol. 12, no. 8, pp. 988–995, 2009.
[48] G. Zeidner, R. Sadja, and E. Reuveny, “Redox-dependent gating of G protein coupled inwardly rectifying K+ channels,” *J. Biol. Chem.*, p. M105189200, Jul. 2001.
[49] D. A. Doyle, J. Morais Cabral, R. A. Pfuetzner, A. Kuo, J. M. Gulbis, S. L. Cohen, B. T. Chait, and R. MacKinnon, “The structure of the potassium channel: molecular basis of K+ conduction and selectivity,” *Science*, vol. 280, no. 5360, pp. 69–77, Apr. 1998.
[50] M. Nishida and R. MacKinnon, “Structural basis of inward rectification: cytoplasmic pore of the G protein-gated inward rectifier GIRK1 at 1.8 A resolution,” *Cell*, vol. 111, no. 7, pp. 957–965, Dec. 2002.
[51] S. Pegan, C. Arrabit, W. Zhou, W. Kwiatkowski, A. Collins, P. A. Slesinger, and S. Choe, “Cytoplasmic domain structures of Kir2.1 and Kir3.1 show sites for modulating gating and rectification,” *Nat. Neurosci.*, vol. 8, no. 3, pp. 279–287, Mar. 2005.
[52] M. Nishida, M. Cadene, B. T. Chait, and R. MacKinnon, “Crystal structure of a Kir3.1-prokaryotic Kir channel chimera,” *EMBO J*, vol. 26, no. 17, pp. 4005–4015, 2007.
[53] M. R. Whorton and R. MacKinnon, “Crystal structure of the mammalian GIRK2 K+ channel and gating regulation by G proteins, PIP2, and sodium,” *Cell*, vol. 147, no. 1, pp. 199–208, Sep. 2011.
[54] X.-Y. Meng, H.-X. Zhang, D. E. Logothetis, and M. Cui, “The Molecular Mechanism by which PIP2 Opens the Intracellular G-Loop Gate of a Kir3.1 Channel,” *Biophysical Journal*, vol. 102, no. 9, pp. 2049–2059, May 2012.
[55] O. B. Clarke, A. T. Caputo, A. P. Hill, J. I. Vandenberg, B. J. Smith, and J. M. Gulbis, “Domain Reorientation and Rotation of an Intracellular Assembly Regulate Conduction in Kir Potassium Channels,” *Cell*, vol. 141, no. 6, pp. 1018–1029, Jun. 2010.
[56] J. Xiao, X. Zhen, and J. Yang, “Localization of PIP2 activation gate in inward rectifier K+ channels,” *Nat. Neurosci.*, vol. 6, no. 8, pp. 811–818, Aug. 2003.
[57] M. A. Wall, D. E. Coleman, E. Lee, J. A. Iñiguez-Lluhi, B. A. Posner, A. G. Gilman, and S. R. Sprang, “The structure of the G protein heterotrimer Gi[alpha]1[beta]1[gamma]2,” *Cell*, vol. 83, no. 6, pp. 1047–1058, Dec. 1995.
[58] D. G. Lambright, J. Sondek, A. Bohm, N. P. Skiba, H. E. Hamm, and P. B. Sigler, “The 2.0 A crystal structure of a heterotrimeric G protein,” *Nature*, vol. 379, no. 6563, pp. 311–319, Jan. 1996.
[59] W. M. Oldham and H. E. Hamm, “Structural Basis of Function in Heterotrimeric G Proteins,” *Quarterly Reviews of Biophysics*, vol. 39, no. 02, pp. 117–166, 2006.
[60] J. Sondek, A. Bohm, D. G. Lambright, H. E. Hamm, and P. B. Sigler, “Crystal structure of a G-protein beta gamma dimer at 2.1A resolution,” *Nature*, vol. 379, no. 6563, pp. 369–374, Jan. 1996.

[61] J. J. G. Tesmer, V. M. Tesmer, D. T. Lodowski, H. Steinhagen, and J. Huber, "Structure of human G protein-coupled receptor kinase 2 in complex with the kinase inhibitor balanol," *J. Med. Chem.*, vol. 53, no. 4, pp. 1867–1870, Feb. 2010.
[62] A. Loew, Y. K. Ho, T. Blundell, and B. Bax, "Phosducin induces a structural change in transducin beta gamma," *Structure*, vol. 6, no. 8, pp. 1007–1019, Aug. 1998.
[63] C. L. Huang, P. A. Slesinger, P. J. Casey, Y. N. Jan, and L. Y. Jan, "Evidence that direct binding of G beta gamma to the GIRK1 G protein-gated inwardly rectifying K+ channel is important for channel activation," *Neuron*, vol. 15, no. 5, pp. 1133–1143, Nov. 1995.
[64] A. Inanobe, K. I. Morishige, N. Takahashi, H. Ito, M. Yamada, T. Takumi, H. Nishina, K. Takahashi, Y. Kanaho, T. Katada, and Y. Kurachi, "Gβγ Directly Binds to the Carboxyl Terminus of the G Protein-Gated Muscarinic K+ Channel, GIRK1," *Biochemical and Biophysical Research Communications*, vol. 212, no. 3, pp. 1022–1028, Jul. 1995.
[65] M. T. Kunkel and E. G. Peralta, "Identification of domains conferring G protein regulation on inward rectifier potassium channels," *Cell*, vol. 83, no. 3, pp. 443–449, Nov. 1995.
[66] G. Krapivinsky, I. Medina, L. Eng, L. Krapivinsky, Y. Yang, and D. E. Clapham, "A novel inward rectifier K+ channel with unique pore properties," *Neuron*, vol. 20, no. 5, pp. 995–1005, May 1998.
[67] T. Ivanina, I. Rishal, D. Varon, C. Mullner, B. Frohnwieser-Steinecke, W. Schreibmayer, C. W. Dessauer, and N. Dascal, "Mapping the Gbetagamma-binding sites in GIRK1 and GIRK2 subunits of the G protein-activated K+ channel," *J. Biol. Chem.*, vol. 278, no. 31, pp. 29174–29183, Aug. 2003.
[68] T. Ivanina, D. Varon, S. Peleg, I. Rishal, Y. Porozov, C. W. Dessauer, T. Keren-Raifman, and N. Dascal, "Galphai1 and Galphai3 differentially interact with, and regulate, the G protein-activated K+ channel," *J. Biol. Chem.*, vol. 279, no. 17, pp. 17260–17268, Apr. 2004.
[69] P. A. Slesinger, E. Reuveny, Y. N. Jan, and L. Y. Jan, "Identification of structural elements involved in G protein gating of the GIRK1 potassium channel," *Neuron*, vol. 15, no. 5, pp. 1145–1156, Nov. 1995.
[70] M. Finley, C. Arrabit, C. Fowler, K. F. Suen, and P. A. Slesinger, "βL–βM loop in the C-terminal domain of G protein-activated inwardly rectifying K+ channels is important for Gβγ subunit activation," *J Physiol*, vol. 555, no. 3, pp. 643–657, Mar. 2004.
[71] C. He, H. Zhang, T. Mirshahi, and D. E. Logothetis, "Identification of a Potassium Channel Site That Interacts with G Protein βγ Subunits to Mediate Agonist-induced Signaling," *Journal of Biological Chemistry*, vol. 274, no. 18, pp. 12517–12524, Apr. 1999.
[72] C. He, X. Yan, H. Zhang, T. Mirshahi, T. Jin, A. Huang, and D. E. Logothetis, "Identification of Critical Residues Controlling G Protein-gated Inwardly Rectifying K+ Channel Activity through Interactions with the βγ Subunits of G Proteins," *Journal of Biological Chemistry*, vol. 277, no. 8, pp. 6088–6096, Feb. 2002.
[73] C. E. Ford, N. P. Skiba, H. Bae, Y. Daaka, E. Reuveny, L. R. Shekter, R. Rosal, G. Weng, C.-S. Yang, R. Iyengar, R. J. Miller, L. Y. Jan, R. J. Lefkowitz, and H. E. Hamm, "Molecular Basis for Interactions of G Protein βγ Subunits with Effectors," *Science*, vol. 280, no. 5367, pp. 1271 –1274, May 1998.
[74] A. M. Albsoul-Younes, P. M. Sternweis, P. Zhao, H. Nakata, S. Nakajima, Y. Nakajima, and T. Kozasa, "Interaction sites of the G protein beta subunit with brain GIRK," *J. Biol. Chem.*, p. M011231200, Jan. 2001.

[75] Q. Zhao, T. Kawano, H. Nakata, Y. Nakajima, S. Nakajima, and T. Kozasa, “Interaction of G protein beta subunit with inward rectifier K(+) channel Kir3,” *Mol. Pharmacol.*, vol. 64, no. 5, pp. 1085–1091, Nov. 2003.
[76] T. Mirshahi, L. Robillard, H. Zhang, T. E. Hébert, and D. E. Logothetis, “Gβ Residues That Do Not Interact with Gα Underlie Agonist-independent Activity of K+ Channels,” *Journal of Biological Chemistry*, vol. 277, no. 9, pp. 7348–7355, Mar. 2002.
[77] T. Mirshahi, V. Mittal, H. Zhang, M. E. Linder, and D. E. Logothetis, “Distinct Sites on G Protein βγ Subunits Regulate Different Effector Functions,” *Journal of Biological Chemistry*, vol. 277, no. 39, pp. 36345–36350, 2002.
[78] L. Li, S. J. Wright, S. Krystofova, G. Park, and K. A. Borkovich, “Heterotrimeric G Protein Signaling in Filamentous Fungi*,” *Annual Review of Microbiology*, vol. 61, no. 1, pp. 423–452, 2007.
[79] N. A. Lambert, “Dissociation of Heterotrimeric G Proteins in Cells,” *Sci. Signal.*, vol. 1, no. 25, p. re5, Jun. 2008.
[80] I. Halperin, B. Ma, H. Wolfson, and R. Nussinov, “Principles of docking: An overview of search algorithms and a guide to scoring functions,” *Proteins*, vol. 47, no. 4, pp. 409–443, Jun. 2002.
[81] M. Karplus and J. A. McCammon, “Molecular dynamics simulations of biomolecules,” *Nat. Struct. Biol.*, vol. 9, no. 9, pp. 646–652, Sep. 2002.
[82] J. Åqvist, C. Medina, and J.-E. Samuelsson, “A new method for predicting binding affinity in computer-aided drug design,” *Protein Engineering, Design and Selection*, vol. 7, no. 3, pp. 385–391, 1994.
[83] D. L. Beveridge and F. M. DiCapua, “Free energy via molecular simulation: applications to chemical and biomolecular systems,” *Annu Rev Biophys Biophys Chem*, vol. 18, pp. 431–492, 1989.
[84] S. Vajda and D. Kozakov, “Convergence and combination of methods in protein–protein docking,” *Current Opinion in Structural Biology*, vol. 19, no. 2, pp. 164–170, Apr. 2009.
[85] T. Lengauer and M. Rarey, “Computational methods for biomolecular docking,” *Curr. Opin. Struct. Biol.*, vol. 6, no. 3, pp. 402–406, Jun. 1996.
[86] G. R. Smith and M. J. E. Sternberg, “Prediction of protein-protein interactions by docking methods,” *Curr. Opin. Struct. Biol.*, vol. 12, no. 1, pp. 28–35, Feb. 2002.
[87] C. Dominguez, R. Boelens, and A. M. J. J. Bonvin, “HADDOCK: A Protein−Protein Docking Approach Based on Biochemical or Biophysical Information,” *J. Am. Chem. Soc.*, vol. 125, no. 7, pp. 1731–1737, Feb. 2003.
[88] M. F. Lensink and S. J. Wodak, “Docking and scoring protein interactions: CAPRI 2009,” *Proteins: Structure, Function, and Bioinformatics*, vol. 78, no. 15, pp. 3073–3084, 2010.
[89] A. Sali and T. L. Blundell, “Comparative protein modelling by satisfaction of spatial restraints,” *J. Mol. Biol.*, vol. 234, no. 3, pp. 779–815, Dec. 1993.
[90] V. M. Tesmer, T. Kawano, A. Shankaranarayanan, T. Kozasa, and J. J. G. Tesmer, “Snapshot of activated G proteins at the membrane: the Galphaq-GRK2-Gbetagamma complex,” *Science*, vol. 310, no. 5754, pp. 1686–1690, Dec. 2005.
[91] R. Chen and Z. Weng, “Docking unbound proteins using shape complementarity, desolvation, and electrostatics,” *Proteins*, vol. 47, no. 3, pp. 281–294, May 2002.
[92] R. Chen, L. Li, and Z. Weng, “ZDOCK: An initial-stage protein-docking algorithm,” *Proteins: Structure, Function, and Genetics*, vol. 52, no. 1, pp. 80–87, 2003.

[93] J. Mintseris, B. Pierce, K. Wiehe, R. Anderson, R. Chen, and Z. Weng, "Integrating statistical pair potentials into protein complex prediction," *Proteins: Structure, Function, and Bioinformatics*, vol. 69, no. 3, pp. 511–520, 2007.
[94] B. Pierce and Z. Weng, "ZRANK: Reranking protein docking predictions with an optimized energy function," *Proteins: Structure, Function, and Bioinformatics*, vol. 67, no. 4, pp. 1078–1086, 2007.
[95] M. F. Lensink and S. J. Wodak, "Blind predictions of protein interfaces by docking calculations in CAPRI," *Proteins*, vol. 78, no. 15, pp. 3085–3095, Nov. 2010.
[96] H. Hwang, T. Vreven, B. G. Pierce, J.-H. Hung, and Z. Weng, "Performance of ZDOCK and ZRANK in CAPRI rounds 13-19," *Proteins*, vol. 78, no. 15, pp. 3104–3110, Nov. 2010.
[97] J. Fernández-Recio, M. Totrov, and R. Abagyan, "Identification of protein-protein interaction sites from docking energy landscapes," *J. Mol. Biol.*, vol. 335, no. 3, pp. 843–865, Jan. 2004.
[98] S. Grosdidier and J. Fernandez-Recio, "Identification of hot-spot residues in protein-protein interactions by computational docking," *BMC Bioinformatics*, vol. 9, no. 1, p. 447, 2008.
[99] S. R. Comeau, D. W. Gatchell, S. Vajda, and C. J. Camacho, "ClusPro: an automated docking and discrimination method for the prediction of protein complexes," *Bioinformatics*, vol. 20, no. 1, pp. 45–50, Jan. 2004.
[100] C. J. Camacho, Z. Weng, S. Vajda, and C. DeLisi, "Free energy landscapes of encounter complexes in protein-protein association," *Biophys. J.*, vol. 76, no. 3, pp. 1166–1178, Mar. 1999.
[101] D. Kozakov, O. Schueler-Furman, and S. Vajda, "Discrimination of near-native structures in protein-protein docking by testing the stability of local minima," *Proteins*, vol. 72, no. 3, pp. 993–1004, Aug. 2008.
[102] C. J. Camacho and S. Vajda, "Protein docking along smooth association pathways," *Proc. Natl. Acad. Sci. U.S.A.*, vol. 98, no. 19, pp. 10636–10641, Sep. 2001.
[103] D. Kozakov, K. H. Clodfelter, S. Vajda, and C. J. Camacho, "Optimal Clustering for Detecting Near-Native Conformations in Protein Docking," *Biophysical Journal*, vol. 89, no. 2, pp. 867–875, Aug. 2005.
[104] N. O'Toole and I. A. Vakser, "Large-scale characteristics of the energy landscape in protein-protein interactions," *Proteins*, vol. 71, no. 1, pp. 144–152, Apr. 2008.
[105] J. J. Gray, S. Moughon, C. Wang, O. Schueler-Furman, B. Kuhlman, C. A. Rohl, and D. Baker, "Protein-Protein Docking with Simultaneous Optimization of Rigid-body Displacement and Side-chain Conformations," *Journal of Molecular Biology*, vol. 331, no. 1, pp. 281–299, Aug. 2003.
[106] B. Pierce and Z. Weng, "A combination of rescoring and refinement significantly improves protein docking performance," *Proteins: Structure, Function, and Bioinformatics*, vol. 72, no. 1, pp. 270–279, 2008.
[107] X. Xu and J. W. Nelson, "Solution structure of tertiapin determined using nuclear magnetic resonance and distance geometry," *Proteins*, vol. 17, no. 2, pp. 124–137, Oct. 1993.
[108] W. Jin, A. M. Klem, J. H. Lewis, and Z. Lu, "Mechanisms of inward-rectifier K+ channel inhibition by tertiapin-Q," *Biochemistry*, vol. 38, no. 43, pp. 14294–14301, Oct. 1999.

[109] Y. Ramu, Y. Xu, and Z. Lu, “Engineered specific and high-affinity inhibitor for a subtype of inward-rectifier K+ channels,” *Proc. Natl. Acad. Sci. U.S.A.*, vol. 105, no. 31, pp. 10774–10778, Aug. 2008.
[110] M. Yokogawa, M. Osawa, K. Takeuchi, Y. Mase, and I. Shimada, “NMR analyses of the Gbetagamma binding and conformational rearrangements of the cytoplasmic pore of G protein-activated inwardly rectifying potassium channel 1 (GIRK1),” *J. Biol. Chem.*, vol. 286, no. 3, pp. 2215–2223, Jan. 2011.
[111] R. Wolfenden, L. Andersson, P. M. Cullis, and C. C. B. Southgate, “Affinities of amino acid side chains for solvent water,” *Biochemistry*, vol. 20, no. 4, pp. 849–855, Feb. 1981.
[112] H. Chuang and S. Lin, “Oxidative challenges sensitize the capsaicin receptor by covalent cysteine modification,” *Proc. Natl. Acad. Sci. U.S.A.*, vol. 106, no. 47, pp. 20097–20102, Nov. 2009.
[113] Q. Zhang, M. A. Pacheco, and C. A. Doupnik, “Gating properties of GIRK channels activated by Galpha(o)- and Galpha(i)-coupled muscarinic m2 receptors in Xenopus oocytes: the role of receptor precoupling in RGS modulation,” *J. Physiol. (Lond.)*, vol. 545, no. Pt 2, pp. 355–373, Dec. 2002.
[114] S. Corey and D. E. Clapham, “The Stoichiometry of Gβγ Binding to G-protein-regulated Inwardly Rectifying K+ Channels (GIRKs),” *Journal of Biological Chemistry*, vol. 276, no. 14, pp. 11409 –11413, Apr. 2001.
[115] E. C. Fieller, “The Biological Standardization of Insulin,” *Supplement to the Journal of the Royal Statistical Society*, vol. 7, no. 1, p. 1, 1940.
[116] V. H. Franz, “Ratios: A short guide to confidence limits and proper use,” *arXiv:0710.2024*, Oct. 2007.
[117] M. J. Knol, W. R. Pestman, and D. E. Grobbee, “The (mis)use of overlap of confidence intervals to assess effect modification,” *Eur J Epidemiol*, vol. 26, no. 4, pp. 253–254, Apr. 2011.